State Planet, 3-slre1, 4, 2024
https://doi.org/10.5194/sp-3-slre1-4-2024

Sea Level Rise in Europe: Observations and projections

Angélique Melet[1], Roderik van de Wal[2,3], Angel Amores[4,5], Arne Arns[6], Alisée A. Chaigneau[1,7], Irina Dinu[8], Ivan D. Haigh[9], Tim H. J. Hermans[2], Piero Lionello[10], Marta Marcos[4,5], H. E. Markus Meier[11], Benoit Meyssignac[12], Matthew D. Palmer[13,14], Ronja Reese[15], Matthew J. R. Simpson[16], and Aimée B. A. Slangen[17]

[1]Mercator Ocean International, Toulouse, 31400, France
[2]Institute for Marine and Atmospheric Research Utrecht, Utrecht University, Princetonplein 5, 3584 CC Utrecht, the Netherlands
[3]Department of Physical Geography, Utrecht University, Princetonlaan 8a, 3584 CB Utrecht, the Netherlands
[4]Mediterranean Institute for Advanced Studies (IMEDEA, UIB-CSIC), Esporles, 07190, Spain
[5]Department of Physics, University of the Balearic Islands, Palma, 07122, Spain
[6]Faculty of Agricultural and Environmental Sciences, University of Rostock, Justus-von-Liebig-Weg 6, 18059 Rostock, Germany
[7]IHCantabria – Instituto de Hidráulica Ambiental de la Universidad de Cantabria, Isabel Torres 15, 39011 Santander, Spain
[8]Department of Interdisciplinary Studies and Coastal Management, Institute for Marine Geology and Geoecology (GeoEcoMar), Bucharest, 024053, Romania
[9]School of Ocean and Earth Science, University of Southampton, European Way, Southampton, SO14 3ZH, United Kingdom
[10]Department of Environmental and Biological Sciences and Technologies, University of Salento, Lecce, Italy
[11]Department of Physical Oceanography and Instrumentation, Leibniz Institute for Baltic Sea Research Warnemünde, 18119 Rostock, Germany
[12]LEGOS (CNES/CNRS/IRD/UT3), Université de Toulouse, 31400 Toulouse, France
[13]Met Office Hadley Centre, FitzRoy Road, Exeter, EX1 3 PB, United Kingdom
[14]School of Earth Sciences, University of Bristol, Bristol, BS8 1UH, United Kingdom
[15]Department of Geography and Environmental Sciences, Northumbria University, Ellison Place, Newcastle Upon Tyne, NE1 8ST, United Kingdom
[16]Norwegian Mapping Authority, Geodetic Institute, Hønefoss, 3511, Norway
[17]Department of Estuarine and Delta Systems, NIOZ Royal Netherlands Institute for Sea Research, Yerseke, 4401 NT, the Netherlands

Correspondence: Angélique Melet (amelet@mercator-ocean.fr) and Roderik van de Wal (r.s.w.vandewal@uu.nl)

Received: 2 December 2023 – Discussion started: 12 December 2023
Revised: 4 June 2024 – Accepted: 14 June 2024 – Published: 29 October 2024

Abstract. Sea level rise (SLR) is a major concern for Europe, where 30 million people live in the historical 1-in-100-year event flood coastal plains. The latest IPCC assessment reports provide a literature review on past and projected SLR, and their key findings are synthesized here with a focus on Europe. The present paper complements IPCC reports and contributes to the Knowledge Hub on SLR European Assessment Report. Here, the state of knowledge of observed and 21st century projected SLR and changes in extreme sea levels (ESLs) are documented with more regional information for European basins as scoped with stakeholders. In Europe, satellite altimetry shows that geocentric sea level trends are on average slightly above the global mean rate, with only a few areas showing no change or a slight decrease such as central parts of the Mediterranean Sea. The spatial pattern of geocentric SLR in European Seas is largely influenced by internal climate modes, especially

Published by Copernicus Publications.

the North Atlantic Oscillation, which varies on year-to-year to decadal timescales. In terms of relative sea level rise (RSLR), vertical land motions due to human-induced subsidence and glacial isostatic adjustment (GIA) are important for many coastal European regions, leading to lower or even negative RSLR in the Baltic Sea and to large rates of RSLR for subsiding coastlines. Projected 21st century local SLR for Europe is broadly in line with projections of global mean sea level rise (GMSLR) in most places. Some European coasts are projected to experience a RSLR by 2100 below the projected GMSLR, such as the Norwegian coast, the southern Baltic Sea, the northern part of the UK, and Ireland. A relative sea level fall is projected for the northern Baltic Sea. RSLR along other European coasts is projected to be slightly above the GMSLR, for instance the Atlantic coasts of Portugal, Spain, France, Belgium, and the Netherlands. Higher-resolution regionalized projections are needed to better resolve dynamic sea level changes especially in semi-enclosed basins, such as the Mediterranean Sea, North Sea, Baltic Sea, and Black Sea. In addition to ocean dynamics, GIA and Greenland ice mass loss and associated Earth gravity, rotation, and deformation effects are important drivers of spatial variations of projected European RSLR. High-end estimates of SLR in Europe are particularly sensitive to uncertainties arising from the estimates of the Antarctic ice mass loss. Regarding ESLs, the frequency of occurrence of the historical centennial-event level is projected to be amplified for most European coasts, except along the northern Baltic Sea coasts where a decreasing probability is projected because of relative sea level fall induced by GIA. The largest historical centennial-event amplification factors are projected for the southern European seas (Mediterranean and Iberian Peninsula coasts), while the smallest amplification factors are projected in macro-tidal regions exposed to storms and induced large surges such as the southeastern North Sea. Finally, emphasis is given to processes that are especially important for specific regions, such as waves and tides in the northeastern Atlantic; vertical land motion for the European Arctic and Baltic Sea; seiches, meteotsunamis, and medicanes in the Mediterranean Sea; and non-linear interactions between drivers of coastal sea level extremes in the shallow North Sea.

1 Introduction

Sea level rise (SLR) is a major concern for Europe, where more than 50 million people live in low-elevation (≤ 10 m) coastal zones and 30 million in the 100-year-event marine coastal flood plains (Neumann et al., 2015).

Sea level (SL) changes at the coast result from processes acting at various spatial scales and timescales, from extreme events to long-term SLR, with the superposition of global, regional, and local variations. SLR is a direct consequence of climate change, which is due to the current energy imbalance of our planet at the top of its atmosphere induced by anthropogenic emissions of greenhouse gases (e.g. Forster et al., 2021). As our planet reemits less energy to space than it receives from the Sun, an excess of energy, mostly in the form of heat, accumulates in the climate system. About 91 % of the excess heat stored in the climate system has been absorbed in the oceans (Cheng et al., 2017; Von Schuckmann et al., 2020), causing a thermal expansion of the ocean, leading to global mean sea level rise (GMSLR). The remainder of the excess heat has been absorbed by the atmosphere, land ice, sea ice, and land surface. As land ice (glaciers, ice sheets) melts and is discharged to the ocean, water is added to the ocean, increasing its mass and volume and thereby rising SL. Changes in land water storage due to natural hydrological cycle and human interventions also lead to ocean mass and SL changes.

SLR has not been and will not be uniform over the ocean (Fox-Kemper et al., 2021). At a regional scale, mean SLR can deviate substantially from GMSLR due to a number of processes, with three key drivers. First, ocean circulations redistribute the seawater mass, heat, and salinity, leading to regional dynamic SL changes. Changes in ocean circulations are mostly driven by surface wind stress but also by air–sea heat and freshwater fluxes (Forget and Ponte, 2015; Meyssignac et al., 2017; Todd et al., 2020) and by intrinsic ocean variability (Llovel et al., 2018; Sérazin et al., 2015). Regional dynamic SL changes are mostly steric (ocean density changes), with a predominance of its thermosteric component. When combined together, the global mean steric SL change and ocean dynamic SL changes are called sterodynamic SL change (Gregory et al., 2019). Second, geographical redistribution of mass over the Earth, including contemporary or past transfers between land and ocean, such as glacier and ice sheet mass loss or land water storage changes, induce changes in Earth gravity and rotation as well as viscoelastic solid Earth deformations (called GRD effects). GRD effects induce SL changes through changes in the geoid and vertical land motion (VLM; Tamisiea, 2011). Glacial isostatic adjustment (GIA; Peltier, 2004) causes contemporary relative SL change due to GRD effects through ongoing viscous changes in the solid Earth caused by past changes in land ice, mostly through the deglaciation following the Last Glacial Maximum ($\sim 20\,000$ years ago). Third, regional changes in atmospheric pressure loading over the ocean (due to changes in atmospheric circulations and moisture content) induce regional changes in the inverted barometer effect at scales longer than about a month (Wunsch and

Stammer, 1997). The inverted barometer effect is a relatively minor driver of regional SL changes at seasonal and longer timescales.

At more coastal scales, relative SL changes can be due to VLM of natural and anthropogenic origins (e.g. sediment compaction in deltas, Earth tectonics, GIA and solid Earth deformation due to contemporary land ice mass loss, pumping of groundwater, and weight of the built environment). In many coastal megacities, including European ones, VLM can induce relative SL trends similar to or larger than trends induced by oceanic and climate factors causing geocentric SL changes (Gregory et al., 2019, also known as absolute sea level changes) (e.g. Nicholls et al., 2021; Wu et al., 2022). In addition, several other processes lead to substantial SL deviations from the open ocean and should be considered when estimating local SL changes at the coast (Woodworth et al., 2019). Among these processes are tides, atmospheric surges, wind wave setup and swash, seiches, coastal waves, and effects of river discharges. Coastal SL variability spans a wide range of temporal and spatial scales (Hughes et al., 2019; Woodworth et al., 2019). Processes driving coastal SL change can also interact (e.g. Idier et al., 2019) due to their effects and their dependence on water depth for instance.

European regional seas (see Jiménez et al., 2024, in this report) and their bordering coasts along Europe present contrasting environments, from open-ocean environments (northeastern Atlantic, European Arctic) to semi-enclosed (North Sea) and quasi-enclosed seas (Baltic Sea, Mediterranean Sea, and Black Sea), microtidal (Mediterranean, Baltic and Black Seas) to mesotidal (European Arctic) and macrotidal environments (northeastern Atlantic, North Sea), deep to shallow seas on the continental shelf (North Sea, Baltic Sea), regions exposed to large swells or storms under the North Atlantic storm track, and regions experiencing different VLM. These contrasted atmospheric and ocean environments induce different past and projected SL changes over European seas. Here, the state of knowledge of observed and 21st century projected changes in mean and extreme SL is documented for European basins as part of the Knowledge Hub on Sea Level Rise Assessment Report.

First, a synthesis of the key findings of recent Intergovernmental Panel on Climate Change (IPCC) assessment reports on past and future SLR is provided in Sect. 2.1, with a European perspective in Sect. 2.2. The following Sects. 3–6 complement the IPCC assessment reports and provide extensive regional information on European observed and projected SL changes, as requested by stakeholders (see Jiménez et al., 2024, in this report). Observations of SLR in Europe from tide gauges (Sect. 3.1) and satellite altimetry (Sect. 3.2) are discussed, together with available SL tools and data portals (Box 1). As VLM due to human-induced subsidence and GIA is important for many coastal European regions, observations of this component of relative sea level rise (RSLR) are discussed in Sect. 3.3. Observed changes in extreme sea levels (ESLs, Sect. 3.4) and a selection of iconic historical storms causing coastal flooding in Europe and their consequences are reported (Box 2). In Sect. 4, drivers of SLR and ESLs are discussed, with a focus on Europe. Projected changes in European SL are presented in Sect. 5, with a focus on projected 21st century changes in mean SL and extremes. A discussion on tipping points, irreversibility, and commitment of SLR is also provided. Finally, a regional focus per European regional sea (northeastern Atlantic, North Sea, Arctic Ocean, Baltic Sea, and Mediterranean and Black seas) with key developments per region is provided in Sect. 6.

2 Summary of previous assessments

2.1 Synthesis of recent IPCC assessment reports

Here we present a synthesis of the key findings of the two most recent assessment reports that provided comprehensive information on past and future SLR: (1) the IPCC Special Report on the Ocean and Cryosphere in a Changing Climate (SROCC; IPCC, 2019; Oppenheimer et al., 2019) and (2) the IPCC Sixth Assessment Report of Working Group I (Fox-Kemper et al., 2021; IPCC, 2021a). The text in this Section is based primarily on the AR6 WG1 and SROCC Summaries for Policy Makers (IPCC, 2019, 2021b), which have been endorsed by international government delegations during the IPCC approval sessions. The IPCC reports synthesize a huge body of literature, and we refer the reader to the above assessment reports and references therein for further discussion on the topics summarized in this section. Recent progress and additional regional information are provided in subsequent Sections.

During the 20th century, global mean SL has risen faster than during any preceding century in at least the last 3000 years. SLR has accelerated since the late 1960s. The average rate was about $1.3\,\mathrm{mm\,yr^{-1}}$ during 1901–1971, increasing to about $1.9\,\mathrm{mm\,yr^{-1}}$ during 1971–2006 and further increasing to about $3.7\,\mathrm{mm\,yr^{-1}}$ during 2006–2018. Our understanding of the physical mechanisms of these past changes has increased through demonstrated closure of the observed GMSL budget, in particular after 1970 (Oppenheimer et al., 2019; Fox-Kemper et al., 2021). For example, the acceleration of GMSLR in recent decades is driven primarily by a 4-fold increase in the rate of ice sheet mass loss since the 1990s. For the period since 2006, ice mass input to the ocean from ice sheets and glaciers exceeds all other contributions to GMSLR. It is now understood that anthropogenic forcing was the main driver of the observed GMSLR since at least 1971 (Slangen et al., 2016). There is also scientific evidence for changes in the drivers of ESL events. There is high confidence that anthropogenic climate change has increased some cyclone-driven ESL events. Extreme wave heights have increased in the Southern Ocean and North Atlantic since the 1980s, and loss of sea ice has been linked to increased wave heights in the Arctic Ocean since the 1990s (Oppenheimer et al., 2019).

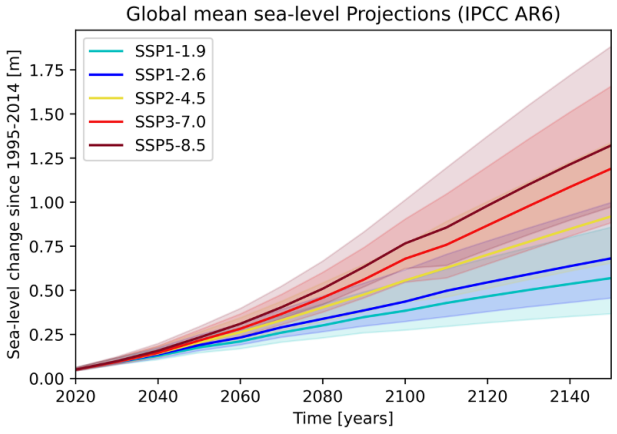

Figure 1. Projected GMSLR from the sixth assessment report of the IPCC relative to 1995–2014. Median (50th percentile) projections for all scenarios are indicated by the solid lines as shown in the figure legend. For each scenario, the shading shows the likely range (17th–83rd percentiles) (Fox-Kemper et al., 2021).

One of the main innovations in AR6 was the use of emulators with multi-model ensembles and observational constraints to develop SL projections that were consistent with the assessment of climate sensitivity (Forster et al., 2021; Fox-Kemper et al., 2021; IPCC, 2021a). Another important innovation was the explicit treatment of the potential for accelerated future SLR associated with deeply uncertain ice sheet instability processes through illustrative high-end storylines, intended to aid decision-making. While these high-end storylines yielded much higher multi-century SLR projections than seen in previous IPCC reports, the likely range (i.e. the central two-thirds of the distribution) of the projections has remained relatively stable since the publication of the IPCC Fifth Assessment Report (Church et al., 2013) despite major advancements in the models and methods used in AR6 (Slangen et al., 2023).

The latest IPCC likely range projections of GMSL yield values at 2100 of 0.32–0.62 m (low GHG emissions, SSP1-2.6) and 0.63–1.01 m (very high GHG emissions, SSP5-8.5), relative to the 1995–2014 average (Fig. 1). Furthermore, GMSLR approaching 2 m by 2100 and 5 m by 2150 cannot be ruled out for a very high GHG emissions scenario, due to deep uncertainty in ice sheet processes. On longer timescales, GMSLR will continue for centuries to millennia due to continued deep-ocean warming and ice sheet melt, as these elements of the Earth system slowly adjust to the anthropogenic warming. Over the next 2000 years AR6 assessed that GMSLR will reach about 2–3 m if surface warming is limited to 1.5 °C relative to pre-industrial values. This rise increases to about 2–6 m with a peak warming of 2 °C and about 19–22 m with a peak warming of 5 °C.

At regional scales, it is virtually certain (99 %–100 % probability) that mean RSLR will continue throughout the 21st century, except in a few regions with large vertical land uplift rates. By 2100 it is projected that ESL events that occurred once per century in the recent past will occur at least annually at more than half of all tide gauge locations around the world due to local mean SLR (Fox-Kemper et al., 2021). SLR will increase the frequency and severity of coastal flooding in low-lying areas and coastal erosion along most sandy coasts. The combination of more frequent ESLs and increased extreme rainfall and river flow events associated with an intensified hydrological cycle will make flooding more probable in coastal cities and settlements by the sea (IPCC, 2021a).

Despite the inevitability of SLR in the coming centuries, the science also shows the benefit of reduced GHG emissions in terms of avoiding the worst future risks and buying more time to adapt to the changes. By the end of the 21st century, scenarios with very low and low GHG emissions would strongly limit the rate of increase in the frequency of ESL events relative to higher GHG emissions scenarios. Excluding uncertain ice sheet processes, the assessed ranges of projected GMSLR at 2300 under a low GHG emissions are substantially lower (0.6–1.0 m in SROCC; 0.3–2.9 m in AR6) than for the very high GHG emissions scenario (2.2–5.3 m in SROCC; 1.7–6.8 m in AR6), implying that strong mitigation is needed to prevent large SLR in 2300.

2.2 The European perspective

Most coastal regions in Europe are currently experiencing a local SLR of a few millimetres per year, but there are large spatial variations across the continent. A key driver of these spatial variations is GIA: the ongoing GRD response to past ice mass changes. The spatial pattern of this land motion is characterized by vertical land uplift in areas covered by ice sheets during the last glacial period and land subsidence in other areas (Sect. 3.3). As a result, much of the northern Scandinavian coastline is currently experiencing a local SL fall, since the long-term rate of land uplift following the last deglaciation exceeds the global-warming-driven contemporary SLR.

Projected local SLR for Europe is broadly in line with projections of GMSL rise in most places (Sect. 5.1). GIA will continue to be an important driver of spatial variations across the continent, with additional spatial differences also arising from the effect of Greenland ice sheet mass loss on Earth's gravity field and also by local oceanographic processes (Fox-Kemper et al., 2021). There may also be highly localized VLM processes active either now or in the future, such as subsidence associated with groundwater and hydrocarbon extraction or tectonic activity (Sect. 3.3). Risk-based decision-making should account for these additional non-climatic processes when assessing potential magnitudes or rates of future SLR.

The scientific consensus is that changes in future coastal flood hazard will be dominated by SLR, rather than changes in the drivers of ESLs such as waves, tides, and surges (e.g.

Fox-Kemper et al., 2021; Howard et al., 2019; Vousdoukas et al., 2018; see van de Wal et al., 2024, in this report for more details). However, systematic changes in these drivers could exacerbate local SLR, and internal variability is expected to play a large role in shaping the evolution of wave and storm surge extremes on decadal timescales (Sects. 3.4 and 5.3). In addition, there is a growing body of scientific evidence that suggests SLR could have substantive effects on local tidal characteristics (Haigh et al., 2020). Combined 21st century projections of SLR, tides, surges, and waves for European coasts found the largest absolute increases in ESLs in the North Sea, followed by the Baltic Sea and Atlantic coasts of the UK and Ireland (Vousdoukas et al., 2017), but in the Mediterranean the relative increase is larger, implying a more urgent need to improve adaptation strategies. Changes in waves and storm surges were found to exacerbate SLR for most coasts with contributions of up to 40 % of the change in ESLs. However, the response of waves and surges under climate change remains a key uncertainty (e.g. Howard et al., 2019). IPCC AR6 concluded that "relative SLR is extremely likely to continue around Europe (except in the northern Baltic Sea), contributing to increased coastal flooding in low-lying areas and shoreline retreat along most sandy coasts (high confidence)" (Ranasinghe et al., 2021).

Box 1: Common practices and available sea level tools and data portals

As the impact of SL change is a local issue, it is important to communicate SL projections in a form that can be used by local decision makers. In this Box, we will provide a non-exhaustive overview of online visualization tools and data portals that provide information on past and projected SL change.

The IPCC AR5 Chap. 13 (Church et al., 2013) made the SL projections available online, through the Integrated Climate Data Centre from the University of Hamburg (Table 1), but this was not actively communicated or referred to in the report, and the online tool was more science-focused than public-oriented. The focus on accessible regional information has increased in the recent IPCC AR6 report, which produced an interactive atlas (https://interactive-atlas.ipcc.ch/, last access: 2 July 2024, Table 1), showing observations and projections of a wide range of climate variables for all IPCC working group 1 reference regions (Gutiérrez et al., 2021). For SL change, this atlas includes the SL projections for the different future climate scenarios. However, the atlas only shows SLR for three time periods for large regions. Therefore, in collaboration with NASA, the IPCC Chap. 9 authors built an additional tool which specifically focuses on SL projections (Table 1). This tool allows the user to select and visualize the projected changes for different time periods (by decade), scenarios, and contributions. It also provides projections at specific tide gauge locations using an interactive map. In addition, all the IPCC AR6 SL projections (global and gridded 1 by 1° regional) can be downloaded by the user from the NASA website and from a Zenodo archive (Table 1).

There are also several other online interactive SL tools. For instance, the INSeaPTION project (an ERA4CS European research consortium) has made a tool which includes IPCC AR5 and SROCC projections but also allows for investigating different scenarios using sliders and high- and low-end scenarios (Table 1). The UK Met Office has made a "sea level dashboard", where global mean projections (total and individual contributions) are connected to observations (Table 1). Focusing on local or national changes, there are also various online tools available. For instance, the Norwegian Mapping Authority has developed a tool that provides users with information on observed and forecasted water levels, predicted tides, extreme still water levels, VLM, and past and future SL for Norway (Table 1). Users can find information on vertical datums (various tidal datums and Norway's national height system NN2000) which are relevant for planning decisions and on SL impacts (more in van de Wal et al., 2024, in this report, Sect. 5).

Several online data portals provide information on past and projected SL changes. The Permanent Service for Mean Sea Level (PSMSL), for instance, provides an overview of tide gauge measurements around the world (Table 1). Regarding coastal ESLs, return levels and simulated time series since 1979 from a global hydrodynamic model forced with atmospheric pressure, wind and tides are available in the Climate Data Store of the Copernicus Climate Change Service (C3S), which also hosts various other SL observation and projection-related datasets (Table 1). The Joint Research Centre hosts a number of datasets as part of the Large Scale Integrated Sea Level and Coastal Assessment Tool, including historical and projected ESLs along the European coasts. A global database of daily maxima storm surges obtained with a data-driven model (Tadesse and Wahl, 2021) is also available at tide gauge sites using five different atmospheric reanalyses as forcing fields (Table 1). The European Marine Observation and Data Network (EMODnet) also provides via its unified Portal, open and free access to integrated and harmonized data from tide gauges (including EuroGOOS platforms), together with specific data products for SLR, including SL trends (relative and geocentric) and relative SL anomalies. Such societally relevant data layers are also made publicly available via the European Atlas of the Seas, a European Commission Communication tool to support public awareness and ocean literacy.

European Copernicus Services also provide SL data, with a free and open access policy (Melet et al., 2021). Altimeter SL products are operationally produced and distributed by the Copernicus Marine Service and by the Copernicus Climate Change Service (C3S) (Legeais et al., 2021), and used to produce Ocean Monitoring Indicators (https://marine.copernicus.eu/access-data/ocean-monitoring-indicators?f%5B0%5D=omi_family:438, last access: 2 July 2024), such as observed mean SLR for the global ocean and regional European seas, as well as regional SL trends. In addition, the Copernicus Marine Service provides tide gauge data and ocean and wave forecasts and reanalyses (Irazoqui Apecechea et al., 2023).

Table 1. Overview of publicly available data portals and online visualization tools of SL data. Please note that this is a non-exhaustive overview, providing entry points to data, with a focus on the IPCC and European-based organizations.

Data source or organization	Access link (last access: 2 July 2024)	Contents
IPCC AR5 WG1 Chap. 13 (Church et al., 2013)	https://www.cen.uni-hamburg.de/en/icdc/data/ocean/ar5-slr.html	IPCC AR5 SL projections viewer and data portal (global)
IPCC AR6 WG1 report	https://interactive-atlas.ipcc.ch	IPCC AR6 climate observations and projections viewer and data portal (global)
IPCC AR6 WG1 Chap. 9 (Fox-Kemper et al., 2021)	https://sealevel.nasa.gov/ipcc-ar6-sea-level-projection-tool	IPCC AR6 SL projections viewer and data portal (global)
PSMSL	https://psmsl.org/	SL observations (tide gauges) data portal (global)
INSeaPTION	http://www.inseaption.eu/index.php/news/23-web-map-of-sea-level-projections	SL projections viewer (global)
UK Met Office	https://climate.metoffice.cloud/sea_level.html	SL observations viewer (global)
Global storm surge reconstruction database (Tadesse and Wahl, 2021)	http://gssr.info/	Observed daily maxima storm surges (global)
Copernicus Climate Data Store	https://cds.climate.copernicus.eu/#!/home	Various datasets on observed and projected sea levels and extreme sea levels (Europe)
Copernicus Marine	https://marine.copernicus.eu/	Satellite altimetry, tide gauge records, ocean and wave reanalyses, ocean and wave forecasts (including for sea level); visualization tool (global and Europe)
EMODnet	https://emodnet.ec.europa.eu/en	SL observations data portal (Europe)
European Atlas of the Seas	https://emodnet.ec.europa.eu/en/eu_atlas_of_the_seas	SL observations data portal (Europe)
Norwegian Mapping Authority	https://www.kartverket.no/en/at-sea/se-havniva/se-havniva-i-kart	Observed and projected sea level change viewer (Norway)
Joint Research Centre	Joint Research Centre Data Catalogue – Large Scale Integrated Sea-level and Coastal Assessment Tool – European Commission (https://data.jrc.ec.europa.eu/collection/liscoast)	Modelled historical and projected extreme sea levels
SONEL	Système d'Observation du Niveau des Eaux Littorales (SONEL, https://www.sonel.org/?lang=en)	Observed sea level trends from tide gauges and VLM trends derived from GNSS at tide gauge sites.

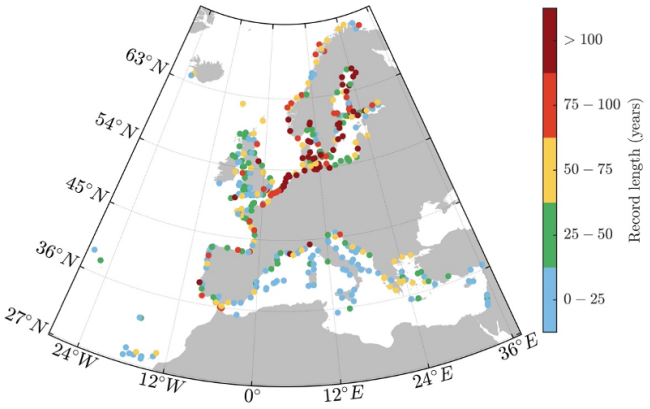

Figure 2. Location of tide gauges in Europe from the PSMSL database with the length of records in years.

3 Regional observations: past mean trends and extreme value intensification

3.1 Tide gauge record

Centennial changes in SL are largely based on tide gauge observations. The European coastlines are home to many of the longest tide gauge records worldwide (Marcos et al., 2021; Raicich, 2020; Woodworth and Blackman, 2004; Wöppelmann et al., 2014; Wöppelmann and Marcos, 2016; Fig. 2). Tide gauges measure SL changes relative to the coastal point where they are installed. This implies that they observe the oceanic component of SL together with VLM driven by a variety of mechanisms (Sect. 3.3). To account for VLM, tide gauge measurements are often complemented with VLM measurements (Global Navigation Satellite System, GNSS) to separate the ocean-related and solid Earth processes from SL records (Wöppelmann and Marcos, 2016).

Tide gauges are installed and operated by national and subnational agencies and also by research institutions, each of which provide access to SL records with a variety of formats, sampling frequencies and quality checks. User access is facilitated by original data providers or data assembly centres and initiatives, including those in the framework of the Global Sea Level Observing System (GLOSS), the Copernicus Marine Service or EMODnet Physics, among others (Table 1). Monthly and annual mean SL records from tide gauges are obtained by national providers and compiled and distributed by the Permanent Service for Mean Sea Level (http://www.psmsl.org, last access: 2 July 2024) (Holgate et al., 2013). A total of 595 tide gauge records are available along the European coasts on the PSMSL website, of which 55 span a period longer than 100 years (Fig. 2). In addition to homogenized tide gauge datasets, the database contains other historical records that provide valuable information on long-term SL changes, such as Amsterdam or Stockholm (see https://psmsl.org/data/longrecords/, last access: 2 July 2024) (Fig. 3a). For studies related to extreme events or storminess, high-frequency SL observations are required. The Global Extreme Sea Level Analysis dataset (http://www.gesla.org, last access: 2 July 2024; Haigh et al., 2022; Woodworth et al., 2016; Caldwell et al., 2001), currently in its version 3, contains a global set of hourly and higher sampling tide gauge observations (Fig. 3b). High-frequency records are needed for ESLs and to capture high-frequency processes contributing to SL changes at the coast such as seiches, meteotsunamis, and infragravity waves (Vilibić and Šepić, 2017).

In Europe, these observations can be obtained from the Copernicus Marine Service (https://marine.copernicus.eu/, last access: 2 July 2024), from EMODnet Physics (https://emodnet.ec.europa.eu/en/physics, last access: 2 July 2024), and from national and subnational agencies (see the GESLA website for more details on data providers). Different data portals may distribute repeated stations, albeit with different metadata, convention names, or ID and distinct levels of processing. An intercomparison of available tide gauge portals is provided by SONEL (https://www.sonel.org/tgcat/, last access: 2 July 2024). As an example of the database contents, there are a total of 1072 tide gauge stations of at least hourly sampling along the European coasts in the GESLA database with a median length of 15 years and of which 48 span a period longer than 100 years, providing essential information (Fig. 2).

3.2 Satellite record

While tide gauges provide point-wise, long-term relative SL (relative to the local land surface to which they are grounded), altimetry measurements provide shorter but spatially coherent and quasi-global measurements of geocentric SL (relative to a reference ellipsoid). Satellite altimetry measures sea level from space with a radar emitter to measure the distance between the satellite and the sea surface and precise positioning instruments to measure the position of the spacecraft. Satellite altimeters allow us to measure the geocentric SL, which is the SL with respect to the centre of mass of the Earth. Since 1993, SL has been monitored routinely on a daily basis with a resolution of $1/4° \times 1/4°$ from 82° S to 82° N (e.g. Legeais et al., 2021). Although SL dynamics are highly heterogeneous, the time and space samplings are enough to effectively resolve the global mean SL dynamics on a weekly basis (Fox-Kemper et al., 2021; Henry et al., 2014; Scharffenberg and Stammer, 2019).

Since 1993, global mean SL has risen by $3.3 \pm 0.3\,\mathrm{mm\,yr^{-1}}$, which represents a total increase in SL of 10 cm (Fig. 5). Over 1993–2018, 46 % of GMSLR is attributed to the ocean thermal expansion, 19 % to melting mountain glaciers, 15 % to land ice mass loss from the Greenland ice sheet, and 9 % from the Antarctic ice sheet (Fox-Kemper et al., 2021). The remaining 11 % is attributed to changes in land water storage such as dam building, groundwater pumping, and aquifer recharge and discharge (Cazenave and Moreira, 2022; WCRP Global Sea Level

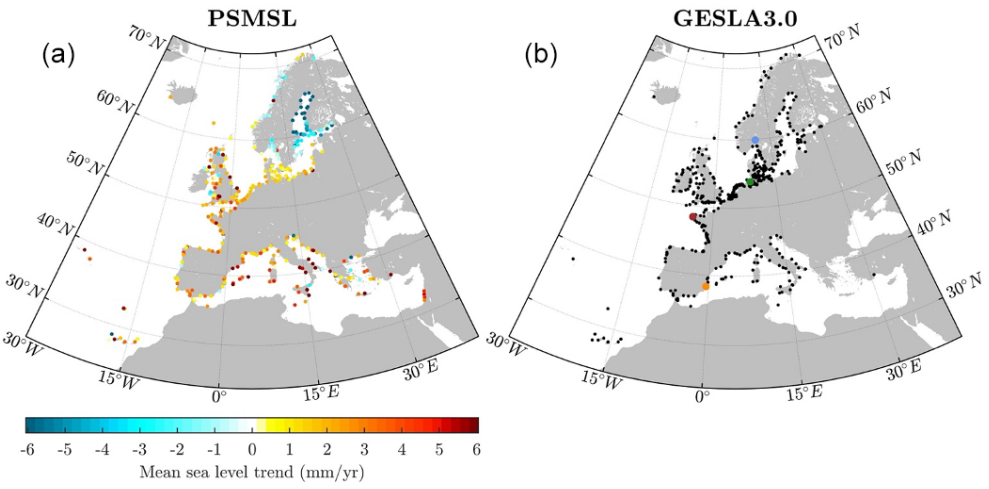

Figure 3. **(a)** Relative SL trends at PSMSL European tide gauges. Note that the tide gauge records are covering different periods (Fig. 2). **(b)** Location of GESLA European tide gauges. Coloured dots indicate the location for which return level curves of storm surges are shown in Fig. 4: blue for Oslo, green for Cuxhaven, purple for Brest, and orange for Alicante.

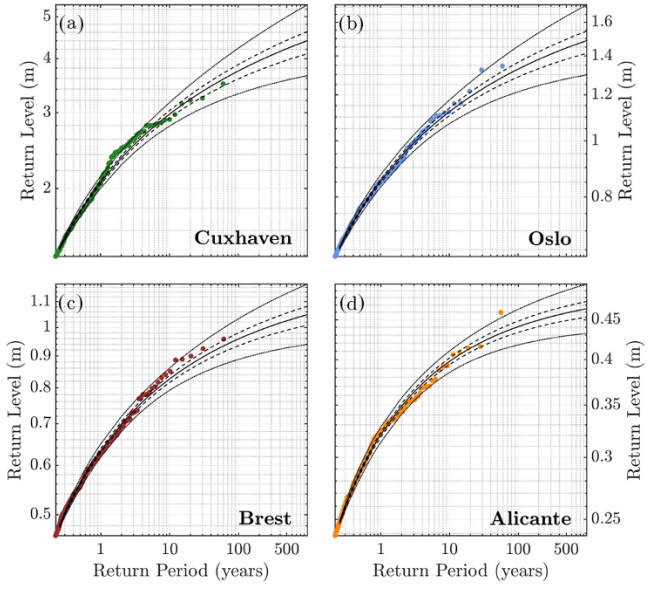

Figure 4. Return level curves of storm surges at four selected GESLA tide gauges from different European basins shown in Fig. 3b. Tide gauge records were de-tided (using Utide MATLAB software; Codiga, 2024), and extremes were selected as peaks over the 95th percentile of each time series, with events separated by at least 3 d to ensure independence. Return levels have then been calculated fitting a generalized Pareto distribution to each record. Uncertainties indicate 30th–70th (dashed lines) and 5th–95th (dotted lines) confidence levels.

Budget Group, 2018). The satellite altimetry SL record also shows an acceleration of $0.11 \pm 0.6\,\mathrm{mm\,yr^{-2}}$ (Guérou et al., 2023). This acceleration since 1993 has mostly been due to an acceleration of ice mass loss from Greenland and to a lesser extent to an acceleration of the contribution from glacier melting and ocean warming (Frederikse et al., 2020b). Studies have shown that present-day GMSLR cannot be explained by internal climate variability and mostly results from anthropogenic forcing (Fasullo and Nerem, 2018; Marcos et al., 2015a, 2017; Richter et al., 2020; Slangen et al., 2016). In Europe, geocentric SL trends since 1993 have been contrasted with high SLR in the Baltic Sea (see Sect. 6.5 and Fig. 7 for RSLR in the Baltic), low SLR in the Mediterranean Sea, and a SLR close to the global mean rate in the Atlantic sector (Fig. 6). Only a few areas, such as central parts of the Mediterranean Sea, show no change or a slight decrease in geocentric SL. On interannual timescales, the global mean SL record shows significant variations, which are mostly generated by El Niño–Southern Oscillation events and its influence on the ocean heat content and global hydrological cycle. During El Niño events, the global mean SL is temporarily increased due to both an increase in ocean mass and in ocean thermal expansion (e.g. Cazenave and Le Cozannet, 2014; Piecuch and Quinn, 2016; Hamlington et al., 2020). Indeed, during El Niño events, more precipitation occurs over the ocean (mostly in the tropics), resulting in a temporary increase in the barystatic component of global mean SL. In addition, the ocean heat content temporarily increases during El Niño, with a dominance of the tropical Pacific Ocean, leading to sizeable increases in global mean steric SL.

To analyse sea level changes at regional scales, gridded altimetric products can be used. Although such products are provided as daily maps on a $1/4° \times 1/4°$ grid, the dynamical content of these maps does not have full $1/4°$ spatial and 1-D temporal resolutions due to the filtering properties of the optimal interpolation. The effective resolution corresponds to the spatiotemporal scales of the features that can be properly resolved in the maps. The temporal effective temporal

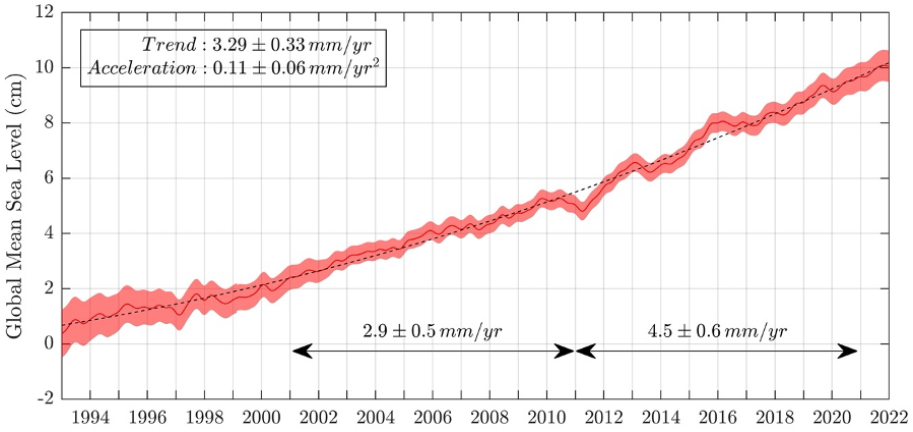

Figure 5. Global mean SL measured by satellite altimetry since 1993 (red curve), shaded area represents the uncertainty and the dotted line shows a trend line with an acceleration. The annual and semi-annual periodic signals are removed and the time series is low-pass filtered (175 d cut-off). The time series is corrected for GIA using the ICE5G-VM2 GIA model (Peltier, 2004) to consider the ongoing movement of land. Over 1993–1998, global mean sea level is corrected for the TOPEX-A instrumental drift, based on comparisons between altimeter and tide gauge measurements (Ablain et al., 2019; Legeais et al., 2020). Over 1993–2022, the GMSLR trend is 3.29 ± 0.33 mm yr^{-1} (uncertainty at 90 % confidence level) and the GMSLR acceleration is 0.11 ± 0.06 mm yr^{-2}. Trends are also reported for the period 2001–2011 and 2011–2021 to highlight the changing decadal trend of global mean sea level. The shaded envelope indicates uncertainties (17th–83rd percentiles). Data source: EU Copernicus Marine Service product (2019b) Ocean Monitoring Indicator based on the C3S altimetric SL product. Credit: C3S/ECMWF/Copernicus Marine.

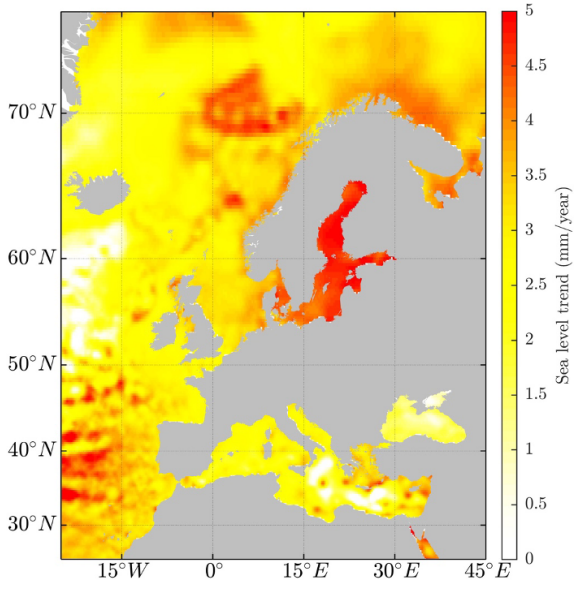

Figure 6. Geocentric SL trends (mm per year) from January 1993 to July 2021. The data have not been adjusted for GIA or for the TOPEX-A instrumental drift. Data source: Copernicus Marine Ocean Monitoring Indicator based on the C3S SL product. Credit: C3S/ECMWF/Copernicus Marine. Geocentric SL does not account for VLM, which is described in Sect. 3.3. The trend of GMSLR observed by altimetry over the same period, with no GIA correction and with the seasonal cycle removed, is 3.20 mm yr^{-1} (Source: AVISO).

resolution has been estimated to around 34 d (spatially varying), and the effective spatial resolution has been estimated to range from 100 to 200 km in the northeastern Atlantic and from 90 to 160 km in the Mediterranean and Black seas (Ballarotta et al., 2019). Satellite altimetry shows that the rate of SL change is spatially highly heterogeneous. The dominant contribution to the regional SL trend patterns is the non-uniform thermal expansion caused by the redistribution of heat within the ocean in response to the wind-forced ocean circulation, and direct exchange of heat between the lower atmosphere and the upper ocean (Forget and Ponte, 2015; Meyssignac et al., 2017). The spatial trend patterns in SL are not stationary, in particular in the North Atlantic, where positive trends shift to negative trends from the first to the second decade of the spatial altimetry SL record and vice versa (e.g. Chafik et al., 2019). This is because spatial trend patterns in SL remain so far mostly driven by the internal climate modes. Several climate modes of variability are influencing sea levels in European seas, such as the North Atlantic Oscillation (NAO) in the Atlantic (see Sect. 6.1), the Arctic Oscillation, and the East Atlantic pattern and the Scandinavian pattern (see Roberts et al., 2016, for an analysis of the climate modes signature on sea level; Boucharel et al., 2023; Wakelin et al., 2003; Jevrejeva et al., 2005; Chafik et al., 2017). Strong differences in SL trends at the sub-basin scale are also recognized in the Mediterranean (Bonaduce et al., 2016; Mohamed et al., 2019; Skliris et al., 2018), in which variability and complexity arise from changes in ocean circulations (Mauri et al., 2019; Meli et al., 2023; Menna et al., 2019, 2021, see Sect. 6.4.1). Near the coast, the altimeter-

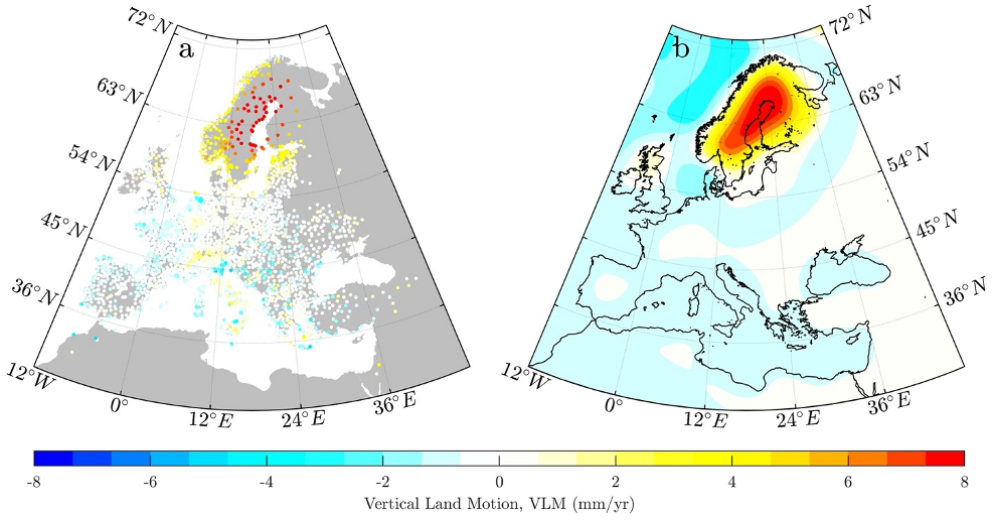

Figure 7. **(a)** Preferred filtered and smoothed present-day VLM field from Piña-Valdés et al. (2022) and based on data from ∼4000 GNSS stations in Europe. **(b)** The present-day VLM from the GIA inversion model from Caron et al. (2018). Values are given in units of millimetres per year.

based SL variations and associated trends are more uncertain than the measurements retrieved in the open ocean (e.g. Birol et al., 2017; Cipollini et al., 2017; Vignudelli et al., 2019). This is due to local factors, such as the distortion of the altimeter radar echo by coastal features, the higher uncertainties of some altimeter corrections (e.g. ocean tides), other local processes that are not captured by satellites (e.g. how far waves wash up the shore), and the spatial resolution of the satellite data. Although more uncertain, recent estimates of the SL at the coast (e.g. Birol et al., 2021) show a general agreement between SLR on European coast and closest SLR in the open ocean in terms of trends and interannual variability, at least when getting as close as a few kilometres from the coast (The Climate Change Initiative Coastal Sea Level Team et al., 2020).

Satellite altimetry has also been used to study the annual, semiannual, and interannual cycles in SL (e.g. Fernández-Montblanc et al., 2020), including in relative SL changes (Ray et al., 2021), which is of relevance for coastal flooding. Along the coasts of Europe, the annual cycle of geocentric SL is characterized by annual maxima during the autumn (except for the Black Sea, where the annual maxima are reached in spring). The annual cycle amplitude ranges from around 5 to 12 cm with the largest amplitude found in the North Sea, Baltic Sea, along the Arctic coast of Norway, and in the western Mediterranean Sea (Fernández-Montblanc et al., 2020; Ray et al., 2021), going up to 20 cm in the German Bight (Dangendorf et al., 2013). Based on altimetric data, it has been shown that the monthly mean SL (including SLR) contribution to ESLs at the coast is mostly larger than that of tides and of the same order of magnitude as that of storm surges in microtidal areas (Black Sea, Baltic and Mediterranean Sea) (Fernández-Montblanc et al., 2020).

3.3 Vertical land motion

VLM is an important component of relative SL change along Europe's coasts as measured by tide gauges. It encompasses all processes leading to a vertical change in the land surface such as GIA due to short- and long-term ice mass loss, tectonics, volcanism, and subsidence owing to groundwater or hydrocarbon withdrawal or sediment compaction. These physical processes operate on different spatial and temporal scales and can be related to climate change, human activities, or natural processes. Several techniques can be used to measure VLM. Historically, repeat levelling has been the main technique. It determines changes in elevation across a network of points and gives a measure of VLM across the levelling network. The repetition of levelling also provides VLM measurements relative to past ones. Repeat levelling has been extensively used in parts of Europe to help constrain VLM, for example, in Scandinavia and the Baltic countries where uplift rates are large (Vestøl et al., 2019). Levelling is also used to measure differences in VLM between global navigation satellite system (GNSS) stations and tide gauges.

Permanent GNSS stations provide a continuous and very accurate (uncertainties smaller than 1 mm yr^{-1}) measure of VLM in the terrestrial reference frame. GNSS thereby gives a high-quality pointwise measurement of VLM but lacks information in areas between stations, where station spacing is typically of several 10s of kilometres. There are several thousand GNSS stations in Europe which are operated in national or regional networks, and are owned by, e.g. national agencies, research institutions, and private companies (Fig. 7a). Efforts to bring together GNSS data and products from across Europe are available from the EUREF (International Association of Geodesy Reference Frame Sub-Commission for Eu-

rope) permanent network (http://www.epncb.oma.be, last access: 2 July 2024), and from the European Plate Observing System (http://www.epos-eu.org, last access: 2 July 2024) research infrastructure. Several analyses have focused on combining European GNSS data (e.g. Kenyeres et al., 2019) with some of those interpolating VLM values for potential use along the coast (e.g. Hammond et al., 2021; Piña-Valdés et al., 2022). For users interested in tide gauges, the International GNSS Service has a programme for analysing GNSS data from stations near or co-located with tide gauges. These data are currently hosted at Système d'Observation du Niveau des Eaux Littorales (http://www.sonel.org, last access: 2 July 2024) (GLOSS data portal for GNSS data at tide gauges). GNSS stations co-located at tide gauges are important for understanding the contribution of VLM to relative SL (Woodworth et al., 2017).

Finally, a more recent technique is interferometric synthetic aperture radar (InSAR), which uses satellite radar to measure VLM with millimetre accuracy. InSAR can image the spatial pattern of VLM and has very good spatial coverage, allowing users to detect local areas of land movement. For example, InSAR has been used in Venice to measure land subsidence (e.g. Teatini et al., 2012). Integrating InSAR and GNSS data can maximize the advantages of both techniques. InSAR data products are newly available from the European Ground Motion Service (https://egms.land.copernicus.eu/, last access: 12 July 2024), which uses Copernicus Sentinel-1 radar images.

The broad pattern of land motion in Europe can be seen from GNSS measurements (Fig. 7). Note that on local scales VLM can deviate significantly from this picture. In European cities like Antwerp, Rotterdam, and Venice, for example, there are complex patterns of localized subsidence (see, e.g. https://egms.land.copernicus.eu/ and Wu et al., 2022). As discussed, subsidence can be natural or human induced. Gas production at the Groningen field, for example, situated in the northeastern Netherlands, has caused measurable subsidence since the 1960s. Understanding the processes causing subsidence and their respective timescales is crucial for sea level studies. This can be particularly challenging in areas where subsidence has multiple causes and requires us to try and disentangle the individual contributions to VLM (Candela and Koster, 2022).

There are several distinct features in the broad VLM field. In northern Europe a dome pattern of uplift due to GIA is clearly visible related to the long-term contribution of unloading since the last ice age. On century timescales we assume this as a constant rate. GNSS observations show a maximum uplift of $\sim 10\,\mathrm{mm\,yr^{-1}}$ in northern Sweden and rates of subsidence exceeding $1\,\mathrm{mm\,yr^{-1}}$ in northern central Europe. Rates of highest uplift correspond to where ice was thickest during the past glacial. Note that GIA also causes gravity and Earth rotation effects on SL, which are around 5 %–10 % of the VLM signal. GIA is the dominant driver of regional VLM in many parts of northern Europe (notably the North Sea, European Arctic, and Baltic basins) (e.g. Kierulf et al., 2021; Milne et al., 2001; Teferle et al., 2009). In those regions VLM can be almost an order of magnitude larger than the climate-driven increase in SL. GIA also largely explains the broad pattern of differences in RSLR in this region.

Land areas adjacent to the Atlantic basin (France and Spain) have generally low rates of VLM. In southern Europe, the GNSS VLM field shows uplift in the Alps. Around the Mediterranean and Black Sea basin there are (volcano)-tectonic deformations in Italy, the Balkans, and Greece, causing a large variability in VLM that is reflected in different relative SL trends.

3.4 Past changes in coastal extreme sea levels

Observations of coastal ESLs rely on high-frequency tide gauge records. In Europe there is a relatively large number of high-quality, long-term tide gauge records with hourly or higher sampling (Haigh et al., 2022, Sect. 3.1, Figs. 2, 3) that have been used to extensively characterize the magnitude and frequency of ESLs as well as their temporal variability (e.g. Marcos and Woodworth, 2017; Fig. 4). Long tide gauge records demonstrate that mean SL change is a major driver of changes in ESLs (Ferrarin et al., 2022; Weisse et al., 2014; Woodworth et al., 2011). However, variability in storm surges unrelated to mean SL has also been identified from observations at interannual and decadal timescales (Dangendorf et al., 2013; Marcos et al., 2015a; Mudersbach et al., 2013; Weisse et al., 2014). In addition, Calafat et al. (2022) determined that long-term trends in storm surges due to a combination of forced changes and internal variability along the European Atlantic coasts have had a contribution comparable to that of mean SLR on changes of ESLs since 1960. Changes in tides have also been evidenced. Although generally small, contemporary past changes in tides were substantial in, e.g. the German Bight (e.g. Haigh et al., 2020). There is also evidence for changes in wave regimes over the past decades notably related to changes in the surface winds in response to climate modes of variability and climate change (e.g. Dodet et al., 2019; for a review, see also Sect. 6 for European seas), but past trends in wind wave characteristics are associated with uncertainties due to the sensitivity of processing techniques, inadequate spatial distribution of observations, and homogeneity issues in available records (Fox-Kemper et al., 2021). Past changes in wind wave regimes imply changes in wave setup and runup (e.g. Melet et al., 2018).

4 Drivers of sea level rise and extremes

4.1 The role of Antarctica and Greenland

Ice loss from the Antarctic and Greenland ice sheets contributes to SLR (e.g. The IMBIE team, 2018, 2020). There is high agreement that for both Antarctica and Greenland, the rates of mass loss and relative contributions to SLR have in-

creased substantially since the 1990s (Otosaka et al., 2023; Fig. 8a). As a consequence, the total mass loss of glaciers and ice sheets has become the dominant term in the SL budget since 2006 (Fox-Kemper et al., 2021). Ice loss reduces the mass of the ice sheets, thereby reducing their gravitational pull, which causes a relative lowering of ambient SL (within ~ 2000 km of ice mass loss) and a relative heightening of far-away SL (further than ~ 7000 km from the ice mass loss). This contemporary GRD effect is sometimes referred to as a SL fingerprint. This means that ice loss in Antarctica raises SL in Europe proportionally more than GMSLR (around 1.25 times the global mean), while ice loss in Greenland raises SL proportionally less than GMSLR over Europe (from around -0.4 to -0.2 times the global mean along the coast of Norway to 0.6–0.8 times the global mean in the eastern Mediterranean Sea and Black Sea, e.g. Tamisiea et al., 2014). Because of higher proximity, the Greenland fingerprint effect is more pronounced in northern European coasts (Bamber and Riva, 2010; Grinsted et al., 2015).

The contribution of the Greenland ice sheet comes from dynamic changes at the margins (Smith et al., 2020), likely caused by changes in the ocean (Holland et al., 2008; Straneo and Heimbach, 2013), as well as a reduction in the surface mass balance due to atmospheric warming (Hanna et al., 2021) which causes increasing surface melt and runoff (Slater et al., 2021), see Fig. 8b. The latter was estimated to account for about 60 % of the mass loss (Van Den Broeke et al., 2016) and both processes are expected to remain relevant over the coming decades (Choi et al., 2021). Projections of mass loss of the Greenland ice sheet until 2100 show a clear greenhouse gas-emission dependency with higher levels of warming leading to higher SL contributions (Goelzer et al., 2020). Uncertainties in atmospheric changes are directly reflected in Greenland projections: higher warming in CMIP6 models in comparison to CMIP5 yield higher mass loss in Greenland due to surface melt (Payne et al., 2021). Ocean-driven processes in Greenland projections are still highly parameterized (Slater et al., 2020). The role of atmospheric dynamics is also uncertain. Increased surface melt was found during atmospheric blocking events (e.g. Fettweis et al., 2013), which are, however, not captured in CMIP5 models (Hanna et al., 2018) and CMIP6 models (Delhasse et al., 2021). As such, van de Wal et al. (2022) added a factor of 2 to the possibility that the current CMIP models underestimate the change in the atmospheric dynamics in their estimate of the high-end contribution to SL change caused by loss of ice in Greenland. Along a similar line of reasoning, Beckmann and Winkelmann (2023) argued for a substantial increase of mass loss in Greenland if extreme warm summers are added to the projections. Other sources of uncertainty in the contribution from Greenland to SLR are related to the sensitivity of regional climate models used for downscaling global climate models results and the calculation of the surface albedo. Finally, there is an uncertainty related to the downscaling of global climate models results with regional climate models. The chain of processes causing mass loss in Greenland is outlined in Fig. 8b.

Antarctica's current mass loss (Rignot et al., 2019; Smith et al., 2020) can be linked to the thinning and enhanced calving of its surrounding ice shelves (Greene et al., 2022; Gudmundsson et al., 2019) driven by warmer ocean water masses; see Fig. 8c. In near-future projections, a further mass loss due to ocean-driven melting is expected to be counteracted by increased surface accumulation (Seroussi et al., 2020). Both processes were found to increase with increasing global forcing, suppressing a scenario dependence of the Antarctic future SL contribution until 2100 (Edwards et al., 2021). The climate forcing of this century will cause SLR over the longer term, and the contrast between lower and higher scenarios will emerge increasingly clearly at longer timescales. Fox-Kemper et al. (2021) assess the Antarctic contribution to global mean SLR in 2300 (without Marine Ice Cliff Instability possible contribution; see Sect. 5.2) to range between -0.14 and $+0.78$ m (17th–83th percentiles) for a low-emission scenario (SSP1-2.6) and between -0.28 and $+3.13$ m for a very high-emission scenario (SSP5-8.5). Critical for the timing of the accelerated mass loss of the Antarctic ice sheet is the timing of the collapse or weakening of ice shelves. As long as the major ice shelves are in place, ice mass loss is limited, but the rate of mass loss can increase strongly if ice shelves lose their buttressing force as enhanced ice discharge will then lead to an acceleration of SLR. For these reasons the Antarctic projections constitute the largest source of uncertainty in SL projections (e.g. Fox-Kemper et al., 2021). The loss of ice shelves is controlled by atmospheric, oceanographic, and glaciological conditions.

Currently, global circulation models that are used to provide the ocean and atmosphere forcing for the ice sheet models in projections do not include the processes on the continental shelf and in ice shelf cavities, which are ultimately determining the changes in sub-shelf melting below the ice shelves and thereby the dynamic mass loss of Antarctica. The sensitivity of melt rates to ocean temperature changes are highly uncertain but explain differences between LARMIP-2 (Levermann et al., 2020) and ISMIP6 projections (Reese et al., 2020; Seroussi et al., 2020). Recent projections with coupled atmosphere–ocean–ice sheet models for Antarctica also show a wide range of results (Park et al., 2023; Siahaan et al., 2022). In the future, ice shelves might also become increasingly vulnerable to atmosphere-driven melting (e.g. van Wessem et al., 2023). It may induce hydrofracturing of the ice shelves. For some shelves, atmospheric process will dominate, while for other shelves oceanographic controlled processes will dominate.

In addition, ice shelf collapse with subsequent self-sustaining ice cliff collapse has been suggested in DeConto and Pollard (2016). This instability is not yet convincingly demonstrated at present, and the importance of this process is debated. A recent paper discussed for example that the presence of ice mélange (a mix of icebergs and sea ice) could

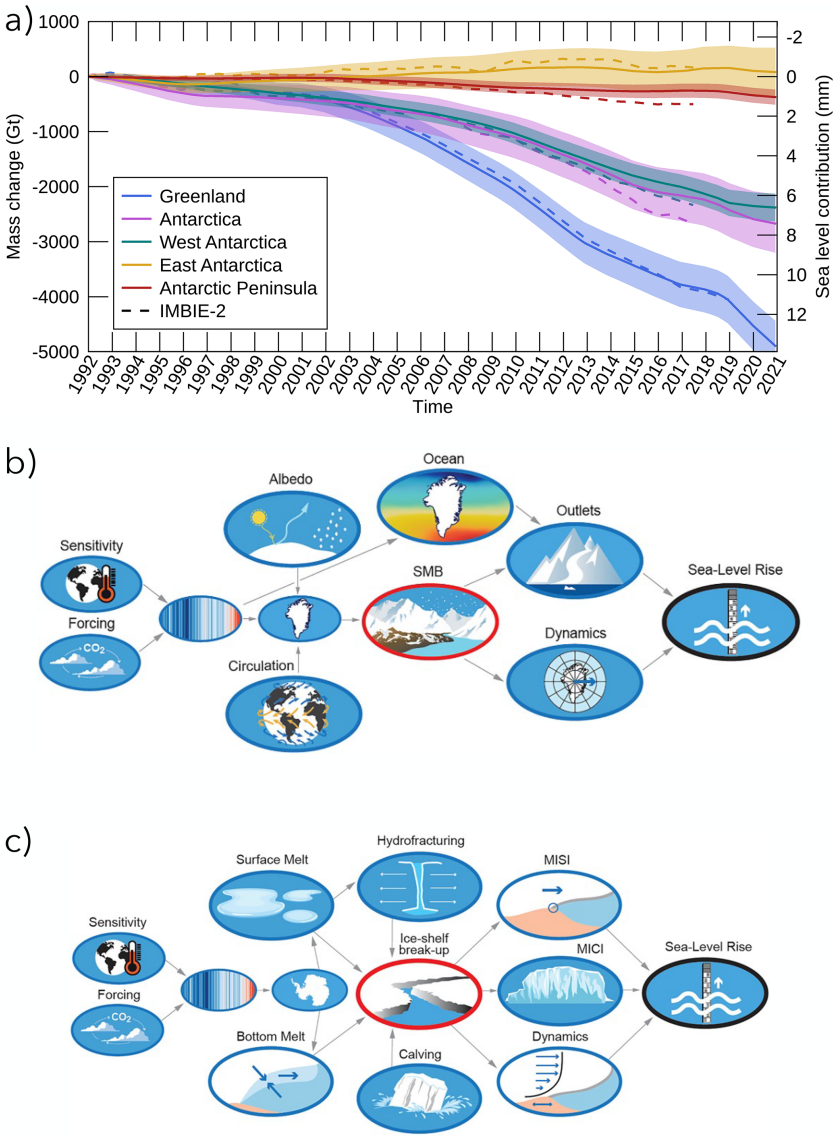

Figure 8. **(a)** Greenland and Antarctic ice sheet mass changes. Credit: reproduced from Fig. 4 of Otosaka et al. (2023). **(b)** Processes that influence Greenland's contribution to SLR and its future uncertainty. Credit: reproduced from Fig. 2 of Van De Wal et al. (2022). **(c)** Processes that influence Antarctica's contribution to SLR and its future uncertainty. Credit: reproduced from Fig. 3 of Van De Wal et al. (2022).

suppress this instability (Bassis et al., 2021; Schlemm et al., 2022). In the recent IPCC, it is treated as "deep uncertainty" (Kopp et al., 2023). The representation of ice shelf calving and damage in the ice constitutes a further uncertainty. Furthermore, uncertainty in processes related to basal sliding may also lead to large rates of ice mass loss (Sun et al., 2020). Hill et al. (2021) report that for the Filchner–Ronne Ice Shelf the range of possible parameters for atmospheric and oceanic changes yield a larger uncertainty than numerical model parameters. An unrealistic upper bound on the ice sheet response due to complete loss of ice shelves is provided by Sun et al. (2020). Problematic in projections for the ice sheets is that the initial state of the ice sheet is poorly constrained (e.g. Aschwanden et al., 2021) and that the Antarctic ice sheet has the potential to cross critical thresholds, which cause irreversible ice loss (see Sect. 5.2) and amplify uncertainty in SL projections (Robel et al., 2019). For this reason, the low-confidence (Fox-Kemper et al., 2021; Kopp et al., 2023) or high-end scenarios (Van De Wal et al., 2022) were developed.

4.2 Sea level budget

On decadal to multi-millennial timescales, global mean SL changes are essentially caused by changes in the Earth energy budget. Since the end of the 19th century, the increase of greenhouse gas concentrations from anthropogenic emis-

sions modified the Earth energy budget such that the amount of outgoing radiation is less than the amount of incoming solar radiation, leading to global warming. Oceans absorbed 90 % of global warming leading to seawater expansion and SLR. A total of 3 % of the excess heat is absorbed by the cryosphere, causing the melting of land ice, such as glaciers and ice sheets, which contributes to SLR. Changes in terrestrial water storage, such as groundwater or water stored in lakes and rivers, also contribute to SLR. Part of the changes in terrestrial water storage are related to the energy budget and the climate variability through the changes in rain patterns that change the amount of water stored in areas such as lakes and rivers. Part of the changes in terrestrial water storage are related to direct anthropogenic activity (such as groundwater depletion and dam building) and thus are independent of the global energy budget.

SL budget analysis over the past century, based on development and application of new statistical methodologies for reconstructing global mean SL (e.g. Dangendorf et al., 2019; Frederikse et al., 2020a) and its contributions (e.g. Bagnell and DeVries, 2020; Frederikse et al., 2020b; Zanna et al., 2019), suggests that the primary factors contributing to GMSLR over 1901–2018 are the mass loss of glaciers (41 ± 15 %), the thermal expansion of seawater due to global warming (38 ± 10 %), and the Greenland ice sheet mass loss (25 ± 8 %). The contribution of Antarctic ice sheets mass loss is relatively small (4 ± 6 %) over this period. The contribution of land water storage is largely uncertain, but it is likely to contribute to a SL fall over 1901–2018 up to -8 ± 20 % (Fox-Kemper et al., 2021). Recent studies show that GMSLR started to accelerate in the 1960s and 1970s, initiated by an acceleration of thermosteric SLR due to an intensification and a basin-scale equatorward shift of Southern Hemispheric westerlies and induced increased ocean heat uptake (Dangendorf et al., 2019). Since the 1990s, accelerated ice mass loss, mostly from the Greenland ice sheet, has also contributed to the GMSLR acceleration (Dangendorf et al., 2019; Frederikse et al., 2020b). Over the period 1971–2018 the SL budget is consistent with the global energy inventory of the climate system, which gives high confidence to the global mean SL budget over this period (Fox-Kemper et al., 2021).

Over a more recent period, since 2006, global mean SL has been monitored by satellite altimetry, thermal expansion of the ocean by Argo floats, and the change in ocean mass by space gravimetry. Consequently, the SL budget is significantly more precise and the closure more accurate. Over 2006–2018, the SL budget is closed with an uncertainty of a few millimetres (Fig. 9). Over 2006–2018, the primary factors contributing to SLR are the thermal expansion of seawater due to global warming (39 %) and the Greenland ice sheet mass loss (17 %). The melting of glaciers represents 17 % of GMSLR over this period, while the Antarctica contribution rose to 10 %. Land water storage changes explain the remaining 17 % (Fox-Kemper et al., 2021, Table 9.5). Percentages

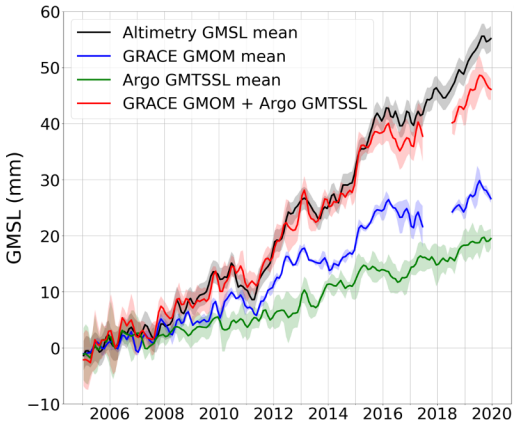

Figure 9. Global mean SL (GMSL) budget from 2006 to 2021. Global mean SL is estimated by satellite altimetry (black curve, data from the Copernicus Marine Environment Monitoring Service). Global mean ocean mass (GMOM) change (sum of ice sheet mass loss, glaciers ice melt, and land water storage changes) is estimated from GRACE and GRACE-FO (blue curve, data taken from the JPL, CSR, and GSFC mascon solutions). Global mean thermosteric sea level (GMTSSL) change is estimated from Argo (green curve, data taken from an ensemble of the NOAA, EN4, SCRIPPS, and JAMSTEC Argo products). From Fig. 2b in Barnoud et al. (2021).

are based on central estimate contributions compared to the central estimate of the sum of contributions.

Since 2018, the global mean SL budget derived from altimeter data has not closed anymore within conventional uncertainty thresholds (Barnoud et al., 2021, Fig. 9). A cause for this non-closure is a drift in the wet tropospheric correction (which is the correction for the path delay in the radar altimeter due to the water vapour content in the atmospheric column) of the Jason-3 altimeter and a drift in Argo salinity sensors. After correction of the spurious Jason-3 drift and after using only thermosteric SLR (and not steric SLR), the non-closure is reduced by 40 % but remains larger than the uncertainty in the components of the SL budget from 2019 on (Barnoud et al., 2023). More research is needed to understand the causes of the residual non-closure of the SL budget over the past few years.

At regional scale, closing the SL budget is more challenging due to the higher variance of the signal, although there have been some attempts to explore the closure from local (Royston et al., 2020) to large basin-wide scales (Purkey et al., 2014). Instead, Camargo et al. (2023) used unsupervised machine learning techniques to identify regions of coherent SL variability. Compared to previous studies, which looked at the regional budget on entire ocean basins, this study identified more and smaller domains. These domains reflect large-scale climate patterns, such as El Niño–Southern Oscillation in the Pacific and NAO in the Atlantic, and highlight which ocean regions are connected through physical processes, such as propagating coastally trapped waves from

Iberia to the northwestern European shelf (Calafat et al., 2012, 2014; Hughes et al., 2019). While in gridded data (for instance a 1×1 rectangular grid) the SL budget cannot be closed everywhere, the budget can be closed in almost all domains identified by self-organizing maps when all contributions, including estimates for deep steric changes, are accounted for and with a residual error of only $0.6\,\mathrm{mm\,yr^{-1}}$ for the period 1993–2016. The regional SL budget has also been closed along coastal regions of coherent variability (Dangendorf et al., 2021), also showing that most of the interannual changes are linked to dynamic SL variability. For example, in the North Sea, observations corrected for VLM display a linear trend of $2.01\,\mathrm{mm\,yr^{-1}}$ (95 % confidence intervals of 1.30–$2.76\,\mathrm{mm\,yr^{-1}}$) over 1960–2012, while the sum of the sterodynamic and barystatic contributions is $2.09\,\mathrm{mm\,yr^{-1}}$ (1.58–$2.52\,\mathrm{mm\,yr^{-1}}$) (Dangendorf et al., 2021). Despite the good agreement in this region, there are uncertainties in VLM that may result in slightly different rates of SL change (e.g. Frederikse et al., 2016, who reported around $1.3\,\mathrm{mm\,yr^{-1}}$ for the same period).

4.3 Drivers of extreme sea levels

Coastal ESLs result from the combined action of mean SL changes, astronomical tides, atmospheric pressure, and surface winds that generate storm surges and wind waves. Higher-frequency processes such as coastal waves, meteotsunamis and seiches (in semi-enclosed basins such as the Adriatic Sea) can also contribute to ESLs at the coast. Thus, ESLs are short-term phenomena (timescale of minutes or hours to a day) triggered by atmospheric perturbations and tides, but they are also modulated by long-term changes in mean SL and by low-frequency variability in storminess (associated with changes in frequency, tracks, and/or severity of weather systems; Woodworth et al., 2019). Return levels for extreme storm surges are shown in Fig. 4 for selected European locations.

Changes in mean SL affect ESLs in several ways: variations in water levels modify the baseline level upon which extremes reach the coastline, and at the same time changes in mean SL interact with other coastal SL contributors like tides, surges, and waves (Idier et al., 2019), for instance through velocity and friction effects over tides and storm surges due to depth changes in coastal shallow waters. Along many European coastlines, astronomical tides are an important component of ESLs and in some regions tide–surge interactions take place, such as in the English Channel (Haigh et al., 2010; Idier et al., 2012), the UK coastline (Horsburgh and Wilson, 2007), and the North Sea (Arns et al., 2020; Wolf, 1981). Changes in mean SL also affect tidal propagation in the same way as storm surges. As these processes take place at subregional spatial scales, further research is needed to explore future changes and the resulting impacts on the coasts (see Sect. 5.3).

Changes in tides (Sect. 3.4) and storminess can also drive changes in ESLs at the coast. Besides storm surges, wind waves are also a driver of coastal hazards, especially when they co-occur with storm surge extremes. Wind waves in the nearshore contribute to coastal ESLs through transfer of momentum due to wave breaking (the so-called wave setup effect) and the wave uprush on a beach or structure (the so-called wave run-up) (Dodet et al., 2019). The magnitude of the wave contribution is locally variable and often difficult to assess from observations, as tide gauges are placed in sheltered areas to avoid instrumental failures. The effect of wind waves on ESLs over broad spatial scales has therefore been assessed mostly using parametric approaches (Melet et al., 2018; Vousdoukas et al., 2017). Coupled hydrodynamic and wind wave models are available, but they need a very high spatial resolution in coastal areas to properly represent wave setup, thus limiting their applicability (Roland et al., 2009).

Despite the relatively good coverage of tide gauges along European coastlines (Sect. 3.1, Figs. 2, 3), their location is sparse and SL records are often incomplete, thus providing only a partial picture of the spatial and temporal footprints of coastal ESLs. One way to overcome the limitation of the observational network is to simulate ESLs using either numerical models or data-driven approaches. Hydrodynamic models, the most common to simulate storm surges, use the shallow water equations to simulate the response of the ocean to atmospheric pressure and surface winds. Ocean general circulation models can also be used for this purpose (e.g. as in Copernicus Marine regional forecasting systems; Irazoqui Apecechea et al., 2023), as they explicitly resolve tides and storm surges, although at higher computational expenses. Model accuracy depends essentially on the available forcing fields and on the model setup, including the spatial resolution of the coastal bathymetry and the coastline. Computational needs and data availability of this type of models are currently one of the main limitations to increase the spatial resolution. For example, available bathymetric data in the German Bight is coarse and inconsistent, and affected by morphodynamic changes at interannual timescales. Hydrodynamic model runs are available at global and European scales spanning several decades, thus allowing us to explore seasonal variability and long-term trends in storm surges (e.g. Fernández-Montblanc et al., 2020; Muis et al., 2020). Alternatively, data-driven approaches rely on establishing a statistical relationship between observed ESLs and a set of predictors from atmospheric and/or oceanic variables. These data-driven approaches can be, in some places, more accurate than hydrodynamic models and require less computational resources (Tadesse et al., 2020). These alternative methods, however, are site dependent and may not be reliable to reproduce an event that is beyond the observational records. Quantitative information on coastal ESLs derived from data-driven approaches or models, in the form of simulated or reconstructed time series, are available online along all European coastlines (see Sects. 3, 5.3, 6).

5 Projections of sea level rise and extremes on global and regional scale

5.1 21st century projections

Projections of future SL change can be computed using global climate model information for the ocean density and dynamics, in combination with dedicated model simulations for the contributions from ice sheets (Sect. 5.1), glaciers, land water storage change, and VLM (Sect. 3.3). The latest IPCC AR6 report provided 21st century SL projections for five different emission scenarios (Fox-Kemper et al., 2021: SSP1-1.9 ("very low"), SSP1-2.6 ("low"), SSP2-4.5 ("intermediate"), SSP3-7.0 ("high") and SSP5-8.5 ("very high"); Fig. 1). These projections include all processes that could be assessed with at least medium confidence, thereby excluding ice sheet processes associated with deep uncertainty as discussed in Sect. 4.1 (see also Sect. 5.2). In addition, low-confidence projections (Fox-Kemper et al., 2021) and high-end projections (Van De Wal et al., 2022) were developed, reflecting the deep uncertainty associated with the contribution of the Antarctic and Greenland ice sheets.

The medium-confidence regional IPCC AR6 projections (Fig. 10) show that some European coasts are projected to experience a RSLR by 2100 below the projected GMSLR, such as the Norwegian coast, the Baltic Sea, the northern part of the UK and Ireland, and the northern coasts in the Mediterranean basin. Other coasts also show projected RSLR above the global mean, for instance the Atlantic coasts of Portugal, Spain, France, Belgium, and the Netherlands. For semi-enclosed basins, the projections can be improved by replacing the ocean density and dynamics component from the IPCC projections by high-resolution regional model results that capture the local dynamics and exchange with the ocean basins in much more detail. More regional information on SLR projections is provided in Sect. 6 per European sea basin.

A new addition to the AR6 report, compared to previous IPCC reports, is the inclusion of SL projections stratified by warming level (Fox-Kemper et al., 2021; their Sect. 9.6.3.4). As SLR is mostly a product of time-integrated warming, rather than instantaneous warming (e.g. Bouttes et al., 2013; Hermans et al., 2021; Kuhlbrodt and Gregory, 2012; Melet and Meyssignac, 2015), it is important to specify the timing of the peak warming. The AR6 projections (Table 2) are based on a global mean surface air temperature increase of 1.5, 2, 3, 4, and 5° by 2081–2100 but do not specify the route to this temperature increase. The differences in the pathways and their effect on the projected SLR are reflected in the uncertainties in the temperature level projections (Table 2).

For decision making around SLR, it may be useful to ask "when" a certain SLR threshold will be crossed (Slangen et al., 2022), as this provides an indication of the time left to prepare adaptive and protective measures for that specific threshold. Figure 11 indicates the first decade in which the median projected regional SL change over European seas has crossed a certain threshold (0.5, 0.75, 1.0 m above the 1995–2014 baseline) under two emissions scenarios. A lower-emission scenario (Fig. 11, left column) typically leads to slower SLR, which in turn leads to a later crossing of thresholds, whereas high-emission scenarios (Fig. 11, right column) have a faster SLR and therefore earlier crossing of thresholds. For thresholds crossed before 2050 there is little dependence on the emission scenario used.

5.2 Tipping points, irreversibility, and commitment

Greenland and the West and East Antarctic ice sheets are considered tipping elements in the climate system (Armstrong McKay et al., 2022; Lenton et al., 2008). In this case, tipping is understood as crossing a critical threshold beyond which ice loss becomes irreversible on human timescales, i.e. the relevant climate forcing (regional oceanic and atmospheric conditions) would need to be reduced substantially below the pre-tipping value to halt or reverse the retreat of the ice sheet.

The tipping behaviour of the Greenland ice sheet is linked to the melt–elevation feedback, where the ice sheet surface lowering brings the ice surface into regions of higher surface air temperatures which causes more melting and thereby further surface lowering (Levermann and Winkelmann, 2016; Weertman, 1961). The Greenland ice sheet was confirmed to exert a tipping behaviour in Robinson et al. (2012); however, in other model simulations, e.g. of a coupled ice and atmosphere general circulation model (Gregory et al., 2020), only the northern part of the ice sheet, corresponding to 2 m of SL equivalent, was found to behave irreversibly. In some cases, examining statistical properties indicate whether the system is close to a tipping point. Boers and Rypdal (2021) suggest that based on surface melt reconstructions the central western Greenland ice sheet is close to a critical transition. Importantly, the timescale of tipping depends on the strength of the forcing scenario. A nearly complete disappearance of the Greenland ice sheet might still take millennia if the threshold is marginally crossed (Robinson et al., 2012), which would imply that rates of SLR are still modest.

A widely accepted mechanism for tipping in Antarctica is the marine ice sheet instability (MISI; Schoof, 2007; Weertman, 1974), where the ice sheet retreats rapidly in marine parts of the ice sheet because of a positive feedback between the seawards ice flux and ice retreat. Since stability conditions for MISI are more complicated than only a retrograde slope for realistic Antarctic conditions (Gudmundsson, 2013; Haseloff and Sergienko, 2018; Pegler, 2018; Sergienko and Wingham, 2022), numerical modelling is required to identify these tipping points. Studies suggest tipping behaviour for the glaciers (e.g. Thwaites and Pine Island) in the Amundsen Sea (Favier et al., 2014; Rosier et al., 2021) and West Antarctica (3 m of SL equivalent; Feldmann and Levermann, 2015). The East Antarctic ice sheet contains marine basins that can

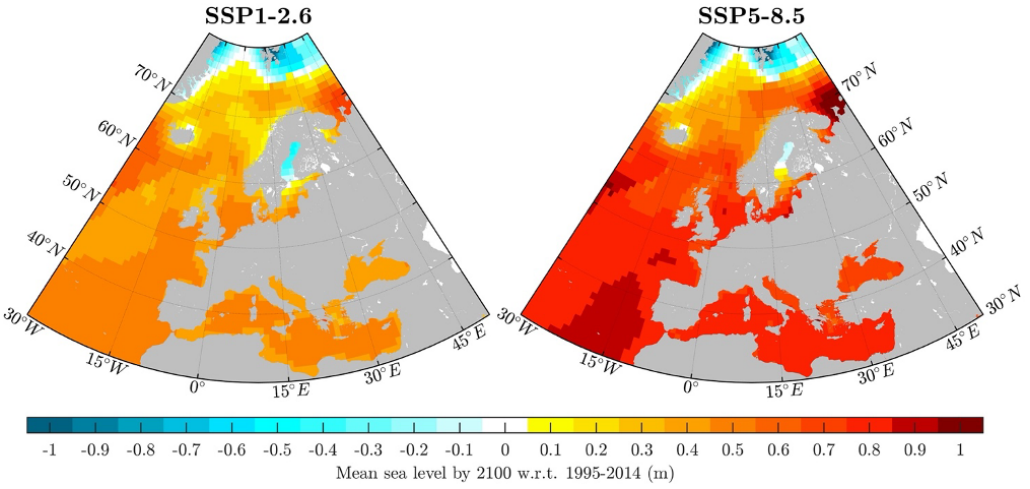

Figure 10. Median relative SL regional projections (medium confidence, i.e. excluding ice sheet processes associated with deep uncertainty) from the IPCC AR6 report around Europe under (left) SSP1-2.6 and (right) SSP5-8.5 in 2100 with respect to 1995–2014 (m) (IPCC AR6 projection data available from https://doi.org/10.5281/zenodo.5914709, Garner et al., 2021).

Table 2. GMSLR projections (m) for exceedance of five global warming levels, defined by sorting global mean surface air temperature in 2081–2100 with respect to 1850–1900. Median values and likely range in 2050 and 2100 relative to a 1995–2014 baseline are given (Fox-Kemper et al., 2021). Data for the temperature pathways are available at https://doi.org/10.5281/zenodo.5914709 (Garner et al., 2021).

GMSLR (m)	1.5°	2.0°	3.0°	4.0°	5.0°
Total (2050)	0.18 (0.16–0.24)	0.20 (0.17–0.26)	0.21 (0.18–0.27)	0.22 (0.19–0.28)	0.25 (0.22–0.31)
Total (2100)	0.44 (0.34–0.59)	0.51 (0.40–0.69)	0.61 (0.50–0.81)	0.70 (0.58–0.92)	0.81 (0.69–1.05)

also show tipping, such as the Wilkes basin (19 m sea level equivalent; Mengel and Levermann, 2014). In addition, the Aurora basin (3.5 m sea level equivalent), which is a large marine-based area, has been suggested to have the potential of tipping. Observations and modelling of continued grounding line retreat in the Amundsen Sea has raised the question whether MISI is already ongoing (Favier et al., 2014; Joughin et al., 2014; Rignot et al., 2014). A recent study by Hill et al. (2023) finds that MISI-driven grounding line retreat is likely not yet underway in Antarctica. However, a collapse of the West Antarctic ice sheet on millennial timescales is possible already under current climate conditions (Reese et al., 2023). This is consistent with Garbe et al. (2020) reporting that retreat of West Antarctic grounding lines could be initiated by around 1–2 °C of global warming above preindustrial levels. Golledge et al. (2021) also find that in a simulation coming from the last interglacial, the West Antarctic ice sheet starts retreating after 1500 years with constant current climate conditions. Oceanic forcing of the Amundsen Sea region is expected to increase, which would push the system faster towards tipping (Naughten et al., 2023). Thus, the general idea is that West Antarctica is unstable for high-forcing scenarios (Oppenheimer et al., 2019), but our insights are not detailed enough to indicate where the threshold is in detail. Importantly, the timescales of tipping also depend on the strength of the forcing scenario, parameter choices, and physical choices made in model set up. Feldmann and Levermann (2015) and Golledge et al. (2019) find that a collapse of the Antarctic ice sheet takes millennia for temperature values close to the threshold, while the unrealistic ice shelf removal in the Antarctic Buttressing Model Intercomparison Project (ABUMIP; Sun et al., 2020) causes the West Antarctic ice sheet to collapse within a few centuries.

An alternative tipping mechanism has been suggested by DeConto and Pollard (2016) based on ice shelf disintegration followed by the collapse of the newly formed vertical ice cliffs is called marine ice cliff instability (MICI), yielding even more rapid rates of mass loss. MICI would be caused by the feedback between ice cliff height and calving. The importance, timescales, and mechanism of this process are debated (e.g. Bassis et al., 2021), and it is for this reason classified as "deep uncertainty" in the latest IPCC report (Fox-Kemper et al., 2021). The importance of both MISI and MICI strongly depends on the extent to which the ice shelves retain their buttressing force to keep the ice sheet in place. Timing of collapse or thinning of the major ice shelves is not foreseen in the 21st century, but DeConto et al. (2021) suggest that increased mass loss due to shelf collapse starts to play a role around 2100 with consequences for enhanced SLR in the early 22nd century.

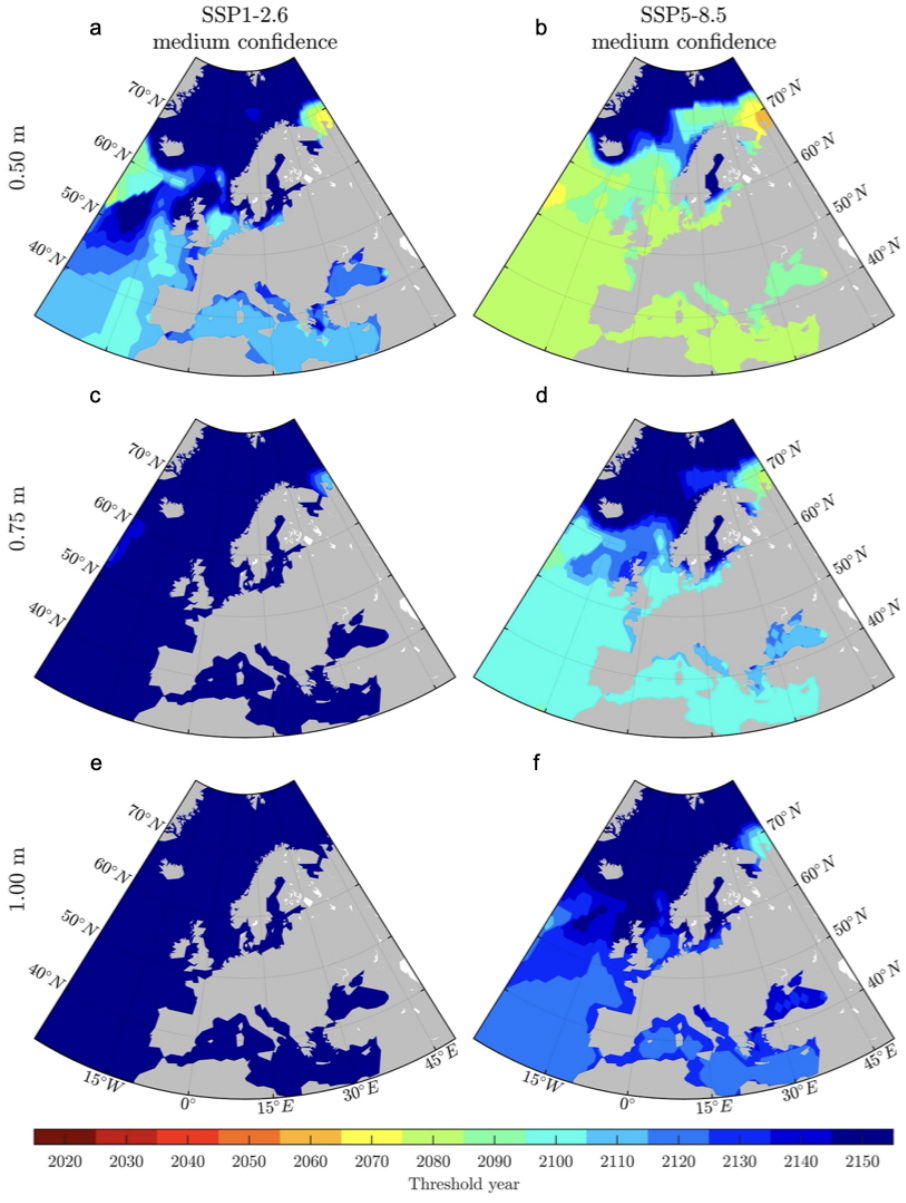

Figure 11. The first year of the decade (between 2020 and 2150) when the median regional SL projections around Europe have crossed a threshold since 1995–2014 of 0.5 m **(a, b)**, 0.75 m **(c, d)**, and 1.0 m **(e, f)** under SSP1-2.6 emissions **(a, c, e)** and SSP5-8.5 **(b, d, f)**. Dark blue indicates no crossing before 2150. Results are based on the medium-confidence IPCC AR6 SL projections (Fox-Kemper et al., 2021; IPCC AR6 projection data available from https://doi.org/10.5281/zenodo.5914709, Garner et al., 2021).

Crossing tipping points would mean an irreversible commitment to SLR unless a rapid temperature decrease is materialized (Bochow et al., 2023). SL commitment is, however, not only due to crossing of tipping points but also because ice sheets respond on long timescales and climate forcing might be hard to reverse. The contribution of the Greenland ice sheet in 2100 that has already been committed through past climate change has been estimated to be around 3.3 cm SLR (Nias et al., 2023). Climate change during this century will commit ice loss over the coming centuries to millennia even without further climate change.

Furthermore, there is a long-term SLR commitment from the ocean, through the key role it plays for uptaking heat from the atmosphere and the consequently induced thermal expansion (e.g. Bouttes et al., 2013). The efficiency of ocean heat uptake (the temporal rate of change of the ocean heat content) depends on how quickly heat gained at the ocean surface is transported to depth. The faster heat is mixed to the deep ocean, the less the surface air temperature warms as more excess heat is taken up by the ocean and the lower the transient climate response (Krasting et al., 2018; Marshall and Zanna, 2014). If emissions of GHG were to stop,

the radiative forcing of GHG that was previously released in the atmosphere would remain quasi-constant with a slow decay over centuries (e.g. Ehlert et al., 2017; Zickfeld et al., 2017). As a result, the global mean surface air temperature would remain quasi-constant. The upper-ocean temperature, which exchanges heat with the atmosphere, tracks the radiative forcing and would thus equilibrate. On the other hand, the deep ocean, which is coupled to the upper ocean through mixing, would continue to warm and to export heat to deeper layers (e.g. Bouttes et al., 2013; Dalan et al., 2005; Ehlert et al., 2017; Melet et al., 2022). Although the ocean heat uptake would decline over time, the large thermal inertia of the deep ocean and the long timescales of its adjustment would result in a net warming of the ocean and related steric SLR that is largely irreversible for at least a millennium after emissions stop (e.g. Zickfeld et al., 2017). Only on very long timescales the deep ocean may release this energy again.

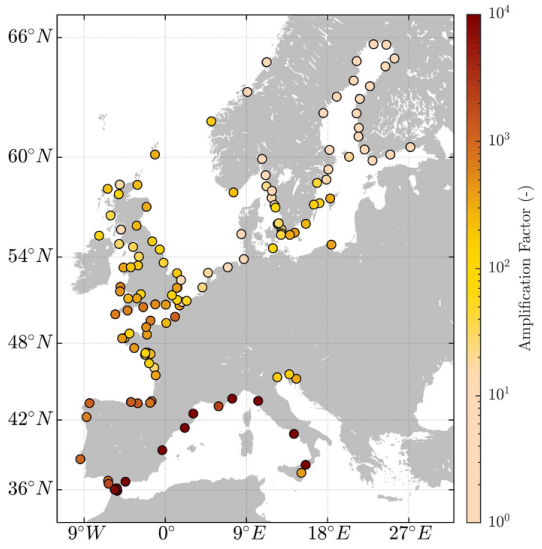

Figure 12. Amplification factors showing the expected change in frequency of the historical centennial SL event in 2100 projected by the IPCC AR6 for Europe under the SSP2-4.5 middle-of-the-road emission scenario (obtained from Fig. 9.32 of Fox-Kemper et al., 2021). Here, an amplification factor of 10 means that the historical centennial SL event will become a decennial event in 2100, while an amplification factor of 100 means that the historical centennial SL event will become an annual event in 2100.

5.3 Projected changes in extremes

Projections of future changes in ESLs generally either only include the effect of an increase in the mean SLR on the baseline height of extremes, assuming that the distribution of ESLs is stationary, or also include non-stationarity in extremes due to changes in storm surges, tides, and/or waves based on numerical modelling (Sect. 4.3).

5.3.1 Projected changes in extremes

Projections of future changes in ESLs due to SLR are often reported through so-called amplification factors, which correspond to the change in the expected frequency of a given contemporary ESL height under climate change scenarios (Buchanan et al., 2016; Fox-Kemper et al., 2021; Frederikse et al., 2020b; Hermans et al., 2023; Jevrejeva et al., 2023; Lambert et al., 2020; Oppenheimer et al., 2019; Rasmussen et al., 2018; Tebaldi et al., 2021; Wahl et al., 2017) or as the height by which coastal defences need to be raised to restore the historical flood probability (called allowances; Hunter, 2012; Hunter et al., 2013; Slangen et al., 2017; Woodworth et al., 2021). For instance, the IPCC AR6 (Fox-Kemper et al., 2021) projected that the SL associated with the historical centennial event, which is the event that historically had a 1 % chance of occurring each year (once per century on average), will be exceeded at least annually (i.e. corresponding to an amplification factor of 100) at 19 %–31 % of 634 tide gauges worldwide in 2050 and at 60 %–82 % in 2100. In Europe, the largest amplification factors of the frequency of ESLs are projected for the south (Mediterranean and Iberian Peninsula coasts), whereas in the northeast of the United Kingdom and in the southeastern North Sea, amplifications are generally smaller because the current variability of ESLs is larger (Fig. 12). Amplifications of the historical centennial event are below 1, implying a decreasing probability of the historical centennial event in the northern Baltic Sea because of the land uplift anticipated for that region associated with GIA (Sects. 3.3 and 6.5). The spatial pattern in Fig. 12 is a robust feature across different studies (e.g. Fox-Kemper et al., 2021; Frederikse et al., 2020b; Oppenheimer et al., 2019).

Projected amplification factors in most of the studies mentioned above are derived by combining inferences of the historical ESL distribution with projected relative SLR, incorporating the uncertainty in both and assuming that the historical extremes distribution remains the same (so-called static or mean SL offset method). Projections of amplification factors are therefore sensitive to the type of extreme value distribution used and to the threshold above which events are defined as extreme (Buchanan et al., 2016; Wahl et al., 2017). A generalized Pareto distribution with the 99th percentile as a threshold was identified to be the preferred approach to assess ESLs at a global scale (Wahl et al., 2017). Acknowledging that the same threshold is not appropriate at all locations, two recent studies implemented an automatic threshold selection (Hermans et al., 2023; Lambert et al., 2020), which substantially affected their results in specific locations. To characterize the events below the threshold, different approximations have been used such as a Gumbel distribution between mean higher high water and the extremes threshold (Buchanan et al., 2016; Fox-Kemper et al., 2021; Rasmussen et al., 2018) or a simple extrapolation (Hermans et al., 2023; Sweet et al., 2022). Rasmussen et al. (2022) applied an extreme value mixture model instead, but the extent to which declustering the data below the threshold is appropriate is

unclear. Furthermore, since wave-sheltered tide gauge measurements are typically used to infer the extreme SL distributions, the effect of waves is not (fully) incorporated in the type of projections in this Section. Incorporating waves generally increases the historical range of extremes at a given location, which leads to smaller projected amplification factors (Lambert et al., 2020).

Most studies have projected the amplification of the historical centennial event. However, information on changes in the probability of a single extreme SL can be of limited salience locally (Rasmussen et al., 2022). For instance, the design height of local protective infrastructure may differ from the height of the historical centennial event, and large amplifications of the historical centennial event do not necessarily affect a large fraction of the local population (Rasmussen et al., 2022). Projections of the population affected by changes in extremes (e.g. Haasnoot et al., 2021; Kirezci et al., 2020, 2023; Rasmussen et al., 2022) or projections of the amplification factors of specifically those ESLs that local coastal protection is designed to withstand (Hermans et al., 2023), help to add context to projections of amplification factors that facilitates translating hazards into impacts (Rasmussen et al., 2022; van de Wal et al., 2024, in this report). Policy-relevant information may also be provided by projecting when certain critical increases in the probability of ESLs may be reached instead of how much that probability will increase in 2100 (Rasmussen et al., 2022), akin to the timing of mean SLR milestones (Cooley et al., 2022; Fox-Kemper et al., 2021; Haasnoot et al., 2019; Slangen et al., 2022). Recent projections of the timing of amplification factors due to SLR indicate that the probability of ESLs that coastal flood defences are designed to withstand will increase substantially within the time it may take to implement large adaptation measures in Europe as well (Hermans et al., 2023).

5.3.2 Projections of dynamic changes in extremes

To account for changes in the distribution of extremes, numerical models can be used to simulate changes in storm surges, tides, and waves due to changes in atmospheric conditions and water depth (e.g. Fig. 13). Barotropic hydrodynamic models (Sect. 4.3) have been used to simulate storm surges, tides, and their future changes, either only as a function of atmospheric changes simulated by regional or global climate models (Palmer et al., 2018; Vousdoukas et al., 2017, 2018; Jevrejeva et al., 2023) or also due to projected mean SLR, imposed in the model as a change in water depth (Muis et al., 2020, 2023). High-resolution baroclinic ocean models, which can simulate both changes in mean SLR and in storm surges, tides and their non-linear interactions, can provide more consistent simulations of dynamic changes in extremes. As these models are computationally more expensive than hydrodynamic models, they are often limited to a specific region (e.g. Northern Atlantic and North Sea in Chaigneau et al., 2022; Chinese Seas in Kim et al., 2021; and Jin et al., 2021). As explained in Sect. 4.3, wave contributions to ESLs and their projections can be evaluated using parameterizations based on numerical wave models outputs (Dodet et al., 2019; Kirezci et al., 2020; Lambert et al., 2020; Melet et al., 2018), but these parameterizations are limited as they are restricted to specific coastal environments, rely on the specification of a local beach slope, and are calibrated with relatively sparse historical field data (Lambert et al., 2020, 2021; Melet et al., 2020).

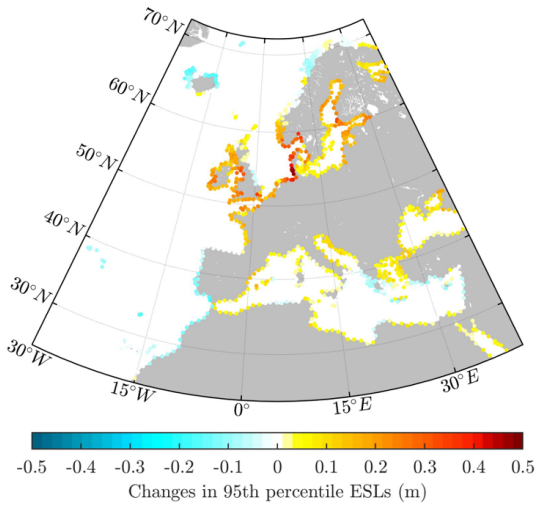

Figure 13. Projected changes in the height of ESLs associated with storm surges and waves only under a worst-case scenario (95th percentile of the centennial event, corresponding to a return period of 0.01 yr^{-1}) by 2100 relative to 1980–2014 along the European coastline (adapted from Fig. 3 of Jevrejeva et al., 2023, using data from Vousdoukas et al., 2018).

Using the models described above, substantial dynamic changes in each contribution to ESLs have been projected for the European coasts, especially under the SSP5-8.5 scenario. The results are presented here for the SSP5-8.5 scenario, since this is the scenario that shows the largest projected changes and that has been the focus in most dynamic approaches in the past years. Forcing a hydrodynamic model with atmospheric simulations from high-resolution climate models (Haarsma et al., 2016), Muis et al. (2023) projected a decrease in storm surges of up to 15 % in southern Europe by mid-21st century. Around the UK, Palmer et al. (2018) and Howard et al. (2019) concluded no projected changes in storm surges due to the spread of the global climate forcing models. For the same region a strong decrease of around −10 % in mean and extreme wave heights and periods (Aarnes et al., 2017; Lobeto et al., 2021b; Mentaschi et al., 2017; Meucci et al., 2020; Morim et al., 2018, 2021), resulting in a decrease in wave setup and runup (Melet et al., 2020), is also expected by the end of the century. In the southern North Sea, Jevrejeva et al. (2023) showed an increase of +50 cm in extreme storm surges and waves under a low-probability high-impact scenario (Fig. 13), in line with early

attempts to account for dynamic changes in storm surges (Woth, 2005; Woth et al., 2006). In addition, non-linear interactions between SL, surges, waves, and tides, for instance through changes in water depth, can impact ESLs and their future changes in Europe (Idier et al., 2019). For example, tidal ranges may change by several tens of centimetres in Europe depending on the spatial variability of SLR, considered SL drivers, and the inclusion of flooding of low-lying topography (Haigh et al., 2020; Idier et al., 2017; Pickering et al., 2017). Extreme significant wave heights are projected to be significantly larger (up to +40 %) at the end of the century under the SSP5-8.5 scenario due to the consideration of mean SLR and tides (Arns et al., 2017; Chaigneau et al., 2023) with implications on wave setup and runup and thus on projections of ESLs. In addition, recent studies have shown, on a global scale and more specifically for Europe, that historical trends in storm surges (Calafat et al., 2022; Reinert et al., 2021; Roustan et al., 2022; Tadesse et al., 2022) and tides (Pineau-Guillou et al., 2021; Jänicke et al., 2021) have been comparable in magnitude to the historical mean SLR trend.

The historical and projected dynamic changes in extremes and their non-linear interactions in Europe suggest that studies using a static approach may miss an important aspect of changes in ESLs (e.g. Boumis et al., 2023). However, recent studies using dynamic approaches concluded that generally mean SLR is the dominating driver of the projected changes in ESLs (Howard et al., 2019; Jevrejeva et al., 2023; Muis et al., 2020; Vousdoukas et al., 2018). For instance, Jevrejeva et al. (2023) concluded that projected changes associated with storm surges and waves contribute less than 10 % to the total increase in ESLs by 2100 in Europe and elsewhere. Nevertheless, these studies typically do not include projected changes in all the coastal SL components (tides, storm surges, waves) nor their non-linear interactions and may therefore underestimate the importance of dynamic changes in extremes. Moreover, most studies projecting dynamic changes in extremes are based on small ensembles of model simulations, often for a single emissions scenario, due to the high computational cost of high-resolution hydrodynamic or 3D ocean and wave models and the limited availability of appropriate forcing data (Jevrejeva et al., 2023; Muis et al., 2020, 2023; Vousdoukas et al., 2017, 2018). The projections may therefore not be robust due to structural differences between the different driving climate models and internal climate variability, as also suggested by Calafat et al. (2022). Furthermore, the driving global climate models often have a relatively low atmospheric resolution, so they cannot resolve historical and future cyclones very well.

In summary, while several studies have concluded that mean SLR is the dominant driver of changes in ESLs at most locations, including in Europe, further research is required to better quantify dynamic changes in extremes.

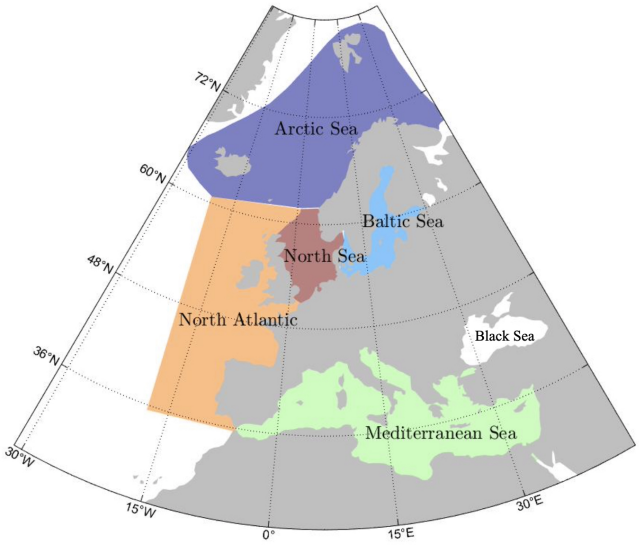

Figure 14. European regional seas domains used in this section, Table 3 and Figs. 15 to 19.

6 Key developments per region

In this section, we provide a regional focus per European regional sea: northeastern Atlantic, North Sea, European Arctic Ocean, Baltic Sea, and Mediterranean and Black seas (Fig. 14). Key developments per region are provided, with first the general context for each regional sea, then past mean and extreme sea level changes, and finally future mean and extreme sea level changes. As key processes can differ across European regional seas, specific discussions are provided in each section.

Rates of RSLR over the recent past (1950–2014) and end of the 21st century under different climate change scenarios are provided in Table 3 for each European regional sea.

In addition, Figs. 15 to 19 provide, for each regional sea, basin-averaged relative SL (with GIA and GRD effects being included) over 1900–2014, basin-averaged projected multi-model ensemble mean relative SL until 2100, linear trends of vertical land motion, and 50-year return levels of extreme still water levels representative of the recent past. For that purpose, different datasets were used in addition to IPCC AR6 projections.

For SL changes over 1900–2014, the global reconstruction of mean sea level changes by Dangendorf et al. (2019) is used. This dataset uses long-tide gauge records, altimetric observations, SL fields from climate models and spatial fingerprints of land-based ice melting (including GIA) to generate a hybrid monthly mean SL reconstruction that accounts for both observed trends and variability on a global $1° \times 1°$ grid. Relative SL with and without the effect of GIA are provided in Dangendorf et al. (2019) and are used to provide RSLR for the European Arctic and Baltic Sea in Table 3, as these regional seas are largely impacted by GIA. In Figs. 15–

Table 3. Rates of RSLR (in mm yr^{-1}) per European regional seas for 1950–2014 (based on Dangendorf et al., 2019), and 2080–2100 under the SSP1-2.6 low-emission, high-mitigation scenario; SSP2-4.5 middle-of-the-road scenario; and SSP5-8.5 very high-emission, low-mitigation scenario from IPCC AR6. Corresponding time series are shown in Fig. 15a for the northeastern Atlantic Ocean, Fig. 16a for the North Sea, Fig. 17a for the European Arctic, Fig. 18a for the Mediterranean Sea and Black Sea, and Fig. 19a for the Baltic Sea. Note that for the European Arctic and the Baltic Sea, rates are also presented over 1950–2014 without GIA contribution (i.e. GIA corrected), as provided by Dangendorf et al. (2019). Reported uncertainties for the 1950–2014 rates correspond to the standard error of the time series only. For 2080–2100, the rate of the median RSLR is reported, together with the trends of the RSLR 17th–83th percentiles in brackets.

mm yr^{-1}	Reconstruction (1950–2014)	SSP1-2.6 (2080–2100)	SSP2-4.5 (2080–2100)	SSP5-8.5 (2080–2100)
Arctic	1.5 ± 0.1	1.6 [−0.7–4.5]	3.4 [1.1–6.8]	5.9 [2.7–10.9]
Arctic (no GIA)	1.4 ± 0.1			
Baltic	-1.1 ± 0.4	0.6 [−1.5–3.2]	4.5 [3.1–7.1]	9.2 [5.0–14.7]
Baltic (no GIA)	1.8 ± 0.4			
Mediterranean	1.2 ± 0.1	4.3 [1.8–7.2]	6.8 [4.4–10.4]	12.6 [9.7–17.2]
NE Atlantic	1.2 ± 0.1	4.4 [1.9–7.3]	7.3 [5.1–10.7]	12.3 [9.5–17.1]
North Sea	1.5 ± 0.1	3.7 [1.6–6.3]	6.7 [5.2–9.5]	11.8 [8.7–16.5]

19, reconstructed relative SL with the effect of GIA (and GRD from contemporary mass loss of land-based ice) are shown. In addition, the vertical reference of the reconstructed relative SL time series has been adjusted to match projected mean sea level records, as it is arbitrary.

Regarding trends of VLM in Figs. 15 to 19, the dataset provided by Oelsmann et al. (2024) is used. This dataset is based on point-wise observations (time series from 11 000 GNSS and from differences between altimetry and 713 tide gauges). Time series were first adjusted or corrected for offsets and outliers. Following this, VLM was reconstructed over 1995–2020 using Bayesian principal component analysis and was finally spatially interpolated along the world's coastlines.

The 50-year return levels of extreme still water levels (still water levels represent coastal sea level including relative mean sea level, tides and surges, as observed by tide gauges) representative of the recent past are provided by different datasets, depending on regional seas. In the northeastern Atlantic, a high-resolution, 3D ocean model including tides and surges is used (IBI-CCS; Chaigneau et al., 2022). In the North Sea and Baltic Sea, the barotropic Global Tide and Surge Model (GTSM) dataset is used (Yan et al., 2020). In the European Arctic, estimates provided by the Norwegian Mapping Authority (Table 1) are used. Finally, for the Mediterranean Sea, computed using a 72-year ocean simulation of coupled hydrodynamic and wave model (Toomey et al., 2022b).

6.1 Atlantic Ocean

6.1.1 General context

The northeastern Atlantic Ocean basin bordering western Europe (Portugal, Spain, France, the UK, Ireland, Fig. 14) is characterized by strong bathymetric gradients, with a deep ocean basin and a continental shelf that is narrow along the Iberian Peninsula and that widens northward up to Ireland. This region includes parts of the North Atlantic subtropical and subpolar gyres, separated by the North Atlantic Current. A slope current flows northward along the continental slope separating the deep ocean from the continental shelf (Clark et al., 2022; Huthnance and Gould, 1989). Strong summer upwellings of deeper, colder water occur along the coasts of Portugal (Fiúza, 1983). On the continental shelf, higher-frequency processes have a more leading role on sea level variability (e.g. Woodworth et al., 2019) and can lead to sea level variability of larger amplitude (due to, for example, tides and storm surges). Although spatial scales of ocean mesoscale dynamics are smaller on continental shelves than in the deep ocean (e.g. Chelton et al., 1998; Hallberg, 2013; LaCasce and Groeskamp, 2020), sea level along the northeastern Atlantic European coast northward of 25° N can also be coherent over thousands of kilometres at decadal timescales (e.g. Calafat et al., 2014) related to coastally trapped waves (Hughes et al., 2019). Along-shore wind forcing is a major contributor to such coastal sea level variability (Calafat et al., 2012).

Tides on the northeastern Atlantic continental shelf are amongst the most energetic ones worldwide, with the principal lunar semidiurnal tidal constituent (M2) dominating. The coasts of Portugal, Spain, the Bay of Biscay, Ireland, and the northern UK experience a lower macrotidal regime (3.5 to 5.0 m tidal range). An upper macrotidal regime along the coasts of the English Channel, Brittany, and southern UK reaches from 5.0 to 10 m of amplitude (e.g. Flemming, 2005).

The North Atlantic mid-latitude storm track induces large waves, swells, and storm surges due to surface winds and low atmospheric pressure that directly impact western Europe. Extreme storm surges along the northeastern Atlantic coasts are therefore directly related to the track location and intensity of extra-tropical cyclones. In addition, swells generated by North Atlantic extratropical storms are reaching western

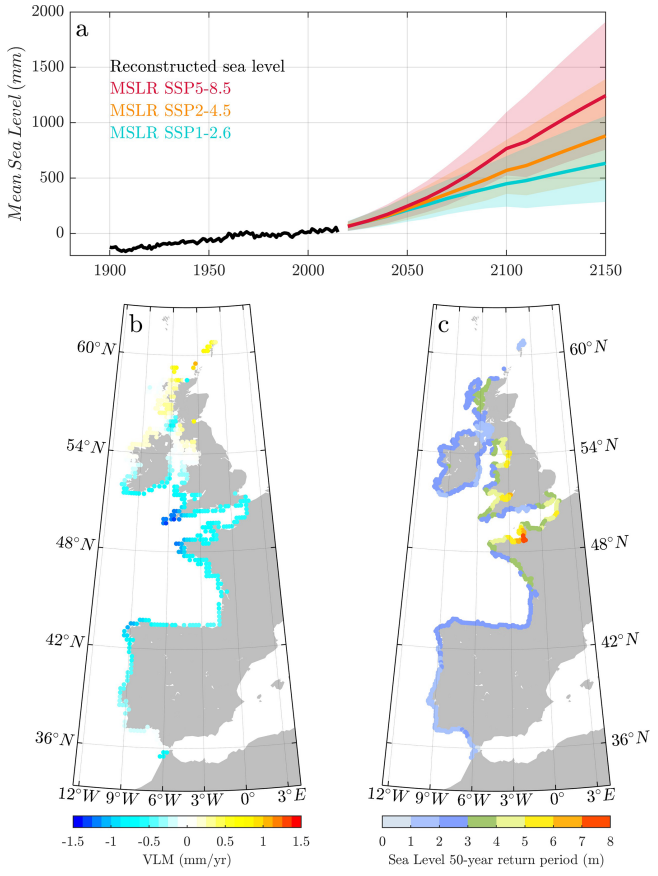

Figure 15. **(a)** Yearly reconstructed basin-average (Fig. 14) mean relative SL over 1900–2014 from Dangendorf et al. (2019) with the effect of GIA and GRD from contemporary mass loss of land-based ice, together with basin-average projected multi-model ensemble mean relative SL until 2100 and relative to 1995–2014 under SSP1-2.6, SSP2-4.5, and SSP5-8.5. Shading indicates the 17th–83rd percentile uncertainties under SSP2-4.5 and SSP5-8.5 obtained from AR6 IPCC. Projections were obtained from AR6 IPCC accounting for VLM (including GIA) effects. **(b)** Linear trends of VLM over 1995–2020 (Oelsmann et al., 2024). **(c)** The 50-year return levels of extreme still water levels that are representative of the recent past computed using a historical regional ocean model forced by a climate model (Chaigneau et al., 2022).

European coasts (e.g. Amores and Marcos, 2020; Bricheno and Wolf, 2018). Under the present climate, the world's highest 50-year return period significant wave heights are found in the northeastern Atlantic (Morim et al., 2023).

VLM in the northeastern Atlantic is rather small, with rates over 1995–2020 ranging from $-1.5\,\mathrm{mm\,yr^{-1}}$ (Brittany in France, Cornwall in the UK) to close to $1.0\,\mathrm{mm\,yr^{-1}}$ (Shetland Islands, UK) (Fig. 15b).

6.1.2 Past sea level changes

SL changes along the coastline of the northeastern Atlantic have been monitored through a rather dense network of tide gauges for decades and up to centuries at specific locations (e.g. at Brest, France, or Newlyn, UK, Fig. 2). Over 1950–2014, the mean RSLR for the northeastern Atlantic was $1.2\,\mathrm{mm\,yr^{-1}}$ (Table 3). Since 1993 and the advent of precise satellite altimetry to monitor SL changes from space, SLR over the coasts of western Europe in the northeastern Atlantic has not largely deviated from the global mean, with most places exhibiting rates ranging between 2 and $4\,\mathrm{mm\,yr^{-1}}$ (Sect. 3.2).

Regional RSLR patterns in this region are mostly explained by ocean dynamics and by GRD effects related to mass loss of the Greenland ice sheet and of mountain glaciers.

The regional pattern of SLR in this region can differ from one decade to another (Sect. 3.2), due to the large influence of the North Atlantic Oscillation (NAO) and other climate modes of variability and teleconnection patterns (e.g. Roberts et al., 2016). The NAO is the most prominent and recurrent pattern of large-scale atmospheric circulation variability over the mid- and high-latitudes of the Northern Hemisphere (e.g. Hurrell et al., 2003). Its strength and phase can be characterized by the difference in surface atmospheric pressure between the Icelandic low-pressure system and the Azores high-pressure system. In addition to its influence on the regional pattern of SL trends, the NAO also influences the year-to-year (or interannual) variability as well as ESLs in the northeastern Atlantic as the variation in pressure patterns influences the strength and location of the jet stream and the path of storms across the North Atlantic. At interannual to decadal timescales, coastal SLs (as recorded by tide gauges) are highly correlated to the NAO (Calafat et al., 2012).

Regarding extremes, storm surges along the coasts of western Europe are related to extra-tropical storms under the storm track and hitting the coasts. The 50-year return period extreme still water levels over the recent past range from 1–2 m for the coast of Portugal to 7–8 m in the macrotidal Mont Saint-Michel Bay (France) (Fig. 15c). During positive NAO phases, the North Atlantic westerlies and storm tracks are shifted northwards. This results in increased (decreased) storminess, storm surges, and precipitation over northern (southern) Europe (e.g. Hurrell and Deser, 2010). The maximum amplitude of surges increases from the coasts of Portugal and Spain to France and the UK in the Atlantic. The 50-year return period level of surges characteristics of the past decades is close to 0.5 m along the coast of Portugal (Cid et al., 2016) and reaches between 1 (e.g. at Brest, France) and 2 m (e.g. at Liverpool, UK) along the Atlantic coasts of northern Europe (Marcos and Woodworth, 2017). The median number of extreme skew surges per year also tends to be larger around the coasts of the UK and in the English Channel than in the Bay of Biscay or the Iberian Peninsula (Marcos and Woodworth, 2017). A skew surge is the difference between the maximum observed SL and the maximum predicted tide regardless of their timing during the tidal cycle – there is one skew surge value per tidal cycle (Pugh and

Woodworth, 2014). The median duration of extreme skew surge events is less than 5 h in most places along the northeastern Atlantic coasts (Marcos and Woodworth, 2017).

In many places, changes in mean SL have been the dominant driver of changes in ESLs since at least 1960 (Sect. 4.3). As such, both mean sea level changes and ESLs are modulated by the NAO in the northeastern Atlantic at interannual timescales. The extreme value distribution of skew surges has been shown to evolve over time along the Atlantic European coasts, even when mean SL changes are discarded (Marcos and Woodworth, 2017). According to a review of storminess over northwestern Europe (Feser et al., 2015), trends in storminess vary with the analysed time period (see also Sect. 5.3). An analysis of tide gauges with at least 25 years of data since 1960 indicates that the amplitude of extreme skew surges tend to have decreased along the northeastern Atlantic coast (Marcos and Woodworth, 2017). In Europe, it has recently been reported that changes in storm surge activity, related to the NAO, have contributed just as much as MSLR to the overall change in ESLs in Europe since 1960 (Calafat et al., 2022). The probability of extreme storm surges since 1960 has been suggested to have increased north of 52° N and decreased south of 52° N (especially so along the coasts of Brittany and the English Channel). This is due to the compounding effect (north of 52° N) or cancelling effect (south of 52° N) of trends in both the storm surge extremes and of regional MSL, which make comparable contributions to the overall change in ESLs in Europe (Calafat et al., 2022).

Along the European Atlantic coast, the timing of the storm surge season is highly correlated with the NAO and the timing of the storm atmospheric events. Extreme storm surges tend to occur earlier in the year in the south (Portugal and Spain) than in the north (English Channel, UK). A consistent spatio-temporal shift in the timing of the storm surge season over the second half of the 20th century has recently been reported (Roustan et al., 2022). The storm surge season has tended to occur earlier along the Atlantic coasts of Europe south of 50° N, at an average pace of around 5 d per decade (e.g. a 25 d shift over 1950–2000).

6.1.3 21st century projections

Projections indicate that 21st century SLR along the coasts of the northeastern Atlantic is expected to be close to GMSLR south of 55° N and lower for northern UK and Ireland (Fig. 10), notably due to VLM (Figs. 7, 15). For instance, under the high-emission, low-mitigation SSP5-8.5 scenario, total mean SL is projected to increase by 0.77 m on global mean, 0.85 m in Cádiz (SP), 0.73 m in Brest (FR), and 0.56 m in Tobermory (UK) in 2100 compared to 1995–2014 (Fox-Kemper et al., 2021; Garner et al., 2021; see also Table 3).

Sterodynamic SLR, which includes global mean thermal expansion of the warming ocean and steric and dynamic SL changes induced by ocean circulations (Gregory et al., 2019), remains the dominant contributor to total SLR along the European Atlantic coast. Regionally downscaled projections of SL changes over parts of the northeastern Atlantic have been produced (Chaigneau et al., 2022; Gomis et al., 2016; Hermans et al., 2022). Hermans et al. (2020) and Chaigneau et al. (2022) have demonstrated the influence of dynamical downscaling on projections of dynamic SL over the 21st century for the northwestern European region. Hermans et al. (2020) have found that projected changes in dynamic SL in the downscaled simulations are up to 15 cm lower than in the GCM simulations for the RCP8.5 scenario. These differences are notably observed in the Celtic Sea, which is poorly resolved in the coarse-resolution GCMs. In Chaigneau et al. (2022), the impact of the regionalization on ocean dynamic SL projections is weaker due to forcings from a higher-resolution GCM, including more spatial details. In the same study, the impact of bias correcting the GCM ocean and atmospheric forcings on the regionally downscaled ocean dynamic SL projections is also highlighted.

The amplitude of the historical centennial climate extreme event (as defined in Sect. 5.3.1) (including storm surges and wave setup) is estimated to range from 1.5 m in the Gulf of Cádiz, increasing northward along the Atlantic European coast to up to 3.0–3.5 m on the western UK coast (Vousdoukas et al., 2017). The 21st century projections indicate a decrease in the overall wave and storm surge contribution to extreme total SL along the Atlantic coast of the Iberian Peninsula and a general increase northward, with values ranging between ±0.3 m by 2100 under a high-emission scenario (Vousdoukas et al., 2017). Along the coast of Portugal and in the Gulf of Cádiz, the projected reduction in surge and wave extremes correspond to an offset of relative SLR by 20 %–30 %.

Future changes in North Atlantic storm positions and intensities will induce changes in mean and extreme wave conditions along the western coasts of Europe. Changes in significant wave height, period, and energy flux in turn contribute to changes in coastal flooding through overflowing or overtopping and in coastal erosion (van de Wal et al., 2024).

Global and regional projections of the wave climate indicate a robust decrease in annual and seasonal mean significant wave height, together with a decrease in the mean wave period over the northeastern Atlantic (e.g. Bricheno and Wolf, 2018; Lobeto et al., 2021a; Morim et al., 2018). This leads to a decreased wave setup contribution to 20-year mean SLR at the coast by the end of the 21st century in this region. Along the Atlantic coast of the Iberian Peninsula, a projected lower wave setup contributes substantially to the regional departure of 20-year mean coastal SL changes from GMSLR (Melet et al., 2020). Changes in wave direction are also relevant for wave impacts at the coast and yet understudied. Indeed, impacts of waves on the coast depend on the wave direction relative to the orientation of the shoreline. For instance, wave setup is largest when wave direction is shore normal. A robust clockwise change in mean wave direction is projected for the Atlantic Iberian coast (e.g. Lobeto et al.,

2022; Morim et al., 2019). Extreme significant wave heights are also consistently projected to decrease over the northeastern Atlantic, with the largest decrease found along the Iberian coasts (Aarnes et al., 2017; Chaigneau et al., 2023; Meucci et al., 2020; Morim et al., 2018, 2021). In an analysis of 14 stations distributed worldwide, Lobeto et al. (2021b) indicate that the stations located along the Atlantic coasts of Europe are the ones exhibiting the strongest projected decrease in wave energy by the end of the 21st century under a high-emission scenario.

Non-linear interactions between the different components of extreme coastal water levels can be substantial in the northeastern Atlantic (e.g. Idier et al., 2019). Tides are sensitive to SLR as increased water depths will alter tidal dynamics (e.g. Haigh et al., 2020; Idier et al., 2017; Sect. 4.3). The English Channel and the Irish Sea are amongst the world regions where tides would change the most substantially in response to SLR (Haigh et al., 2020) and induced shifts in amphidromic points (Idier et al., 2017; Pickering et al., 2017). Changes in M2 amplitude would be spatially heterogenous and might be up to 10 % of the MSLR within the next century (e.g. Palmer et al., 2018; Pickering et al., 2017; Schindelegger et al., 2018).

Wave–SL interactions can lead to a substantial increase in significant wave heights and water levels in macro-tidal areas of the northeastern Atlantic during extreme events (e.g. Calvino et al., 2023; Chaigneau et al., 2023; Staneva et al., 2017). In terms of coastal impacts, accounting for wave–water level interactions can increase the centennial wave setup event by +10 % at some locations and the wave energy flux by up to +40 % in 2100 under a high-emission, low-mitigation scenario (Chaigneau et al., 2023). Sea-state-induced processes also modulate ESLs in the northeastern Atlantic (Bonaduce et al., 2023).

6.2 North Sea

6.2.1 General context

The North Sea is a shallow continental shelf sea bordering France, Belgium, The Netherlands, Denmark, Norway, and the United Kingdom. Due to the prevailing westerly winds over the North Sea, the ocean circulation in the North Sea is predominantly cyclonic (Sündermann and Pohlmann, 2011). The North Sea receives relatively saline and warm water from the North Atlantic Ocean from the south, through the English Channel, and from the north, through the Orkney–Shetland section, the Shetland shelf area, and the Norwegian Trench. In the east it is also connected to the Baltic Sea, from which it receives relatively cool and fresh water. Water exits the North Sea mainly along the Norwegian coast.

Astronomical tides significantly influence the dynamics of the North Sea (Sündermann and Pohlmann, 2011) and contribute to the height of extreme water levels. The semidiurnal tides of the North Sea are driven by co-oscillation with northern Atlantic tides and travel anticlockwise through the North Sea. As the tidal wave propagates from the deep ocean towards the shallower shelf, it is deformed by shallow water and frictional effects, resulting in overtides (having multiple periods of the fundamental constituents) and compound tides (as linear combinations of multiple constituents). The largest tidal ranges are observed along UK east coast (Pugh, 2004), reaching spring tidal ranges of up to 3.60 m at Aberdeen and 6.20 m at Immingham (Horsburgh and Wilson, 2007). Mean tidal ranges amount to 3.40 m in the UK, 1.98 m along the Dutch west coast, 2.33 m along the northern Dutch coast, and 2.82 m along the German coast (Jänicke et al., 2021). The northern and central North Sea are stratified from early summer to early autumn, but the southern North Sea has no thermocline throughout the year due to strong tidal mixing (Sündermann and Pohlmann, 2011). Large non-linear interactions between the tidal and non-tidal components of water level have been recognized and studied for a long time, particularly in the southern North Sea. For example, Doodson (1929) noticed a tendency for surge maxima in the Thames Estuary in the UK to occur most frequently on the rising tide; this phenomenon has been studied in depth by many authors (e.g. Horsburgh and Wilson, 2007; Prandle and Wolf, 1978; Proudman, 1955, 1957; Williams et al., 2016; Wolf, 1981). Large historic changes in tides have been observed in the North Sea (Haigh et al., 2020; Jänicke et al., 2021; Woodworth et al., 1991).

The North Sea has a long history of severe coastal flooding, which accelerated the development in coastal flood risk management such as the 1953 flood that killed more than 2000 people around the coastlines of the southern North Sea (Baxter, 2005; Gerritsen, 2005; McRobie et al., 2005) and the 1962 flood in the German Bight, in which more than 300 people lost their lives (Von Storch and Woth, 2008). Today, settlements along the North Sea coast are much better protected against the impacts of ESLs, relying on ongoing improvements in flood warnings and defences (van den Hurk et al., 2022).

6.2.2 Past sea level changes

Based on tide gauge records, relative SL averaged over the North Sea rose at a rate of $1.4 \pm 0.3\,\mathrm{mm\,yr^{-1}}$ during 1958–2014 (Frederikse et al., 2016). Reconstructed RSLR indicates rates of $1.5 \pm 0.1\,\mathrm{mm\,yr^{-1}}$ over 1950–2014 (Dangendorf et al., 2019, Table 3). Observed trends over the 20th and early parts of the 21st century vary by one to three tenths of a millimetre per year between different parts of the North Sea region (Wahl et al., 2013). Several assessments of sea level trends around the British Isles (e.g. Woodworth et al., 1999, 2009; Haigh et al., 2009; Woodworth et al., 2017; Hogarth et al., 2020, 2021) include tide gauge sites in the North Sea and again observed trends typically range between one to three tenths of a millimetre per year over the last century. The rates over this period match well with the sum of the rates of ob-

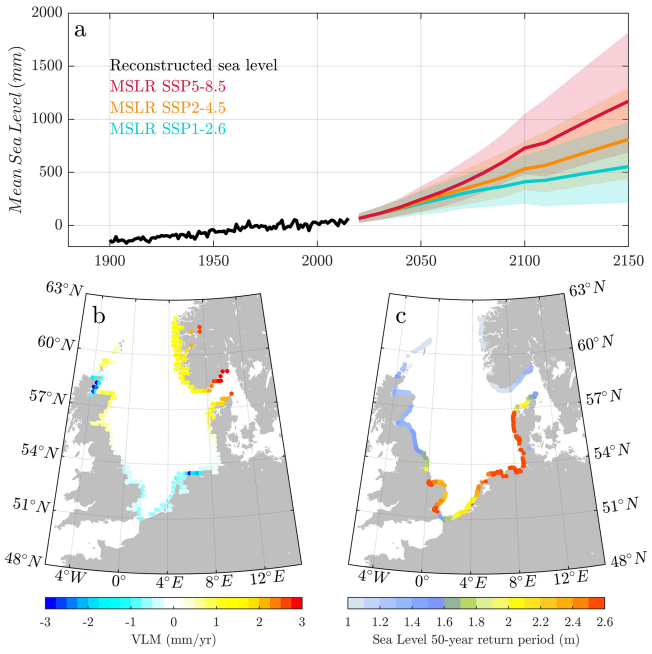

Figure 16. **(a)** Yearly reconstructed basin-average (Fig. 14) mean relative SL over 1900–2014 from Dangendorf et al. (2019) with the effect of GIA and GRD from contemporary mass loss of land-based ice, together with basin-average projected multi-model ensemble mean relative SL until 2100 and relative to 1995–2014 under SSP1-2.6, SSP2-4.5, and SSP5-8.5. Shading indicates the 17th–83rd percentile uncertainties under SSP2-4.5 and SSP5-8.5 obtained from AR6 IPCC. Projections were obtained from AR6 IPCC accounting for VLM (including GIA) effects. **(b)** Linear trends of VLM over 1995–2020 (Oelsmann et al., 2024). **(c)** The 50-year return levels of extreme still water levels representative of the recent past from GTSM dataset (Yan et al., 2020).

served individual components, with the sterodynamic component contributing the most (both to the observed trend and temporal variability) (Dangendorf et al., 2021; Frederikse et al., 2016). The relative SL change measured at tide gauges in the North Sea is also influenced by VLM due to glacial isostatic adjustment, present-day ice mass loss, and other processes such as tectonic activity and naturally or anthropogenically driven subsidence (Fig. 16b). Near regions that were covered by ice sheets during the last glacial maximum, such as Scandinavia and the UK, GIA causes relatively large land uplift contributing to a relative SL fall, whereas further away, in the southeastern North Sea, the land is gradually subsiding due to a collapse of the forebulge, contributing to relative SLR (Frederikse et al., 2016; Peltier et al., 2015). Estimates of the contributions of GIA and other sources of VLM to relative sea level rise rates, however, are relatively uncertain (Wahl et al., 2013). An estimate over 1995–2020 shows VLM rates ranging from $-3\,\mathrm{mm\,yr^{-1}}$ in the northeastern UK to $3\,\mathrm{mm\,yr^{-1}}$ in southern Norway in the Skagerrak Strait (Fig. 16b, Oelsmann et al., 2024).

Based on satellite altimetry, which measures geocentric sea level change, linear SL trends estimated for 1993–2014 vary spatially over the North Sea from 1.3 to $3.9\,\mathrm{mm\,yr^{-1}}$, with the highest rates found in the southeastern North Sea (Sterlini et al., 2017). Averaged over the wider northwestern European Shelf, the SL trend seen by satellites during 1993–2022 was $3.1\,\mathrm{mm\,yr^{-1}}$ (Copernicus Marine Service, Ocean Monitoring Indicator; Box 1). However, interannual to decadal SL variability has a large impact on the estimated SLR trends in the North Sea when evaluated over periods of only a few decades, especially in the southeastern North Sea where the variability is largest (Calafat and Chambers, 2013; Dangendorf et al., 2014; Gerkema and Duran-Matute, 2017; Tinker et al., 2020). Consequently, temporal SL variability is projected to continue to be the dominant source of uncertainty in SL change in the North Sea for the coming decades (Palmer et al., 2018).

Observational and model studies have shown that seasonal (Frederikse and Gerkema, 2018) and interannual to decadal SL variability (Dangendorf et al., 2014; Frederikse et al., 2016; Hermans et al., 2020; Tinker et al., 2020) in the North Sea is primarily caused by the variability in local wind and SL pressure and to a lesser extent also by variability in buoyancy fluxes (Hermans et al., 2020). After removing part of the SL variability driven by local wind and SL pressure variability from tide gauge records, recent studies have found statistically significant accelerations of SLR in the southeastern North Sea (Dutch coast) (Keizer et al., 2023; Steffelbauer et al., 2022). At timescales of years to decades, a spatially coherent SL variability can be found along the eastern boundary of the North Atlantic Ocean, extending from the Canary Islands all the way up to the Norwegian Sea, which is thought to also affect the North Sea (Dangendorf et al., 2014, 2021; Frederikse et al., 2016). This signal is thought to be caused by remote along-shore winds and the subsequent northward propagation of coastally trapped waves (Calafat et al., 2012, 2013; Dangendorf et al., 2014; Frederikse et al., 2016; Hermans et al., 2020; Hughes et al., 2019), but it may also be caused by open-ocean steric anomalies that follow from decadal variability in the strength of the Subpolar North Atlantic Gyre (Chafik et al., 2019).

In terms of extreme still water levels, the 50-year return levels of the recent past range from 1 m (coast of Norway) to less than 3 m in parts of the southern North Sea such as the German Bight (Fig. 16c).

Trends and variability in mean SL influence the baseline height of ESLs (Sect. 5.3). Furthermore, storm surges, waves, and tides, which constitute ESLs in the North Sea, have also been observed to change. For instance, Calafat et al. (2022) concluded that historical trends in the height of storm surges are similar in magnitude to trends in mean SL. They found positive trends in storm surges mainly along the northwestern North Sea coastline (northeastern UK), and negative trends along the southern and southeastern North Sea coasts. The changes along the English North Sea coast were mainly at-

tributed to internal climate variability and partly to forced change associated with the strengthening and eastward extension of the North Atlantic storm track that is also projected for the 21st century (Calafat et al., 2022). Besides changes in storminess, the historically increasing water depth (due to SLR) has been shown to affect storm surges, wave height, and tides non-linearly in the German Bight, with the largest changes found in the Wadden Sea due to spatially variable changes in tidal constituents (Arns et al., 2015).

Changes in water depth and other non-astronomical factors, such as changes in stratification and large construction measures, affect tides along the North Sea coast (e.g. Jänicke et al., 2021; Jensen, 1984; Jensen and Mudersbach, 2007; Mudersbach et al., 2013; Woodworth et al., 2017), including in estuaries (e.g. Amin, 1983; Keller, 1901; Jiang et al., 2020) and harbours (e.g. Doodsen, 1924; Marmer, 1935; Schureman, 1934; Vellinga et al., 2014). However, a comprehensive and generalized analysis is still missing.

6.2.3 21st century projections

Recent SL projections (Fox-Kemper et al., 2021; Palmer et al., 2018; KlimaatScenario's 2023, https://www.knmi.nl/klimaatscenarios23-toolkit, last access: 12 July 2024) suggest that 21st century SLR in the North Sea will be close to or slightly higher than GMSLR at southern North Sea coasts, whereas at the more northern North Sea coasts, projected SLR is lower than the global mean (Sect. 5.1, Table 3). For example, for the emissions scenario SSP5-8.5, the IPCC AR6 projects a SLR of 76–85 cm at the southeastern UK, Belgian, Dutch, and German coasts for 2100, whereas at the northern UK and southern Norwegian coastlines, the projected rise is typically below 70 cm for the same period (Fox-Kemper et al., 2021; Garner et al., 2021). This gradient is predominantly caused by GIA (Sect. 3.3) and the gravitational imprint of the melt of the Greenland ice sheet (Fox-Kemper et al., 2021; Palmer et al., 2018). In contrast, the projected sterodynamic SLR is spatially relatively uniform over the North Sea and slightly higher than elsewhere on the northwestern European continental shelf (Fox-Kemper et al., 2021; Hermans et al., 2022, their Supplementary Fig. 1).

The sterodynamic SLR in the North Sea is typically projected using simulations of global climate models, several of which have a too coarse resolution to capture important bathymetric and topographic features influencing the North Sea circulation such as the Norwegian Trench and the English Channel. Downscaling the simulations of global climate models with a high-resolution regional ocean model can have large effects on the projected ocean dynamic SL change for the North Sea depending on the global climate model (up to 30 % of the total sterodynamic sea-level rise simulated for the 21st century; Hermans et al., 2020), but downscaling has not been applied to large ensembles of global climate models yet. Besides changes in annual mean ocean dynamic SL, CMIP6 global climate models also simulate changes in the amplitude and phase of the seasonal SL cycle (Hermans et al., 2022; Widlansky et al., 2020). The projected changes are largest in the southeastern and eastern parts of the North Sea and may have implications for intertidal ecosystems.

Several studies have projected changes in the frequency of ESLs in the North Sea due to future SLR using the static approach described in Sect. 5.3.1. Compared to other regions, the projected frequency amplification factors of the historical centennial event and other return heights are small in most of the North Sea (see Fig. 12), because the current variability of extremes is large (Fox-Kemper et al., 2021; Frederikse et al., 2020a; Hermans et al., 2023; Oppenheimer et al., 2019). These studies did not consider changes in ESLs due to dynamic changes such as changes in storminess or the effect of an increasing water depth (due to SLR) on surges, tides, and waves.

The impact of changes in water depth induced by SLR on surges, tides, and waves is more important in the North Sea than elsewhere in Europe since the North Sea is a shallow sea, especially near the southern coasts. Haigh et al. (2020) and Idier et al. (2017) both demonstrated a +10 cm and +10 % increase in the semi-diurnal component of the tide along the southeastern North Sea coast, respectively, for a hypothetical increase of +2 m and + 80 cm. Arns et al. (2017) used fine-scale (1 km) numerical modelling in the German Bight to highlight that the long-term SLR would generate waves of greater amplitude (around +48 %–56 % depending on the scenario). Chaigneau et al. (2023) showed with regional climate modelling (6 km resolution) that future mean significant wave heights could become up to +8 % higher in the southern North Sea than at present if SL would rise by 80 cm. These important future changes will also impact the interactions between processes (e.g. tide–surge interactions; Arns et al., 2020; Bonaduce et al., 2020; Staneva et al., 2021) and lead to further changes in ESLs in the North Sea.

The potential contribution of changes in atmospheric storminess to changes in ESLs in the North Sea is uncertain and strongly depends on the (large-scale) atmospheric forcing used to project such changes (Howard et al., 2019; Palmer et al., 2018; Vousdoukas et al., 2016; Woth et al., 2006). For instance, based on a small ensemble of high-resolution regional model simulations forced with downscaled atmospheric changes from CMIP5 models, Palmer et al. (2018) and Howard et al. (2019) find that storm surges around the UK may change by -1 to 1 mm yr^{-1} depending on the model but that the ensemble mean change is close to 0. Under a high-emission scenario, Vousdoukas et al. (2016) project increases in the height of storm surge events with return periods of 5 to 100 years of several percent but report that the disagreement between models is large elsewhere in the region. In conclusion, the amount by which changes in storminess affect ESLs in the North Sea is uncertain, but studies agree that these changes are small compared to the effect of mean SLR itself. In Lobeto et al. (2021a), Chaigneau et al. (2023), and Aarnes et al. (2017), mean and extreme wave character-

istics slightly decrease in the north of the North Sea under the SSP5-8.5 scenario. The amplitude of storm surges does not appear to be significantly modified by mid-century in Muis et al. (2023) under a very high-emission scenario. In contrast, Jevrejeva et al. (2023) showed an increase of +50 cm in extreme storm surges and waves under a low-probability, high-impact scenario in the southern North Sea, in line with early attempts providing future changes in storm surges (Woth, 2005; Woth et al., 2006).

6.3 European Arctic

6.3.1 General context

The European Arctic basin is defined here as the area covering the Nordic Seas, i.e. the Norwegian Sea, Icelandic Sea, and Greenland Sea (Fig. 14). European countries considered in this report and within the European Arctic basin are Iceland and the middle to northern coast of Norway, including Svalbard.

An important component of SL change in the European Arctic is VLM. The broad pattern of VLM in the region can generally be ascribed to past ice mass loss and GIA (e.g. Kierulf et al., 2021; Milne et al., 2001; Vestøl et al., 2019). A regional semi-empirical model of VLM and gravity changes (Vestøl et al., 2019) has been applied in several regional SL studies. Over 1995–2020, rates of VLM were estimated to range between 1 and 6 mm yr^{-1} along the coast of Norway (Oelsmann et al., 2024, Fig. 17b).

There are important contributions to VLM from ongoing ice mass loss on Iceland (Compton et al., 2015) and Svalbard (e.g. Kierulf et al., 2022) driving high rates of local elastic land uplift and variability. GIA on Iceland, where there is a low-viscosity Earth structure that deforms on short timescales, is thought to be dominated by ice mass changes over the past ∼100 years (Auriac et al., 2013). VLM on Iceland is further complicated by significant tectonic and volcanic movements. Recent studies have also shown that ice mass loss in the Arctic and from Greenland produces widespread non-negligible elastic VLM in the European Arctic (e.g. Coulson et al., 2021; Frederikse et al., 2016; Kierulf et al., 2021; Richter et al., 2012). These show that during years of high mass loss from Greenland rates of uplift in Scandinavia reach ∼0.7 mm yr^{-1}.

6.3.2 Past sea level changes

Measuring SL in the European Arctic is challenging due to (1) its remote location and lack of land masses, limiting the number of tide gauges in this region, and (2) hampered measurements from satellites by, e.g. sea ice and limited satellite coverage at high latitudes. In a recent analysis of the Arctic Ocean SL record from altimetry, Rose et al. (2019) found a rate of 3.19 mm yr^{-1} (3.10–3.37 95 % confidence interval) between 1991 and 2018 for the sector covering the European Arctic. Reconstructed RSLR indicate rates of

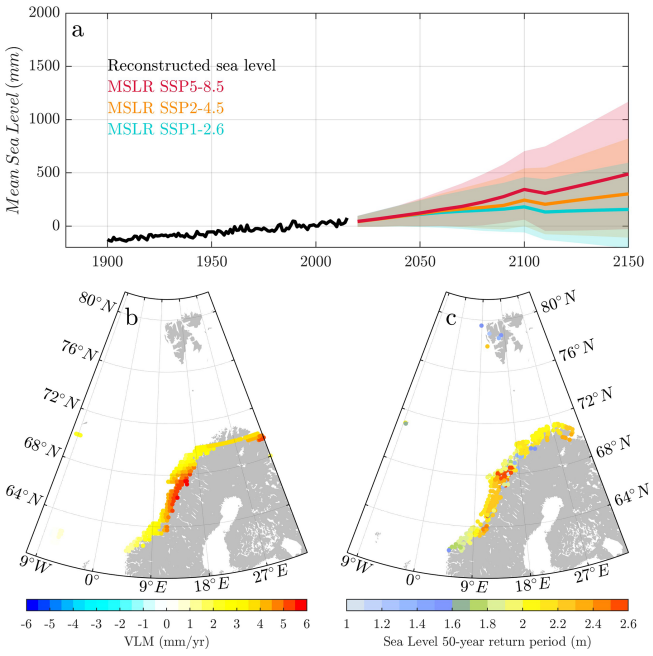

Figure 17. **(a)** Yearly reconstructed basin-average (Fig. 14) mean relative SL over 1900–2014 from Dangendorf et al. (2019) with the effect of GIA and GRD from contemporary mass loss of land-based ice, together with basin-average projected multi-model ensemble mean relative SL until 2100 and relative to 1995–2014 under SSP1-2.6, SSP2-4.5, and SSP5-8.5. Shading indicates the 17th–83rd percentile uncertainties under SSP2-4.5 and SSP5-8.5 obtained from AR6 IPCC. Projections were obtained from AR6 IPCC accounting for VLM (including GIA) effects. **(b)** Linear trends of VLM over 1995–2020 (Oelsmann et al., 2024). **(c)** The 50-year return levels of extreme still water levels representative of the recent past computed using the average conditional exceedance rate method (Skjong et al., 2013; https://www.kartverket.no/til-sjos/se-havniva, last access: 9 June 2023).

1.5 ± 0.1 mm yr^{-1} in the European Arctic over 1950–2014 (or 1.4 ± 0.1 mm yr^{-1} after removal of GIA effects, Dangendorf et al., 2019, Table 3, Fig. 17a).

A number of studies in the region have looked at coastal SL variability and trends with particular focus on Norway (e.g. Breili, 2022; Breili et al., 2017; Frederikse et al., 2016; Henry et al., 2012; Mangini et al., 2022; Richter et al., 2012). Interannual SL variability can be largely explained by atmospheric forcing on wind and the inverse barometer effect. Decadal variability appears to largely reflect steric changes that have been linked to a remote forcing and wind-driven coastally trapped waves that can travel over long distances and reach up to the Arctic (e.g. Calafat et al., 2013; Dangendorf et al., 2014; Frederikse et al., 2016). Studies have shown that the long-term trends and regional SL budgets can be explained by mass, steric, and VLM changes (e.g. Frederikse et al., 2016; Richter et al., 2012).

In terms of extreme still levels, the 50-year return levels of the recent past range from 1 to 2.6 m, with a large spatial variability along the coast of Norway (Fig. 17c).

6.3.3 21st century projections

Projections for the European Arctic indicate the region will experience a SL change somewhat below GMSLR (e.g. Simpson et al., 2017; Table 3, Fig. 17a).

Apart from GIA, several components of projected SL changes are relevant for the European Arctic. (1) Owing to its relatively close proximity to Arctic glaciers and the Greenland ice sheet, GRD effects cause a negative or less than average SLR in the region. Compared to other basins the European Arctic is particularly sensitive to the pattern of ice melt on Greenland (e.g. Mitrovica et al., 2018), inducing a below average regional SLR. (2) At the same time, projections generally indicate that steric dynamic SLR in the Arctic will be larger than the global average. Here the halosteric term is positive and dominates due to ocean freshening (e.g. Pardaens et al., 2011). We note that the large projected steric dynamic SLR in this region also has a large model spread.

As discussed in Sect. 5.3, there is considerable uncertainty attached to projections of changes to storm surges and waves. However, these changes tend to be smaller than the projected mean SL change (e.g. Howard et al., 2019). Projections of future wave climate in the period 2070–2100 generally indicate a lower mean significant wave height in the northeastern Atlantic (e.g. Aarnes et al., 2017). The RCP8.5 scenario yields the strongest reduction in wave height. The exception to this is the northwestern part of the Norwegian Sea and the Barents Sea, where receding ice cover gives longer fetch and higher waves.

6.4 Mediterranean Sea and Black Sea

6.4.1 General context

The Mediterranean Sea is a semi-enclosed basin connected to the Atlantic Ocean, to which it exports around 1 Sv (1 Sverdrup $= 10^6\ m^3\ s^{-1}$) of Mediterranean waters through the narrow Strait of Gibraltar. The mass component is considered the dominant contributor to the mean SL trend in the Mediterranean Sea (Calafat et al., 2010; Pinardi et al., 2014), while the steric component accounts for approximately 20 % of the total variance (Calafat et al., 2012). At the sub-basin scale, however, there are large differences, and the steric component can explain a substantial part of the total SL variance, such as in the Aegean, southern central Mediterranean, and Levantine basin (Mohamed and Skiliris, 2022). The southeastern Mediterranean is affected by warm and salty waters flowing through the Suez Canal from the Red Sea, also altering the steric signal, especially since the early 1990s. Mean SL variability at long timescales (interannual to decadal) averaged over the basin has been shown to be consistent with the nearby Atlantic (Calafat et al., 2012). At the regional scale, however, SL changes within the basin deviate from the mean value, due to ocean circulation, heat redistribution, and atmospheric–ocean momentum fluxes. Storm surges are particularly relevant due to the microtidal nature of the basin and are generated both by incoming atmospheric perturbations from the North Atlantic and by regional cyclogenesis, which occasionally generates tropical-like cyclones in the basin (see Sect. 6.4.7). The Mediterranean Sea is also a hotspot for atmospherically induced high-frequency SL oscillations known as meteorological tsunamis (see Sect. 6.4.8) that affect various locations in the basin.

Coastal VLM is a significant contributor to changes in relative SL in the Mediterranean Sea (Wöppelmann and Marcos, 2012). GIA-related subsidence (Sect. 3.3) is small in comparison to northern European regions and is estimated to be, on average, $0.5\ mm\ yr^{-1}$ over the last millennia, albeit spatially varying (Vacchi et al., 2018). In situ VLM observations from GNSS and from the combination of altimetry and tide gauges used in Oelsmann et al. (2024) are concentrated over the European coast and around the southern Black Sea, with very little information in northern Africa. Linear trends obtained from these observations are mapped in Fig. 18b. The results display regional variability of VLM in the Mediterranean basin with a median value of $-0.4\ mm\ yr^{-1}$ and highlight areas with differential VLM, as is the case of Venice. However, local variability in VLM is much larger, due to active neo-tectonics and volcano-tectonics affecting large part of the Mediterranean coasts.

The Black Sea is an enclosed basin connected to the Mediterranean Sea through the Marmara Sea and the Turkish straits: the Bosphorus and Dardanelles straits. The Mediterranean and Black seas are microtidal basins. The Black Sea receives freshwater from the Danube, Dnieper, and Don rivers especially. The salinity of the Black Sea (~ 18 psu at the surface) is much lower than that of the Mediterranean Sea (~ 38 psu at the surface). In the Black Sea, most of the steric SLR appears to be related to salinity reduction (implying a SLR), rather than to an increase in temperature (Tsimplis et al., 2004).

6.4.2 Past sea level changes

In the Mediterranean and Black seas there is a geographical bias in coastal SL monitoring, with most tide gauge stations located along the northern coasts of the basin and the Black Sea (see Pérez Gómez et al., 2022, for a recent summary of all stations and operators). Although most tide gauges have been deployed since the 1980s, some records date back to the 19th century. This is the case of Marseille and Genoa, which indicate a centennial mean SL trend of $1.3–1.4\ mm\ yr^{-1}$ since the late 19th century. Over 1950–2014, reconstructed RSLR rates were estimated to be $1.2 \pm 0.1\ mm\ yr^{-1}$ on average in the Mediterranean Sea (Table 3, Fig. 18a, Dangendorf et al., 2019). Linear mean SL trends from satellite altimetry since 1993, with a GIA correction applied, display

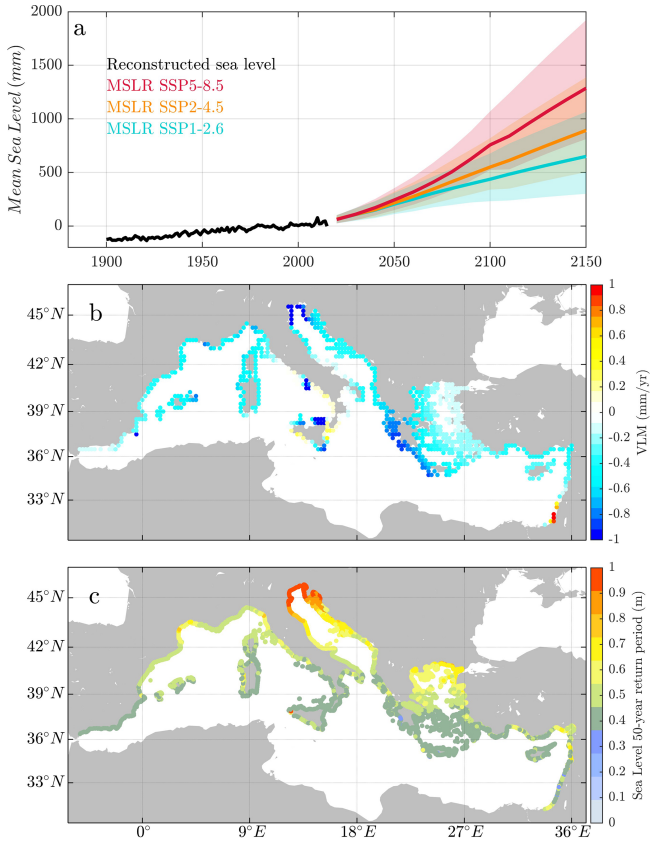

Figure 18. **(a)** Yearly reconstructed basin-average (Fig. 14) mean relative SL over 1900–2014 from Dangendorf et al. (2019) with the effect of GIA and GRD from contemporary mass loss of land-based ice, together with basin-average projected multi-model ensemble mean relative SL until 2100 and relative to 1995–2014 under SSP1-2.6, SSP2-4.5, and SSP5-8.5. Shading indicates the 17th–83rd percentile uncertainties under SSP2-4.5 and SSP5-8.5 obtained from AR6 IPCC. Projections were obtained from AR6 IPCC accounting for VLM (including GIA) effects. **(b)** Linear trends of VLM over 1995–2020 (Oelsmann et al., 2024). Note that North African coasts have not been represented due to lack of data. **(c)** The 50-year return levels of coastal extreme SLs computed using a 72-year ocean simulation of coupled hydrodynamic and wave model (Toomey et al., 2022a).

positive values among most of the Mediterranean and Black Sea basins (Fig. 6) with an average rate of 2.5 mm yr^{-1} over 1993–2022 for the Mediterranean Sea and 1.4 mm yr^{-1} for the Black Sea (EU Copernicus Marine Service, 2019c, a). SL trends as observed by altimetry over 1993–2020 are lower than the global mean (and the European Seas mean) in the eastern Mediterranean Sea and Black Sea (Prandi et al., 2021, Fig. 6). In addition, a slight deceleration of SLR has also been observed in the eastern Mediterranean Sea and more substantially in the Black Sea (Prandi et al., 2021).

The combination of in situ and remote measurements allows reconstructing SL changes over the basin for long periods of time. Temporal variability at multidecadal to interannual timescales is evidenced by tide gauge records (e.g. Marcos and Tsimplis, 2008). At decadal and multi-decadal timescales, the basin-average SL rates range between −5 and +7 mm yr^{-1} and respond, to a large extent, to variations in the nearby northeastern Atlantic Ocean. Part of this variability is coherent along all the European coasts and is driven by along-shore winds propagating northwards along the European continental shelves (Calafat et al., 2012; Hughes et al., 2019). At interannual timescales, nearby records are very coherent. At these timescales, mean SL is largely correlated to large-scale atmospheric circulation patterns, particularly the North Atlantic Oscillation that has been shown to force Mediterranean SL through different mechanisms (Martínez-Asensio et al., 2014; Masina et al., 2022; Volkov and Landerer, 2015). Temporal and spatial variability also results from satellite altimetry data, where non-linearity in SL trend occurs due to oceanographic processes at the sub-basin scale, being also reflected at the basin scale. Main changes in SL trend occur around 1997, 2006, 2010, and 2016, driven by variations in thermohaline circulation and mass redistribution in the Ionian Sea and other sub-basins (Meli et al., 2023). Subannual SL fluctuations in the Aegean Sea, the Mediterranean basin, and the Black Sea are correlated, with the Black Sea lagging behind the Aegean Sea (Volkov and Landerer, 2015). The time lag between the Aegean Sea–Sea of Marmara SL and the Black Sea SL increases from approximately 10 d for monthly averages, to nearly 40 d for 9-months averages. The response of the Black Sea SL is due to barotropic flow anomalies through the Bosphorus Strait, constrained mainly by friction and the strait geometry (Volkov et al., 2016). Black Sea elevation changes are also forced by SL pressure, wind stress along the Bosphorus, and the net freshwater flux into the Black Sea. In their study on the Thrace Peninsula in Türkiye, a vulnerable area to SLR bordered by the Sea of Marmara, Aegean Sea, and Black Sea (Ozsahin et al., 2023) recommend using local mean SL measurements. As highlighted by Kopp et al. (2014), this reflects the need for specific SLR information to generate more accurate projections of SLR.

Coastal ESLs generated by storm surges can be assessed using high-frequency tide gauge records or model hindcasts. Largest values of storm surges are observed at tide gauges located in the northern Adriatic Sea (Marcos et al., 2009) and along the Tunisian and Aegean coasts (Cid et al., 2016). Wind waves, when co-occurring with storm surges, exacerbate the coastal hazard (Lionello et al., 2017). The 50-year return levels of coastal SL extremes obtained with a 72-year run of a hydrodynamic model coupled with wind waves (Toomey et al., 2022b) are mapped in Fig. 18c, showing a consistent picture with observations. Values exceeding 1 m are found in the northern Adriatic and the Gulf of Lions and along the Tunisian and Libyan coasts. Along the rest of the coasts, 50-year return levels are smaller than 50 cm. Besides changes linked to mean SL variations, storm surges also display long-term to interannual variability unrelated to mean

SL and associated with changes in storminess. Decadal variations, such as those observed in the tide gauge records from Trieste (Raicich, 2003) and Marseille (Marcos et al., 2015b), are geographically consistent and related to large-scale atmospheric patterns (Lionello et al., 2021b; Marcos et al., 2015b). The same applies to changes in storm surges at interannual timescales (Masina and Lamberti, 2013).

The wave climate of the Mediterranean Sea is characterized by two well-defined seasons (winter and summer, with spring and autumn having mixed characteristics). In winter, mean and extreme waves are highest in the western Mediterranean, mostly caused by the dominant northwesterly mistral wind. In summer, waves are lower, with a mean wave maximum in the Levantine basin, caused by the Etesian winds and extreme wave maximum in the western basin (Barbariol et al., 2021; Lionello and Sanna, 2005). Along the coastal regions, the largest waves are found in areas with longer fetch distance, such as the Balearic Islands, the west coast of Sardinia, and the northern Algerian coast, with 100-year return levels exceeding 4 m (Toomey et al., 2022b). In contrast, values smaller than 1 m are typical of continental coasts protected by small islands, as on the Dalmatian coast and in parts of the Aegean Sea (Toomey et al., 2022b).

Multidecadal trends from wave gauges have been computed only in the northern Adriatic Sea (Pomaro et al., 2017), while in other locations time series are too short (e.g. Amarouche et al., 2022). Multidecadal trends based on satellite data are still associated with large uncertainties (e.g. Dodet et al., 2020). Therefore, analyses of trends have commonly been based on hindcasts with no overall consensus on trends, possibly associated with the selected period. Trends in the mean wave height are negative or non-significant during the second part of the 20th century (Lionello and Sanna, 2005; Musić and Nicković, 2008; Ratsimandresey et al., 2008), and become positive, particularly in winter, in the western Mediterranean since the 1980s (Amarouche and Akpinar, 2021; Barbariol et al., 2021).

6.4.3 21st century projections

Mean SL projections of the Mediterranean Sea were explored by Sannino et al. (2022) under the RCP8.5 climate scenario, using a high-resolution ocean model capable of resolving the water exchanges through the Strait of Gibraltar. The increase in model resolution together with improved SL information at the Atlantic lateral boundary and the adequate treatment of the complex, hydraulically driven dynamics across the Gibraltar Strait resulted in an improved description of the subregional SL patterns. They concluded that the resulting basin-average mean SL change was within the uncertainties of the multi-model ensemble of global coarser-resolution models from CMIP5 (excluding models without an open connection between the basin and the Atlantic Ocean). This study is in line with Adloff et al. (2018), who pointed at the mean SL in the nearby Atlantic Ocean as a major driver of projected mean SL changes in the Mediterranean. Therefore, projected regional mean SL time series averaged over the Mediterranean Sea are nowadays obtained from multi-model ensemble from CMIP6 (Fig. 18a, Table 3). It is worth mentioning that available climate models have a relatively coarse spatial resolution over the oceans, of around 1 ° in latitude and longitude, that misrepresent water exchanges through the Strait of Gibraltar, which are a major component of SL changes in this semi-enclosed basin. Thus, caution must be taken using the sterodynamic contribution from such models in the Mediterranean Sea. Projected mean SL values reach, under the SSP5-8.5 climate change scenario, 0.79 m (0.64–1.06 m likely ranges 17 %–83 %) by 2100 and 1.22 m (0.91–1.78 m) by 2150 with respect to the period 1995–2014 (Ali et al., 2022). Under SSP2-4.5, projected mean SL by 2100 is 0.57 m (0.44–0.79 m). Few studies assessed projected SL changes in the enclosed Black Sea. According to Görmüs and Ayat (2019), relative SLR for the Black Sea would be within ±20 % of GMSLR.

Projections of storm surges based on hydrodynamic runs forced with climate models show small and mostly negative changes in southern Europe during the 21st century (Conte and Lionello, 2013; Muis et al., 2020; Vousdoukas et al., 2017). Considering the small changes of marine storminess in climate projections, mean SLR will be the dominant driver of increasing coastal ESLs also in the future, but the overall decrease in meteorological surges and storm wave severity is expected in the Adriatic Sea (Benetazzo et al., 2022; Lionello et al., 2021b).

Regarding wind waves, 21st century projections tend to agree that mean significant wave height will decrease as a consequence of anthropogenic climate change (Lionello et al., 2008; Casas-Prat and Sierra, 2013; De Leo et al., 2020).

6.4.4 Medicanes: past and future projections

Medicanes are mesoscale maritime extratropical cyclones developing over the Mediterranean, whose structure resembles tropical cyclones. Analysis of their past trends has not been possible until now, but evidence is for a future decrease in their frequency and an increase of intensity, as a consequence of future sea surface temperature increase (González-Alemán et al., 2019; Koseki et al., 2021; Romero and Emanuel, 2013, 2017). Projected changes in medicane-induced coastal hazards do not exceed 20 % of present-day values in terms of storm surges and wind waves, although there is poor agreement among model projections (Toomey et al., 2022a).

6.4.5 Meteotsunamis: past, present, and future

Meteotsunamis are atmospherically induced high-frequency (< 2 h) oceanic waves generated by travelling atmospheric perturbations (Monserrat et al., 2006). There are different mechanisms by which an atmospheric disturbance can

generate a meteotsunami wave in the open sea, such as Proudman resonance (Proudman, 1929), Greenspan resonance (Greenspan, 1956), front-line passages, and even atmospheric Lamb waves (Villalonga et al., 2023). Analogously to seismically generated tsunamis, meteotsunami waves can travel long distances across the ocean, being amplified when they reach the coastline under specific bathymetric and morphological conditions. The Mediterranean Sea is a hotspot for meteotsunami events. These have been observed at various locations within the basin and sometimes have reached heights of several metres along the coast of Croatia (Orlić, 2015), the Balearic Islands (Rabinovich and Monserrat, 1998; Vilibić et al., 2021), Algeria (Okal, 2021), and the Black Sea (Šepić et al., 2018). In addition, meteotsunamis can also significantly contribute to ESLs generated by other mechanisms (Ruić et al., 2023; Vilibić and Šepić, 2017). For example, recently a meteotsunami has been identified as a contributor to an extreme SL event in Venice (Ferrarin et al., 2023).

Forecasting meteotsunami events is challenging due to the high-computational load required to simulate all high-resolution processes involved. Some examples have recently been implemented in the Balearic Islands (Mourre et al., 2021; Romero et al., 2019). Alternatively, other proxy-based methods use the relationship between observed high-frequency SL oscillations and synoptic atmospheric patterns, which is validated using reported meteotsunami events and atmospheric reanalyses (Vilibić et al., 2018; Zemunik et al., 2022). As it is plausible that the effects of climate change will affect atmospheric circulation and synoptic patterns, it will also imply an effect on the frequency and intensity of meteotsunamis (Vilibić et al., 2018). Therefore, these proxy-based methods have also been applied to explore projected changes in meteotsunamis (Denamiel et al., 2023; Vilibić et al., 2018). An analysis of selected events suggests that the intensity of meteotsunamis could increase under the higher-emission climate scenario (Denamiel et al., 2022).

6.5 Baltic Sea

6.5.1 General context

The semi-enclosed and shallow Baltic Sea (mean depth < 54 m; see Seifert and Kayser, 1995) is located in northern Europe in the highly variable transition zone between the maritime North Atlantic region (warm and wet) and the continental Siberian climates (cold and dry). During winter, about 50 % of the climate variability is explained by the North Atlantic Oscillation (Hurrell, 1995; Weisse et al., 2021; see also Chen and Omstedt, 2005). As the Baltic Sea is connected to the adjacent North Sea only through the narrow and shallow Danish straits, SL oscillations on timescales shorter than 1 month are characterized by oscillations of a quasi-closed system. Pronounced seiches have been observed but all in all, they are energetically insignificant, i.e. are not detectable as a peak in the spectrum (Neumann, 1941; Wubber and Krauss, 1979). Combined with storm surges, seiches can lead to extreme compound events (Weisse et al., 2021). In addition, the amplitude of the diurnal and semi-diurnal tides is small within the Baltic Sea in clear contrast to the North Sea (Maagard and Krauss, 1966).

On timescales longer than 1 month, the mean SL in the Baltic Sea approximately follows the SL in Kattegat, outside the Baltic Sea, but with larger variance at the northernmost and easternmost bays (Samuelsson and Stigebrandt, 1996).

It is expected that SLR in the southern Baltic Sea approximately follows the projected GMSLR (or slightly less) due to the melting of ice sheets and glaciers and the expansion of the warming water (Hieronymus and Kalén, 2020; Meier et al., 2022a; Pellikka et al., 2020; Weisse et al., 2021). However, in the northern sub-basins of the Baltic Sea, GIA (Sect. 3.3) is the dominant driver (Ekman, 1996). Land uplift with a maximum of about 10 mm per year close to the Swedish city Luleå, and slight subsidence along the southern Baltic Sea coasts were found (Vestøl et al., 2019) (Fig. 7). Over 1995–2020, rates of VLM were estimated to range between $0\,\mathrm{mm\,yr^{-1}}$ in the southern Baltic Sea to $10\,\mathrm{mm\,yr^{-1}}$ in the northern Baltic Sea in the Gulf of Bothnia (Oelsmann et al., 2024, Fig. 19b).

Due to the seasonality of the wind fields over the Baltic Sea region, SL in winter is generally highest, especially in mild winters with a high North Atlantic Oscillation index. During periods of strong westerly winds, the Baltic Sea temporarily fills with additional water from the North Sea, also leading to higher storm surges. Storm surges are a threat to low-lying Baltic Sea coastlines (Dieterich et al., 2019; Meier et al., 2004; Wolski et al., 2014).

6.5.2 Past sea level changes

During the 20th century, the global mean SL and thus also the geocentric mean SL in the Baltic Sea rose by about $1–2\,\mathrm{mm\,yr^{-1}}$ (Madsen et al., 2019; Meier et al., 2022b; Oppenheimer et al., 2019; Stramska and Chudziak, 2013; Weisse et al., 2021, Sect. 3.1). In Stockholm, for example, geocentric SL rose by about 20 cm between 1886 and 2009 (Hammarklint, 2009). Over 1950–2014, rates of reconstructed RSLR over the Baltic Sea were estimated at $-1.1 \pm 0.4\,\mathrm{mm\,yr^{-1}}$ when GIA effects are included and $1.8 \pm 0.4\,\mathrm{mm\,yr^{-1}}$ after removal of GIA effects (Table 3, Dangendorf et al., 2019, Fig. 19a). Over the last 2–3 decades, global mean SL rose at rates of $3–4\,\mathrm{mm\,yr^{-1}}$ (Oppenheimer et al., 2019; Weisse et al., 2021; Sect. 2.2; Fig. 6). However, such rates are spatially non-uniform and include impacts of multidecadal variations in wind fields (Passaro et al., 2021). Although the Baltic Sea is warming faster than other coastal seas worldwide (Belkin, 2009), the impact of local thermal expansion is smaller than wind effects (Gräwe et al., 2019). The current acceleration of SLR in the Baltic Sea is small and could only be detected through spatial averaging of ob-

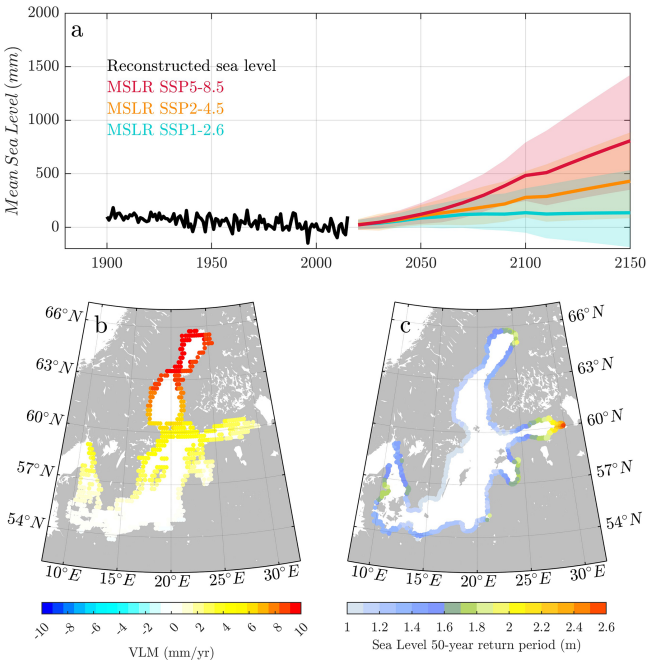

Figure 19. **(a)** Yearly reconstructed basin-average (Fig. 14) mean relative SL over 1900–2014 from Dangendorf et al. (2019) with the effect of GIA and GRD from contemporary mass loss of land-based ice, together with basin-average projected multi-model ensemble mean relative SL until 2100 and relative to 1995–2014 under SSP1-2.6, SSP2-4.5, and SSP5-8.5. Shading indicates the 17th–83rd percentile uncertainties under SSP2-4.5 and SSP5-8.5 obtained from AR6 IPCC. Projections were obtained from AR6 IPCC accounting for VLM (including GIA) effects. **(b)** Linear trends of VLM over 1995–2020 (Oelsmann et al., 2024). **(c)** The 50-year return levels of coastal extreme SLs from the GTSM dataset (Yan et al., 2020).

servations (Hünicke and Zorita, 2016). However, the amplitude of the seasonal cycle significantly increased during the 20th century (Hünicke and Zorita, 2008). The land uplift in the northern Baltic Sea as a result of GIA is still faster than geocentric SLR, so the SL there is currently falling relative to the land (Groh et al., 2017; Hill et al., 2010; Hünicke et al., 2015; Richter et al., 2012; Vestøl et al., 2019; Weisse et al., 2021).

For the 20th century, ESLs in the Baltic Sea probably did not rise more than global mean SL (Donner et al., 2012; Madsen et al., 2019; Meier et al., 2022b; Ribeiro et al., 2014; Wolski et al., 2014). In terms of extreme still levels, the 50-year return levels of the recent past range from 1 m along a large part of the eastern coast of Sweden to 2.6 m in the Gulf of Finland (Fig. 19c).

ESLs in the Baltic Sea are caused by pronounced atmospheric cyclones that sometimes interact with seiches on daily timescales and with volume changes on weekly timescales. As long-term changes in wind fields (frequency, intensity, and position of cyclones) on timescales longer than 100 years have not been detected and changes in other drivers such as tides or non-linear interactions are small, ESLs therefore have not significantly changed relative to the mean SL. This conclusion is supported by a paleoclimate model study for the adjacent North Sea that shows no difference between the impact of warmer and colder climate periods on ESLs (Lang and Mikolajewicz, 2019). Studies that nevertheless report an increase in ESLs such as Ribeiro et al. (2014) might be affected by the influence of the pronounced multidecadal variability of the wind fields (Marcos et al., 2015b; Marcos and Woodworth, 2017; Wahl and Chambers, 2016).

6.5.3 21st century projections

As the Baltic Sea is almost completely landlocked and has a complex, highly variable coastline and topography with many individual sub-basins, internal sills, and underwater channels, global climate models such as in CMIP6 cannot sufficiently resolve the physics and processes of the Baltic Sea in general and water level oscillations in particular. Therefore, projections of ESLs for this basin require high-resolution regional climate models, which are driven by global models, for example, using the statistical and dynamical downscaling approaches (Gröger et al., 2021). An overview about the most recent projections is given by Weisse et al. (2021) and Meier et al. (2022a).

Under medium- and high-emission scenarios, global mean and, thus, Baltic Sea SL will continue to rise during the 21st century (Bamber et al., 2019; Oppenheimer et al., 2019, Table 3). For the Baltic Sea, the contemporary GRD-induced SLR (Gregory et al., 2019) from the melting Antarctic ice sheet will be more pronounced than that from the melting Greenland ice sheet (Grinsted et al., 2015; Hieronymus and Kalén, 2020). Pellikka et al. (2018, 2020) regionalized nine GMSLR projections based on different methods (process-based, semi-empirical) and different emission scenarios (RCP2.6, 4.5, 6.0, 8.5) and found that the SL in the Baltic Sea will rise by about 90 % of the global mean rate.

Future changes in ESLs in the Baltic Sea depend on future changes in mean SL and large-scale atmospheric circulation in combination with changing wind patterns. Model projections do not agree on changes in atmospheric circulation, and therefore their relevance for future ESLs remains unclear (Christensen et al., 2022; Meier et al., 2022a; Räisänen, 2017). For the Baltic Sea, changes in mean SL are expected to have a greater impact on future extreme values than changes in atmospheric circulation (Gräwe and Burchard, 2012). SL fluctuations are dampened by the sea ice cover during winter when the ocean surface is shielded from the wind stress. Therefore, it can be concluded with a relatively high degree of confidence that future sea ice loss caused by warming will result in higher ESLs in the northern Baltic Sea in those regions that have previously been ice covered and that will be free of ice in future (Meier et al., 2022b). This would lead to an increase in significant wave height, coastal erosion, and resuspension of sediment (Girjatowicz, 2004;

Leppäranta, 2013; Orviku et al., 2011). Available projections of ESLs on the European coasts have so far considered all influencing factors by linear superposition, i.e. geocentric mean SLR and land uplift, tides (negligible in the Baltic Sea), storm surges, and waves (e.g. Vousdoukas et al., 2016, 2017). The results of some studies, such as Vousdoukas et al. (2016, 2017), suggested that ESLs will rise more than mean SL due to small changes in the large-scale atmospheric circulation, such as a northward shift of Northern Hemisphere storm tracks and westerly winds and an increase in the North Atlantic and Arctic oscillations (e.g. IPCC, 2013). Similar results were recently reported by Dieterich and Radtke (2024). However, these changes in the large-scale atmospheric circulation over the Baltic Sea region are not consistently depicted in the CMIP5 and CMIP6 global climate models, meaning that these ESL projections have only little confidence.

For further details, the reader is referred to the Baltic Earth Assessment Reports (e.g. Meier et al., 2023; Christensen et al., 2022; Meier et al., 2022b, a; Rutgersson et al., 2022; Weisse et al., 2021).

Box 2: A selection of historical storms causing coastal flooding in Europe and their consequences

Many severe marine flooding events have affected European coastlines throughout history (Ferrarin et al., 2022; Haigh et al., 2015, 2017; Paprotny et al., 2018). For example, large numbers of people (perhaps as many as 10 000 to 100 000 people per event) may have been killed around the coastline of the North Sea during events in 1099, 1206, 1287, 1421, 1446, 1507, and 1717 (Gönnert et al., 2001). The "Big Flood" of 31 January–1 February 1953 killed 1836 in the Netherlands, 28 in Belgium, 307 in England, and 19 in Scotland, and damage costs were over EUR 2 billion in today's prices (Gerritsen, 2005; McRobie et al., 2005). This event, together with the 16–17 February 1962 flood in Germany, were the driving force for major improvements in sea defences (e.g. the Delta Programme in the Netherlands) and led to the establishment of storm surge forecasting and warning services (Gerritsen, 2005; Gilbert and Horner, 1986). On 3 January 2018, Storm Eleanor crossed the North Sea and caused large storm surges along the coasts of the Netherlands. Based on the water level forecasts, five barriers of the Delta Works were closed. In particular, the automated closure of the Maeslantkering, one of the largest mobile storm surge barriers worldwide, was tested during Eleanor by adjusting the water level critical threshold, leading to the second closure of the storm surge barrier since its completion in 1997. On the other side of the North Sea, the Thames Barrier was also raised to protect London from flooding.

During the winter of 2013/14, the UK, France, and Spain experienced an unusual sequence of storms and some of the most significant coastal floods in the last 60 years (Garrote et al., 2018; Spencer et al., 2015; Toimil et al., 2017).

Venice and the northern Adriatic Sea have long suffered the impact of rising SL, experiencing several coastal floods, with the most intense events occurring in 1966, 1979, 2018, and 2019 (Lionello et al., 2021b). It is worth noting that four of the eight largest flooding events in Venice since 1872 happened in 2018 and 2019 (Lionello et al., 2021b), suggesting a possible change in frequency. Below, a focus is given on the Venice case, and on two storms: Xynthia and Gloria.

Venice: November 1966, November 2019 (Mediterranean Sea)

Since the mid-20th century, the frequency of floods of the historical centre of Venice has been progressively increasing (Lionello et al., 2021a). Two extreme water levels, namely the floods of 4 November in 1966 (De Zolt et al., 2006) and 12 November 2019 (Ferrarin et al., 2021), have dramatically exposed the issue of the security of the local monumental heritage and economic activity. The November 2019 extreme water level was analysed in detail by Giesen et al. (2021), and the Copernicus Marine Service could forecast the anomaly 3 d in advance. This has motivated the construction of the MoSE defence system, which was first operated to prevent the flooding of the city in 2020 (Lionello et al., 2021a). MoSE temporarily closes the inlets of the Venice Lagoon, preventing the ESLs from reaching the city centre. MoSE relies on an accurate SL forecast (see Umgiesser et al., 2021, for a review), which failed in the case of 12 November 2019 (Ferrarin et al., 2021) and is based on the concept that the frequency and duration of closures are limited. This principle might become unrealistic in the second part of the 21st century, where long closures will have negative impact on the lagoon ecosystems and the ship traffic.

The highest floods are produced by the southeasterly wind blowing above the shallow northern Adriatic Sea and associated with the passage of a mid-latitude cyclones above northern Italy (Lionello et al., 2021b). On 12 November 2019, an unprecedented substantial contribution of a small mesoscale cyclone was among the multiple causes of the extreme event (Ferrarin et al., 2021). The increased frequency of floods is produced by the increase in the relative mean SL (Lionello et al., 2021a) at a rate of 2.5 mm yr^{-1} in the past 150 years, resulting from approximately equal contributions of vertical land movements and mean SLR (Zanchettin et al., 2021).

The likely range of North Adriatic relative level projections at the end of the 21st century goes from 32 cm (lower limit of the RCP2.6 low emission scenario) to 110 cm (upper limit of the RCP8.5 high emission scenario), and it might reach 1.8 m in a high-end scenario (Zanchettin et al., 2021). However, divergence among scenarios occurs after 2050, the time at which all values are in the range 20–40 cm (Zanchettin et al., 2021). It is estimated that preventing the flood of the city centre would require the closure of the inlets for 2–3 weeks, 2 months, and 6 months per year in correspondence with RSLR of 30, 50, and 75 cm, respectively (see Lionello et al., 2021a, and references therein).

Storm Xynthia (northeastern Atlantic)

The Storm Xynthia hit the Atlantic coast of France, especially Vendée and Charente-Maritime, during the night of 27–28 February in 2010 (Fig. 20). Xynthia caused 41 flood-related deaths (Vinet et al., 2012), 79 injured, and 500 000 affected people. Dikes were overtopped and damages were estimated to a total of EUR 2.5 billion with 4800 houses flooded, 120 km of coast eroded, failure and damages to flood defences occurred along a coastline of 200 km, and 50 000 ha of land areas flooded (e.g. Kolen et al., 2013).

Although the storm characteristics (atmospheric pressure, winds) were less exceptional than previous storms such as Storm Martin in December 1999 or Storm Klaus in 2009, it resulted in exceptional coastal floods as the peak of the storm surge (reaching 1.53 m at La Rochelle) was reached during spring high tides (+3.0 m with a coefficient of 102 at La Rochelle)

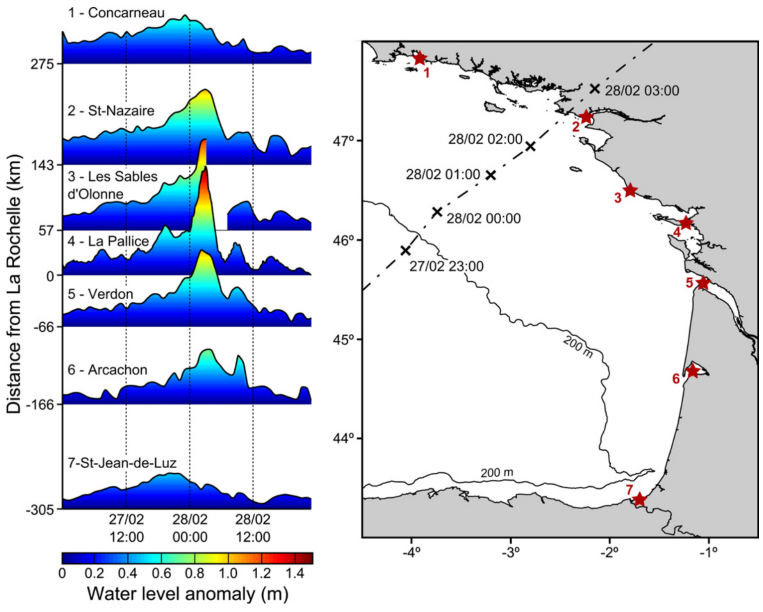

Figure 20. Storm surge during Xynthia along the French coast of the Bay of Biscay, showing a maximum at La Pallice station (station 4). Extracted from Bertin et al. (2012).

and with high waves (7.5 m of maximum significant wave height). Tide gauges recorded water levels reaching +4.51 m NGF (official levelling in France) at La Rochelle (8.01 m with respect to hydrological zero). Such water levels are well above the centennial level for Vendée and Charente-Maritime, estimated at +4.0 m NGF (Simon, 2008), and are estimated to correspond to a 200–250-year return period.

Xynthia was a tipping point for adaptation to coastal floods and associated risk management for France due to its high impact. Following Xynthia, different measures were implemented. A national coastal flood early warning system was developed by national agencies (SHOM and Météo-France), and the prevention fund for major natural hazards, known as the Barnier Fund, was extended to marine flooding. As such, since April 2010, owners of houses that were severely damaged or are threatened due to their location in areas with a high risk of coastal flooding have been allowed to sell their property to the French state. A total of 1176 properties were sold to the French state for a total of EUR 330 million. Dikes were repaired for an amount of EUR 300 million, and more than 300 local priority coastal risk prevention plans were defined.

Storm Gloria (Mediterranean Sea)

Storm Gloria was formed by a low-pressure system of Atlantic origin that intensified over the western Mediterranean starting on 19 January 2020 and lasting until 26 January 2020. It affected the eastern coasts of Spain and the Balearic Islands, with intense and sustained winds that led to record-breaking wind waves (Fig. 21) and heavy precipitation (Amores et al., 2020; de Alfonso et al., 2021; Pérez-Gómez et al., 2021; Toomey et al., 2022a). It caused severe damage along the coasts of the Spanish mainland and the east of the Balearic Islands, including a total of 13 fatalities, flooding and strong erosion, with economic losses of several million euros and damage to power supply networks.

In situ wave observations from deep-water buoys provided measurements of significant wave height over 8 m, exceeding all historical records and corresponding to return periods of several centuries when only previous measurements are accounted for (de Alfonso et al., 2021). Likewise, in situ SL observations from tide gauges along the eastern Spanish coasts measured storm surges over 50 cm (Amores et al., 2020; Pérez-Gómez et al., 2021). In particular, in the southern Gulf of Valencia, a hydrodynamic-wave-coupled model simulation quantified the effect of wave setup as large as 40 % of the total storm surge observed, which was close to 70 cm (Fig. 21) due to sustained strong winds (Amores et al., 2020).

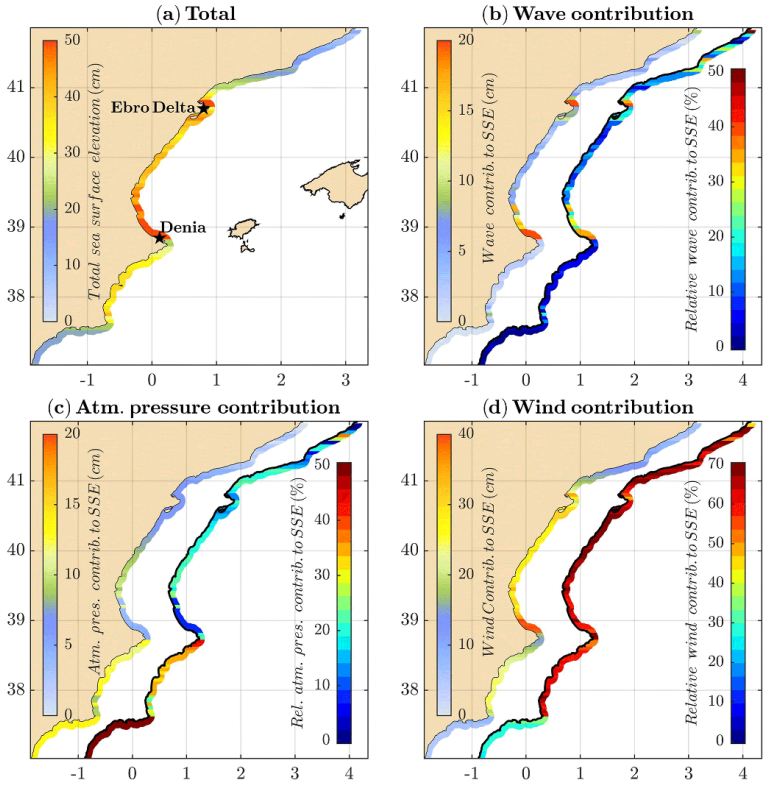

Figure 21. Storm Gloria **(a)** total sea surface elevation (SSE) along a coastal strip affected by the storm in the western Mediterranean Sea and contributions to SSE: **(b)** wave setup, **(c)** atmospheric pressure, and **(d)** wind setup contributions to the storm surge. In panels **(b)–(d)**, the absolute (relative) contributions are indicated by the profile on the left (right). Values for contributions to SSE in absolute terms are given in centimetres. Values for contributions to SSE in relative terms are given as percentages. Note that the colour scales for the wind contribution have higher limits. From Fig. 6 in Amores et al. (2020).

7 Conclusions

This paper provides an assessment of regional to local historic and future SL changes in Europe, both for the long-term trends and for extremes. It complements existing global and European assessments by providing additional geographical and contextual details, as scoped with stakeholders during dedicated regional workshops and the Sea Level Rise Conference 2022 (see Jiménez et al., 2024, in this report). European regional seas present contrasting environments, from the microtidal and enclosed Mediterranean and Black seas, to the open ocean in the northeastern Atlantic with large tides and exposition to extra-tropical storms, to the uplifting northern Baltic Sea and European Arctic. The main drivers of RSLR and of ESLs thus vary along European coastlines. Key processes and drivers or specificities of each European regional sea with regard to SL changes are reviewed.

In terms of SLR, geocentric SL trends since 1993 have been on average slightly above the global mean rate, with only a few areas showing no change or a slight decrease. VLM, notably due to GIA and human activities, can lead to substantial regional to local deviations between geocentric and relative SL changes, especially over the uplifting northern Baltic and hotspots of coastal subsidence.

Projected mean RSLR is the largest in the northeastern Atlantic, North Sea, and Mediterranean and Black seas and lowest in the European Arctic and Baltic Sea. The Baltic Sea exhibits strong spatial gradients of projected RSLR, with SLR close to the global mean in the southern basin, and relative SL fall in the northern Baltic due to GIA.

ESLs will occur more frequently along most European coasts during the 21st century. Amplification factors of the frequency at which ESLs will occur during the 21st century broadly show a meridional gradient, mostly related to the spatial amplitudes of tides and of storm-induced SL variability. The largest amplification factors are projected for southern Europe, especially in the microtidal Mediterranean Sea. The lowest (but positive) amplification factors are projected for northern Europe, in macro-tidal regions exposed to storms and induced large surges such as the southeastern North Sea. ESLs are projected to occur less frequently in the northern Baltic Sea due to a relative mean SL fall.

Several knowledge gaps are identified. An important one concerns ESLs, including the contribution from wind waves, dynamic changes in tides, surges, and wave setup and runup; non-linear interactions between these drivers of ESLs; and marine and fluvial or pluvial extreme compound events. Regionally downscaled projections or more local information of relative mean and ESL changes are needed with characterized uncertainties. A major uncertainty for SLR remains attached to ice sheets instabilities and overall contributions, and more robust projections beyond 2100 are needed. Finally, the interpretation of regional SLR variations for local perceptions and decision-making is also an area needing improvement.

Appendix A: List of acronyms

ABUMIP	Antarctic Buttressing Model Intercomparison Project
AR5	Fifth Assessment Report of the IPCC
AR6	Sixth Assessment Report of the IPCC
CMIP6	Coupled Model Intercomparison Project Phase 6
C3S	Copernicus Climate Change Service
EMODnet	European Marine Observation and Data Network
ESL	Extreme sea level
EuroGOOS	European Global Ocean Observing System
GESLA	Global Extreme Sea Level Analysis
GHG	Greenhouse gases
GIA	Glacial isostatic adjustment
GLOSS	Global Sea Level Observing System
GMSLR	Global mean sea level rise
GNSS	Global Navigation Satellite Systems
GRD	Gravity, rotation, deformation
InSAR	Interferometric Synthetic Aperture Radar
IPCC	Intergovernmental Panel on Climate Change
ISMIP6	Ice Sheet Model Intercomparison Project for CMIP6
LARMIP	Linear Antarctic Response to Basal Melting Model Intercomparison Project
MICI	Marine ice cliff instability
MISI	Marine ice sheet instability
NAO	North Atlantic Oscillation
NASA	National Aeronautics and Space Administration (USA)
PSMSL	Permanent Service for Mean Sea Level
RCP	Representative Concentration Pathways
RSLR	Relative sea level rise
SL	Sea level
SLR	Sea level rise
SONEL	Système d'Observation du Niveau des Eaux Littorales (France)
SROCC	IPCC Special Report on the Ocean and the Cryosphere in a Changing Climate
SSP	Shared Socioeconomic Pathways
VLM	Vertical land motion
WCRP	World Climate Research Programme

Data availability. Data used in this paper are available from IPCC AR6 (projection data available from https://doi.org/10.5281/zenodo.5914709, Garner et al., 2021), GESLA (https://doi.org/10.7289/V5V40S7W, Caldwell et al., 2001; Woodworth et al., 2016), PSMSL (http://www.psmsl.org/data/obtaining/, PSMSL, 2024; Holgate et al., 2013), Copernicus Marine Service (https://doi.org/10.48670/MOI-00215, EU Copernicus Marine Service, 2019a; https://doi.org/10.48670/MOI-00237, EU Copernicus Marine Service, 2019b; https://doi.org/10.48670/MOI-00264, EU Copernicus Marine Service, 2019c), and the Copernicus Climate Data Store (https://doi.org/10.24381/cds.8c59054f, Yan et al., 2020). Data from Dangendorf et al. (2019) are available from the corresponding author on request. Data from Jevrejeva et al. (2023) are available from their Supplementary Files. Statistics on present-day uplift, geoid, gravity, and Stokes coefficient rates derived from Caron et al. (2018) are available at https://vesl.jpl.nasa.gov/solid-earth/gia (Jet Propulsion Laboratory, 2024). The authors acknowledge the use of the Utide software (https://www.mathworks.com/matlabcentral/fileexchange/46523-utide-unified-tidal-analysis-and-prediction-functions, Codiga, 2024).

Author contributions. AM and RvdW coordinated the paper. AM led the writing of the abstract, conclusions, and Sect. 1. MDP led the writing of Sect. 2. MM, MJRS, BM, and AM led the writing of Sect. 3. RR, RvdW, BM, MM, and AM led the writing of Sect. 4. ABAS, RR, RvdW, AM, THJH, and AAC led the writing of Sect. 5; AM, ArA, THJH, MJRS, MM, and HEMM led the writing of Sect. 6. ABAS led the writing of Box 1, while AM and MM led the writing of Box 2. AnA, MM, MDP, ABAS, MJRS, and THJH created the figures. All authors participated in the iteration and revision of the paper.

Competing interests. The contact author has declared that none of the authors has any competing interests.

Disclaimer. Publisher's note: Copernicus Publications remains neutral with regard to jurisdictional claims made in the text, published maps, institutional affiliations, or any other geographical representation in this paper. While Copernicus Publications makes every effort to include appropriate place names, the final responsibility lies with the authors.

Acknowledgements. This paper is part of the 1st Assessment Report of the Knowledge Hub on Sea Level Rise (https://knowledgehubsealevelrise.org/, last access: 25 September 2024), a joint initiative by the Joint Programming Initiatives for Connecting Climate Knowledge for Europe (https://jpi-climate.eu/, last access: 25 September 2024) and Healthy and Productive Seas and Oceans (https://jpi-oceans.eu/en, last access: 25 September 2024), and is endorsed as a UN Ocean Decade project. This assessment report has been made possible through the dedicated efforts of the knowledge hub experts, authors, editors, reviewers, and contributors to scoping workshops and the Sea Level Rise Conference 2022 held in Venice in October 2022.

Financial support. Roderik van de Wal, Tim H. J. Hermans, and Aimée B. A. Slangen were supported by PROTECT. This publication was also supported by PROTECT. The project has received funding from the European Union's Horizon 2020 research and innovation programme under grant agreement no. 869304, PROTECT contribution number 101. Angélique Melet and Benoit Meyssignac were supported by CoCliCo, which has received funding from the European Union's Horizon 2020 research and innovation programme under grant agreement no. 101003598. Ronja Reese has been funded by the TiPACCs project, which receives funding from the European Union's Horizon 2020 research and innovation programme under grant agreement no. 820575.

Review statement. This paper was edited by Kristin Richter and reviewed by two anonymous referees.

References

Aarnes, O., Reistad, M., Breivik, O., Bitner-Gregersen, E., Eide, L. I., Gramstad, O., Magnusson, A. K., Natvig, B., and Vanem, E.: Projected changes in significant wave height towards the end of the 21st century- Northeast Atlantic, J. Geophys. Res.-Oceans, 122, 3394–3403, 2017.

Ablain, M., Meyssignac, B., Zawadzki, L., Jugier, R., Ribes, A., Spada, G., Benveniste, J., Cazenave, A., and Picot, N.: Uncertainty in satellite estimates of global mean sea-level changes, trend and acceleration, Earth Syst. Sci. Data, 11, 1189–1202, https://doi.org/10.5194/essd-11-1189-2019, 2019.

Adloff, F., Jordà, G., Somot, S., Sevault, F., Arsouze, T., Meyssignac, B., Li, L., and Planton, S.: Improving sea level simulation in Mediterranean regional climate models, Clim. Dynam., 51, 1167–1178, https://doi.org/10.1007/s00382-017-3842-3, 2018.

Ali, E., Cramer, W., Carnicer, J., Georgopoulou, E., Hilmi, N., Le Cozannet, G., and Lionello, P.: Cross-Chapter Paper 4: Mediterranean Region, in: Climate Change 2022: Impacts, Adaptation and Vulnerability. Contribution of Working Group II to the Sixth Assessment Report of the Intergovernmental Panel on Climate Change, edited by: Pörtner, H.-O., Roberts, C. D., Tignor, M., Poloczanska, E., Mintenbeck, K., Alegria, A., Craig, M., Langsdorf, S., Löschke, S., Möller, V., Okem, A., and Rama, B., Cambridge, UK and New York, NY, USA, 2233–2272, https://doi.org/10.1017/9781009325844.021, 2022.

Amarouche, K. and Akpinar, A.: Increasing Trend on Storm Wave Intensity in the Western Mediterranean, Climate, 9, 11, https://doi.org/10.3390/cli9010011, 2021.

Amarouche, K., Bingölbali, B., and Akpinar, A.: New wind-wave climate records in the Western Mediterranean Sea, Clim. Dynam., 1899–1922, https://doi.org/10.1007/s00382-021-05997-1, 2022.

Amin, M.: On perturbations of harmonic constants in the Thames Estuary, Geophys. J. Int., 73, 587–603, https://doi.org/10.1111/j.1365-246X.1983.tb03334.x, 1983.

Amores, A. and Marcos, M.: Ocean Swells along the Global Coastlines and Their Climate Projections for the Twenty-First Century, J. Climate, 33, 185–199, https://doi.org/10.1175/JCLI-D-19-0216.1, 2020.

Amores, A., Marcos, M., Carrió, D. S., and Gómez-Pujol, L.: Coastal impacts of Storm Gloria (January 2020) over the northwestern Mediterranean, Nat. Hazards Earth Syst. Sci., 20, 1955–1968, https://doi.org/10.5194/nhess-20-1955-2020, 2020.

Armstrong McKay, D. I., Staal, A., Abrams, J. F., Winkelmann, R., Sakschewski, B., Loriani, S., Fetzer, I., Cornell, S. E., Rockström, J., and Lenton, T. M.: Exceeding 1.5 °C global warming could trigger multiple climate tipping points, Science, 377, eabn7950, https://doi.org/10.1126/science.abn7950, 2022.

Arns, A., Wahl, T., Dangendorf, S., and Jensen, J.: The impact of sea level rise on storm surge water levels in the northern part of the German Bight, Coast. Eng., 96, 118–131, https://doi.org/10.1016/j.coastaleng.2014.12.002, 2015.

Arns, A., Dangendorf, S., Jensen, J., Talke, S., Bender, J., and Pattiaratchi, C.: Sea-level rise induced amplification of coastal protection design heights, Sci. Rep., 7, 40171, https://doi.org/10.1038/srep40171, 2017.

Arns, A., Wahl, T., Wolff, C., Vafeidis, A. T., Haigh, I. D., Woodworth, P., Niehüser, S., and Jensen, J.: Nonlinear interaction modulates global extreme sea levels, coastal flood exposure, and impacts, Nat. Commun., 11, 1918, https://doi.org/10.1038/s41467-020-15752-5, 2020.

Aschwanden, A., Bartholomaus, T. C., Brinkerhoff, D. J., and Truffer, M.: Brief communication: A roadmap towards credible projections of ice sheet contribution to sea level, The Cryosphere, 15, 5705–5715, https://doi.org/10.5194/tc-15-5705-2021, 2021.

Auriac, A., Spaans, K. H., Sigmundsson, F., Hooper, A., Schmidt, P., and Lund, B.: Iceland rising: Solid Earth response to ice retreat inferred from satellite radar interferometry and visoelastic modeling, J. Geophys. Res.-Sol. Ea., 118, 1331–1344, https://doi.org/10.1002/jgrb.50082, 2013.

Bagnell, A. and DeVries, T.: Correcting Biases in Historical Bathythermograph Data Using Artificial Neu-

ral Networks, J. Atmos. Ocean. Tech., 37, 1781–1800, https://doi.org/10.1175/JTECH-D-19-0103.1, 2020.

Ballarotta, M., Ubelmann, C., Pujol, M.-I., Taburet, G., Fournier, F., Legeais, J.-F., Faugère, Y., Delepoulle, A., Chelton, D., Dibarboure, G., and Picot, N.: On the resolutions of ocean altimetry maps, Ocean Sci., 15, 1091–1109, https://doi.org/10.5194/os-15-1091-2019, 2019.

Bamber, J. and Riva, R.: The sea level fingerprint of recent ice mass fluxes, The Cryosphere, 4, 621–627, https://doi.org/10.5194/tc-4-621-2010, 2010.

Bamber, J. L., Oppenheimer, M., Kopp, R. E., Aspinall, W. P., and Cooke, R. M.: Ice sheet contributions to future sea-level rise from structured expert judgment, P. Natl. Acad. Sci. USA, 116, 11195–11200, https://doi.org/10.1073/pnas.1817205116, 2019.

Barbariol, F., Davison, S., Falcieri, F. M., Ferretti, R., Ricchi, A., Sclavo, M., and Benetazzo, A.: Wind Waves in the Mediterranean Sea: An ERA5 Reanalysis Wind-Based Climatology, Front. Mar. Sci., 8, 760614, https://doi.org/10.3389/fmars.2021.760614, 2021.

Barnoud, A., Pfeffer, J., Guérou, A., Frery, M., Siméon, M., Cazenave, A., Chen, J., Llovel, W., Thierry, V., Legeais, J., and Ablain, M.: Contributions of Altimetry and Argo to Non-Closure of the Global Mean Sea Level Budget Since 2016, Geophys. Res. Lett., 48, e2021GL09282, https://doi.org/10.1029/2021GL092824, 2021.

Barnoud, A., Pfeffer, J., Cazenave, A., Fraudeau, R., Rousseau, V., and Ablain, M.: Revisiting the global mean ocean mass budget over 2005–2020, Ocean Sci., 19, 321–334, https://doi.org/10.5194/os-19-321-2023, 2023.

Bassis, J. N., Berg, B., Crawford, A. J., and Benn, D. I.: Transition to marine ice cliff instability controlled by ice thickness gradients and velocity, Science, 372, 1342–1344, https://doi.org/10.1126/science.abf6271, 2021.

Baxter, P. J.: The east coast Big Flood, 31 January–1 February 1953: a summary of the human disaster, Philos. Trans. R. Soc. Math. Phys. Eng. Sci., 363, 1293–1312, https://doi.org/10.1098/rsta.2005.1569, 2005.

Beckmann, J. and Winkelmann, R.: Effects of extreme melt events on ice flow and sea level rise of the Greenland Ice Sheet, The Cryosphere, 17, 3083–3099, https://doi.org/10.5194/tc-17-3083-2023, 2023.

Belkin, I. M.: Rapid warming of Large Marine Ecosystems, Prog. Oceanogr., 81, 207–213, https://doi.org/10.1016/j.pocean.2009.04.011, 2009.

Benetazzo, A., Davison, S., Barbariol, F., Mercogliano, P., Favaretto, C., and Sclavo, M.: Correction of ERA5 Wind for Regional Climate Projections of Sea Waves, Water, 14, 1590, https://doi.org/10.3390/w14101590, 2022.

Bertin, X., Bruneau, N., Breilh, J.-F., Fortunato, A. B., and Karpytchev, M.: Importance of wave age and resonance in storm surges: The case Xynthia, Bay of Biscay, Ocean Model., 42, 16–30, https://doi.org/10.1016/j.ocemod.2011.11.001, 2012.

Birol, F., Fuller, N., Lyard, F., Cancet, M., Niño, F., Delebecque, C., Fleury, S., Toublanc, F., Melet, A., Saraceno, M., and Léger, F.: Coastal applications from nadir altimetry: Example of the X-TRACK regional products, Adv. Space Res., 59, 936–953, https://doi.org/10.1016/j.asr.2016.11.005, 2017.

Birol, F., Léger, F., Passaro, M., Cazenave, A., Niño, F., Calafat, F. M., Shaw, A., Legeais, J.-F., Gouzenes, Y., Schwatke, C., and Benveniste, J.: The X-TRACK/ALES multi-mission processing system: New advances in altimetry towards the coast, Adv. Space Res., 67, 2398–2415, https://doi.org/10.1016/j.asr.2021.01.049, 2021.

Bochow, N., Poltronieri, A., Robinson, A., Montoya, M., Rypdal, M., and Boers, N.: Overshooting the critical threshold for the Greenland ice sheet, Nature, 622, 528–536, https://doi.org/10.1038/s41586-023-06503-9, 2023.

Boers, N. and Rypdal, M.: Critical slowing down suggests that the western Greenland Ice Sheet is close to a tipping point, P. Natl. Acad. Sci. USA, 118, e2024192118, https://doi.org/10.1073/pnas.2024192118, 2021.

Bonaduce, A., Pinardi, N., Oddo, P., Spada, G., and Larnicol, G.: Sea-level variability in the Mediterranean Sea from altimetry and tide gauges, Clim. Dynam., 47, 2851–2866, https://doi.org/10.1007/s00382-016-3001-2, 2016.

Bonaduce, A., Staneva, J., Grayek, S., Bidlot, J.-R., and Breivik, Ø.: Sea-state contributions to sea-level variability in the European Seas, Ocean Dynam., 70, 1547–1569, https://doi.org/10.1007/s10236-020-01404-1, 2020.

Bonaduce, A., Pham, N., Staneva, J., Grayek, S., Raj, R. P., and Breivik, Ø.: Sea state contribution to steric sea-level, EGU General Assembly 2023, Vienna, Austria, 24–28 April 2023, EGU23-9307, https://doi.org/10.5194/egusphere-egu23-9307, 2023.

Boucharel, J., David, M., Almar, R., and Melet, A.: Contrasted influence of climate modes teleconnections to the interannual variability of coastal sea level components–implications for statistical forecasts, Clim. Dynam., 61, 4011–4032, https://doi.org/10.1007/s00382-023-06771-1, 2023.

Boumis, G., Moftakhari, H. R., and Moradkhani, H.: Coevolution of Extreme Sea Levels and Sea-Level Rise Under Global Warming, Earths Future, 11, e2023EF003649, https://doi.org/10.1029/2023EF003649, 2023.

Bouttes, N., Gregory, J. M., and Lowe, J. A.: The Reversibility of Sea Level Rise, J. Climate, 26, 2502–2513, https://doi.org/10.1175/JCLI-D-12-00285.1, 2013.

Breili, K.: Evolution of sea-level trends along the Norwegian coast from 1960 to 2100, Ocean Dynam., 72, 115–136, https://doi.org/10.1007/s10236-021-01492-7, 2022.

Breili, K., Simpson, M. J. R., and Nilsen, J. E. Ø.: Observed Sea-Level Changes along the Norwegian Coast, J. Mar. Sci. Eng., 5, 29, https://doi.org/10.3390/jmse5030029, 2017.

Bricheno, L. M. and Wolf, J.: Future Wave Conditions of Europe, in Response to High-End Climate Change Scenarios, J. Geophys. Res.-Oceans, 123, 8762–8791, https://doi.org/10.1029/2018JC013866, 2018.

Buchanan, M. K., Kopp, R. E., Oppenheimer, M., and Tebaldi, C.: Allowances for evolving coastal flood risk under uncertain local sea-level rise, Clim. Change, 137, 347–362, https://doi.org/10.1007/s10584-016-1664-7, 2016.

Calafat, F. M. and Chambers, D. P.: Quantifying recent acceleration in sea level unrelated to internal climate variability, Geophys. Res. Lett., 40, 3661–3666, https://doi.org/10.1002/grl.50731, 2013.

Calafat, F. M., Marcos, M., and Gomis, D.: Mass contribution to Mediterranean Sea level variability for the period 1948–2000, Glob. Planet. Change, 73, 193–201, https://doi.org/10.1016/j.gloplacha.2010.06.002, 2010.

Calafat, F. M., Chambers, D. P., and Tsimplis, M. N.: Mechanisms of decadal sea level variability in the eastern North Atlantic and the Mediterranean Sea: Decadal Sea Level Variability, J. Geophys. Res.-Oceans, 117, C09022, https://doi.org/10.1029/2012JC008285, 2012.

Calafat, F. M., Chambers, D. P., and Tsimplis, M. N.: Interannual to decadal sea-level variability in the coastal zones of the Norwegian and Siberian Seas: The role of atmospheric forcing, J. Geophys. Res.-Oceans, 118, 1287–1301, https://doi.org/10.1002/jgrc.20106, 2013.

Calafat, F. M., Chambers, D. P., and Tsimplis, M. N.: On the ability of global sea level reconstructions to determine trends and variability, J. Geophys. Res.-Oceans, 119, 1572–1592, https://doi.org/10.1002/2013JC009298, 2014.

Calafat, F. M., Wahl, T., Tadesse, M. G., and Sparrow, S. N.: Trends in Europe storm surge extremes match the rate of sea-level rise, Nature, 603, 841–845, https://doi.org/10.1038/s41586-022-04426-5, 2022.

Caldwell, P. C., Merrifield, M. A., and Thompson, P. R.: Sea level measured by tide gauges from global oceans as part of the Joint Archive for Sea Level (JASL) since 1846, NOAA National Centers for Environmental Information [data set], https://doi.org/10.7289/V5V40S7W, 2001.

Calvino, C., Dabrowski, T., and Dias, F.: A study of the wave effects on the current circulation in Galway Bay, using the numerical model COAWST, Coast. Eng., 180, 104251, https://doi.org/10.1016/j.coastaleng.2022.104251, 2023.

Camargo, C. M. L., Riva, R. E. M., Hermans, T. H. J., Schütt, E. M., Marcos, M., Hernandez-Carrasco, I., and Slangen, A. B. A.: Regionalizing the sea-level budget with machine learning techniques, Ocean Sci., 19, 17–41, https://doi.org/10.5194/os-19-17-2023, 2023.

Candela, T. and Koster, K.: The many faces of anthropogenic subsidence, Science, 376, 1381–1382, https://doi.org/10.1126/science.abn3676, 2022.

Caron, L., Ivins, E. R., Larour, E., Adhikari, S., Nilsson, J., and Blewitt, G.: GIA Model Statistics for GRACE Hydrology, Cryosphere, and Ocean Science, Geophys. Res. Lett., 45, 2203–2212, https://doi.org/10.1002/2017GL076644, 2018.

Casas-Prat, M. and Sierra, J. P.: Projected future wave climate in the NW Mediterranean Sea: Projected Waves in the NW Mediterranean, J. Geophys. Res.-Oceans, 118, 3548–3568, https://doi.org/10.1002/jgrc.20233, 2013.

Cazenave, A. and Le Cozannet, G.: Sea level rise and its coastal impacts, Earths Future, 2, 15–34, 2014.

Cazenave, A. and Moreira, L.: Contemporary sea-level changes from global to local scales: a review, Proc. R. Soc. Math. Phys. Eng. Sci., 478, 20220049, https://doi.org/10.1098/rspa.2022.0049, 2022.

Chafik, L., Nilsen, J., and Dangendorf, S.: Impact of North Atlantic Teleconnection Patterns on Northern European Sea Level, J. Mar. Sci. Eng., 5, 43, https://doi.org/10.3390/jmse5030043, 2017.

Chafik, L., Nilsen, J. E. Ø., Dangendorf, S., Reverdin, G., and Frederikse, T.: North Atlantic Ocean Circulation and Decadal Sea Level Change During the Altimetry Era, Sci. Rep., 9, 1041, https://doi.org/10.1038/s41598-018-37603-6, 2019.

Chaigneau, A. A., Reffray, G., Voldoire, A., and Melet, A.: IBI-CCS: a regional high-resolution model to simulate sea level in western Europe, Geosci. Model Dev., 15, 2035–2062, https://doi.org/10.5194/gmd-15-2035-2022, 2022.

Chaigneau, A. A., Law-Chune, S., Melet, A., Voldoire, A., Reffray, G., and Aouf, L.: Impact of sea level changes on future wave conditions along the coasts of western Europe, Ocean Sci., 19, 1123–1143, https://doi.org/10.5194/os-19-1123-2023, 2023.

Chelton, D. B., deSzoeke, R. A., Schlax, M. G., El Naggar, K., and Siwertz, N.: Geographical Variability of the First Baroclinic Rossby Radius of Deformation, J. Phys. Oceanogr., 28, 433–460, https://doi.org/10.1175/1520-0485(1998)028<0433:GVOTFB>2.0.CO;2, 1998.

Chen, D. and Omstedt, A.: Climate-induced variability of sea level in Stockholm: Influence of air temperature and atmospheric circulation, Adv. Atmos. Sci., 22, 655–664, https://doi.org/10.1007/BF02918709, 2005.

Cheng, L., Trenberth, K. E., Fasullo, J., Boyer, T., Abraham, J., and Zhu, J.: Improved estimates of ocean heat content from 1960 to 2015, Sci. Adv., 3, e1601545, https://doi.org/10.1126/sciadv.1601545, 2017.

Choi, Y., Morlighem, M., Rignot, E., and Wood, M.: Ice dynamics will remain a primary driver of Greenland ice sheet mass loss over the next century, Commun. Earth Environ., 2, 26, https://doi.org/10.1038/s43247-021-00092-z, 2021.

Christensen, O. B., Kjellström, E., Dieterich, C., Gröger, M., and Meier, H. E. M.: Atmospheric regional climate projections for the Baltic Sea region until 2100, Earth Syst. Dynam., 13, 133–157, https://doi.org/10.5194/esd-13-133-2022, 2022.

Church, J. A., Clark, P. U., Cazenave, A., Gregory, J. M., Jevrejeva, S., Levermann, A., Merrifield, M. A., Milne, G. A., Nerem, R. S., Nunn, P. D., Payne, A. J., Pfeffer, W. T., Stammer, D., and Unnikrishnan, A. S.: Climate Change 2013: The Physical Science Basis. Contribution of Working Group I to the Fifth Assessment Report of the Intergovernmental Panel on Climate Change, edited by: Stocker, T. F., Qin, D., Plattner, G.-K., Tignor, M., Allen, S. K., Boschung, J., Nauels, A., Xia, Y., Bex, V., and Midgley, P. M., Cambridge University Press, Cambridge, United Kingdom and New York, NY, USA, ISBN 9781107415324, 2013.

Cid, A., Menéndez, M., Castanedo, S., Abascal, A. J., Méndez, F. J., and Medina, R.: Long-term changes in the frequency, intensity and duration of extreme storm surge events in southern Europe, Clim. Dynam., 46, 1503–1516, https://doi.org/10.1007/s00382-015-2659-1, 2016.

Cipollini, P., Calafat, F. M., Jevrejeva, S., Melet, A., and Prandi, P.: Monitoring Sea Level in the Coastal Zone with Satellite Altimetry and Tide Gauges, Surv. Geophys., 38, 33–57, https://doi.org/10.1007/s10712-016-9392-0, 2017.

Clark, M., Marsh, R., and Harle, J.: Weakening and warming of the European Slope Current since the late 1990s attributed to basin-scale density changes, Ocean Sci., 18, 549–564, https://doi.org/10.5194/os-18-549-2022, 2022.

Codiga, D.: UTide Unified Tidal Analysis and Prediction Functions, MATLAB Central File Exchange [code], https://www.mathworks.com/matlabcentral/fileexchange/46523-utide-unified-tidal-analysis-and-prediction-functions (last access: 17 July 2024), 2024.

Compton, K., Bennett, R. A., and Hreinsdóttir, S.: Climate-driven vertical acceleration of Icelandic crust measured by continuous GPS geodesy, Geophys. Res. Lett., 42, 743–750, https://doi.org/10.1002/2014GL062446, 2015.

Conte, D. and Lionello, P.: Characteristics of large positive and negative surges in the Mediterranean Sea and their attenuation in future climate scenarios, Glob. Planet. Change, 111, 159–173, https://doi.org/10.1016/j.gloplacha.2013.09.006, 2013.

Cooley, S., Schoeman, D., Bopp, L., Boyd, P., Donner, S., Ghebrehiwet, D. Y., Ito, S.-I., Kiessling, W., Martinetto, P., Ojea, E., Racault, M.-F., Rost, B., and Skern-Mauritzen, M.: Oceans and Coastal Ecosystems and Their Services, in: Climate Change 2022: Impacts, Adaptation and Vulnerability. Contribution of Working Group II to the Sixth Assessment Report of the Intergovernmental Panel on Climate Change, edited by: Pörtner, H.-O., Roberts, D. C., Tignor, M., Poloczanska, E. S., Mintenbeck, K., Alegría, A., Craig, M., Langsdorf, S., Löschke, S., Möller, V., Okem, A., and Rama, B., Cambridge University Press, Cambridge, UK and New York, NY, USA, 379–550, https://doi.org/10.1017/9781009325844.005, 2022.

Coulson, S., Lubeck, M., Mitrovica, J. X., Powell, E., Davis, J. L., and Hoggard, M. J.: The Global Fingerprint of Modern Ice-Mass Loss on 3-D Crustal Motion, Geophys. Res. Lett., 48, e2021GL095477, https://doi.org/10.1029/2021GL095477, 2021.

Dalan, F., Stone, P. H., and Sokolov, A. P.: Sensitivity of the Ocean's Climate to Diapycnal Diffusivity in an EMIC. Part II: Global Warming Scenario, J. Climate, 18, 2482–2496, https://doi.org/10.1175/JCLI3412.1, 2005.

Dangendorf, S., Wahl, T., Mudersbach, C., and Jensen, J.: The Seasonal Mean Sea Level Cycle in the Southeastern North Sea, J. Coast. Res., 165, 1915–1920, https://doi.org/10.2112/SI65-324.1, 2013.

Dangendorf, S., Calafat, F. M., Arns, A., Wahl, T., Haigh, I. D., and Jensen, J.: Mean sea level variability in the North Sea: Processes and implications, J. Geophys. Res.-Oceans, 119, 2014JC009901, https://doi.org/10.1002/2014JC009901, 2014.

Dangendorf, S., Hay, C., Calafat, F. M., Marcos, M., Piecuch, C. G., Berk, K., and Jensen, J.: Persistent acceleration in global sea-level rise since the 1960s, Nat. Clim. Change, 9, 705–710, https://doi.org/10.1038/s41558-019-0531-8, 2019.

Dangendorf, S., Frederikse, T., Chafik, L., Klinck, J. M., Ezer, T., and Hamlington, B. D.: Data-driven reconstruction reveals large-scale ocean circulation control on coastal sea level, Nat. Clim. Change, 11, 514–520, https://doi.org/10.1038/s41558-021-01046-1, 2021.

de Alfonso, M., Lin-Ye, J., García-Valdecasas, J. M., Pérez-Rubio, S., Luna, M. Y., Santos-Muñoz, D., Ruiz, M. I., Pérez-Gómez, B., and Álvarez-Fanjul, E.: Storm Gloria: Sea State Evolution Based on in situ Measurements and Modeled Data and Its Impact on Extreme Values, Front. Mar. Sci., 8, 646873, https://doi.org/10.3389/fmars.2021.646873, 2021.

DeConto, R. M. and Pollard, D.: Contribution of Antarctica to past and future sea-level rise, Nature, 531, 591–597, https://doi.org/10.1038/nature17145, 2016.

DeConto, R. M., Pollard, D., Alley, R. B., Velicogna, I., Gasson, E., Gomez, N., Sadai, S., Condron, A., Gilford, D. M., Ashe, E. L., Kopp, R. E., Li, D., and Dutton, A.: The Paris Climate Agreement and future sea-level rise from Antarctica, Nature, 593, 83–89, https://doi.org/10.1038/s41586-021-03427-0, 2021.

De Leo, F., De Leo, A., Besio, G., and Briganti, R.: Detection and quantification of trends in time series of significant wave heights: An application in the Mediterranean Sea, Ocean Eng., 202, 107155, https://doi.org/10.1016/j.oceaneng.2020.107155, 2020.

Delhasse, A., Hanna, E., Kittel, C., and Fettweis, X.: Brief communication: CMIP6 does not suggest any atmospheric blocking increase in summer over Greenland by 2100, Int. J. Climatol., 41, 2589–2596, https://doi.org/10.1002/joc.6977, 2021.

Denamiel, C., Tojčić, I., and Vilibić, I.: Meteotsunamis in orography-free, flat bathymetry and warming climate conditions, J. Geophys. Res.-Oceans, 127, 1167863, https://doi.org/10.1029/2021JC017386, 2022.

Denamiel, C., Belušić, D., Zemunik, P., and Vilibić, I.: Climate projections of meteotsunami hazards, Front. Mar. Sci., 10, 1167863, https://doi.org/10.3389/fmars.2023.1167863, 2023.

De Zolt, S., Lionello, P., Nuhu, A., and Tomasin, A.: The disastrous storm of 4 November 1966 on Italy, Nat. Hazards Earth Syst. Sci., 6, 861–879, https://doi.org/10.5194/nhess-6-861-2006, 2006.

Dieterich, C. and Radtke, H.: Higher quantiles of sea levels rise faster in Baltic Sea Climate projections, Clim. Dynam., 62, 3709–3719, https://doi.org/10.1007/s00382-023-07094-x, 2024.

Dieterich, C., Gröger, M., Arneborg, L., and Andersson, H. C.: Extreme sea levels in the Baltic Sea under climate change scenarios – Part 1: Model validation and sensitivity, Ocean Sci., 15, 1399–1418, https://doi.org/10.5194/os-15-1399-2019, 2019.

Dodet, G., Melet, A., Ardhuin, F., Bertin, X., Idier, D., and Almar, R.: The Contribution of Wind-Generated Waves to Coastal Sea-Level Changes, Surv. Geophys., 40, 1563–1601, https://doi.org/10.1007/s10712-019-09557-5, 2019.

Dodet, G., Piolle, J.-F., Quilfen, Y., Abdalla, S., Accensi, M., Ardhuin, F., Ash, E., Bidlot, J.-R., Gommenginger, C., Marechal, G., Passaro, M., Quartly, G., Stopa, J., Timmermans, B., Young, I., Cipollini, P., and Donlon, C.: The Sea State CCI dataset v1: towards a sea state climate data record based on satellite observations, Earth Syst. Sci. Data, 12, 1929–1951, https://doi.org/10.5194/essd-12-1929-2020, 2020.

Donner, R. V., Ehrcke, R., Barbosa, S. M., Wagner, J., Donges, J. F., and Kurths, J.: Spatial patterns of linear and nonparametric long-term trends in Baltic sea-level variability, Nonlin. Processes Geophys., 19, 95–111, https://doi.org/10.5194/npg-19-95-2012, 2012.

Doodsen, A. T.: Perturbations of harmonic tidal constants, Proc. R. Soc. Lond. Ser. Contain. Pap. Math. Phys. Character, 106, 513–526, https://doi.org/10.1098/rspa.1924.0085, 1924.

Doodson, A. T.: Report on Thames floods, HM Stationery Office, London, https://books.google.fr/books?id=QwgiAQAAIAAJ (last access: 2 July 2024), 1929.

Edwards, T. L., Nowicki, S., Marzeion, B., Hock, R., Goelzer, H., Seroussi, H., Jourdain, N. C., Slater, D. A., Turner, F. E., Smith, C. J., McKenna, C. M., Simon, E., Abe-Ouchi, A., Gregory, J. M., Larour, E., Lipscomb, W. H., Payne, A. J., Shepherd, A., Agosta, C., Alexander, P., Albrecht, T., Anderson, B., Asay-Davis, X., Aschwanden, A., Barthel, A., Bliss, A., Calov, R., Chambers, C., Champollion, N., Choi, Y., Cullather, R., Cuzzone, J., Dumas, C., Felikson, D., Fettweis, X., Fujita, K., Galton-Fenzi, B. K., Gladstone, R., Golledge, N. R., Greve, R., Hattermann, T., Hoffman, M. J., Humbert, A., Huss, M., Huybrechts, P., Immerzeel, W., Kleiner, T., Kraaijenbrink, P., Le Clec'H, S., Lee, V., Leguy, G. R., Little, C. M., Lowry, D. P., Malles, J.-H., Martin, D. F., Maussion, F., Morlighem, M., O'Neill, J. F., Nias, I., Pattyn, F., Pelle, T., Price, S. F., Quiquet, A., Radić, V., Reese, R., Rounce, D. R., Rückamp, M., Sakai, A.,

Shafer, C., Schlegel, N.-J., Shannon, S., Smith, R. S., Straneo, F., Sun, S., Tarasov, L., Trusel, L. D., Van Breedam, J., Van De Wal, R., Van Den Broeke, M., Winkelmann, R., Zekollari, H., Zhao, C., Zhang, T., and Zwinger, T.: Projected land ice contributions to twenty-first-century sea level rise, Nature, 593, 74–82, https://doi.org/10.1038/s41586-021-03302-y, 2021.

Ehlert, D., Zickfeld, K., Eby, M., and Gillett, N.: The Sensitivity of the Proportionality between Temperature Change and Cumulative CO_2 Emissions to Ocean Mixing, J. Climate, 30, 2921–2935, https://doi.org/10.1175/JCLI-D-16-0247.1, 2017.

Ekman, M.: A consistent map of the postglacial uplift of Fennoscandia, Terra Nova, 8, 158–165, https://doi.org/10.1111/j.1365-3121.1996.tb00739.x, 1996.

EU Copernicus Marine Service: Black Sea Mean Sea Level time series and trend from Observations Reprocessing, Mercator Ocean International [data set], https://doi.org/10.48670/MOI-00215, 2019a.

EU Copernicus Marine Service: Global Ocean Mean Sea Level time series and trend from Observations Reprocessing, Mercator Ocean International [data set], https://doi.org/10.48670/MOI-00237, 2019b.

EU Copernicus Marine Service: Mediterranean Sea Mean Sea Level time series and trend from Observations Reprocessing, Mercator Ocean International [data set], https://doi.org/10.48670/MOI-00264, 2019c.

Fasullo, J. T. and Nerem, R. S.: Altimeter-era emergence of the patterns of forced sea-level rise in climate models and implications for the future, P. Natl. Acad. Sci. USA, 115, 12944–12949, https://doi.org/10.1073/pnas.1813233115, 2018.

Favier, L., Durand, G., Cornford, S. L., Gudmundsson, G. H., Gagliardini, O., Gillet-Chaulet, F., Zwinger, T., Payne, A. J., and Le Brocq, A. M.: Retreat of Pine Island Glacier controlled by marine ice-sheet instability, Nat. Clim. Change, 4, 117–121, https://doi.org/10.1038/nclimate2094, 2014.

Feldmann, J. and Levermann, A.: Collapse of the West Antarctic Ice Sheet after local destabilization of the Amundsen Basin, P. Natl. Acad. Sci. USA, 112, 14191–14196, https://doi.org/10.1073/pnas.1512482112, 2015.

Fernández-Montblanc, T., Gómez-Enri, J., and Ciavola, P.: The Role of Mean Sea Level Annual Cycle on Extreme Water Levels Along European Coastline, Remote Sens., 12, 3419, https://doi.org/10.3390/rs12203419, 2020.

Ferrarin, C., Bajo, M., Benetazzo, A., Cavaleri, L., Chiggiato, J., Davison, S., Davolio, S., Lionello, P., Orlić, M., and Umgiesser, G.: Local and large-scale controls of the exceptional Venice floods of November 2019, Prog. Oceanogr., 197, 102628, https://doi.org/10.1016/j.pocean.2021.102628, 2021.

Ferrarin, C., Lionello, P., Orlić, M., Raicich, F., and Salvadori, G.: Venice as a paradigm of coastal flooding under multiple compound drivers, Sci. Rep., 12, 5754, https://doi.org/10.1038/s41598-022-09652-5, 2022.

Ferrarin, C., Orlić, M., Bajo, M., Davolio, S., Umgiesser, G., and Lionello, P.: The contribution of a mesoscale cyclone and associated meteotsunami to the exceptional flood in Venice on November 12, 2019, Q. J. Roy. Meteor. Soc., 149, 2929–2942, https://doi.org/10.1002/qj.4539, 2023.

Feser, F., Barcikowska, M., Krueger, O., Schenk, F., Weisse, R., and Xia, L.: Storminess over the North Atlantic and northwestern Europe – A review, Q. J. Roy. Meteor. Soc., 141, 350–382, https://doi.org/10.1002/qj.2364, 2015.

Fettweis, X., Franco, B., Tedesco, M., van Angelen, J. H., Lenaerts, J. T. M., van den Broeke, M. R., and Gallée, H.: Estimating the Greenland ice sheet surface mass balance contribution to future sea level rise using the regional atmospheric climate model MAR, The Cryosphere, 7, 469–489, https://doi.org/10.5194/tc-7-469-2013, 2013.

Fiúza, A. F. G.: Upwelling Patterns off Portugal, in: Coastal Upwelling Its Sediment Record, edited by: Suess, E. and Thiede, J., Springer US, Boston, MA, 85–98, https://doi.org/10.1007/978-1-4615-6651-9_5, 1983.

Flemming, B. W.: Tidal environments, in: Encyclopedia of coastal science, edited by: Schwartz, M., Berlin, Germany, 1180–1185, ISBN 978-1402019036, 2005.

Forget, G. and Ponte, R. M.: The partition of regional sea level variability, Prog. Oceanogr., 137, 173–195, https://doi.org/10.1016/j.pocean.2015.06.002, 2015.

Forster, P., Storelvmo, T., Armour, K., Collins, W., Dufresne, J.-L., Frame, D., Lunt, D. J., Mauritsen, T., Palmer, M. D., Watanabe, M., Wild, M., and Zhang, H.: The Earth's Energy Budget, Climate Feedbacks, and Climate Sensitivity, in: Climate Change 2021: The Physical Science Basis. Contribution of Working Group I to the Sixth Assessment Report of the Intergovernmental Panel on Climate Change, edited by: Masson-Delmotte, V., Zhai, P., Pirani, A., Connors, S. L., Péan, C., Berger, S., Caud, N., Chen, Y., Goldfarb, L., Gomis, M. I., Huang, M., Leitzell, K., Lonnoy, E., Matthews, J. B. R., Maycock, T. K., Waterfield, T., Yelekci, O., Yu, R., and Zhou, B., Cambridge, United Kingdom and New York, NY, USA, 923–1054, ISBN 978-1-00-915789-6, 2021.

Fox-Kemper, B., Hewitt, H. T., Xiao, C., Aðalgeirsdóttir, G., Drijfhout, S. S., Edwards, T. L., Golledge, N. R., Hemer, M. A., Kopp, R. E., Krinner, G., Mix, A., Notz, D., Nowicki, S., Nurhati, I. S., Ruiz, L., Sallee, J.-B., Slangen, A. B. A., and Yu, Y.: Ocean, Cryosphere and Sea Level Change, in: Climate Change 2021: The Physical Science Basis. Contribution of Working Group I to the Sixth Assessment Report of the Intergovernmental Panel on Climate Change, edited by: Masson-Delmotte, V., Zhai, P., Pirani, A., Connors, S. L., Pean, C., Berger, N., Caud, N., Chen, Y., Goldfarb, L., Gomis, M. I., Huang, M., Leitzell, K., Lonnoy, E., Matthews, J. B. R., Maycock, T., Waterfield, T., Yelekci, O., Yu, R., and Zhou, B., Cambridge University Press, Cambridge, United Kingdom and New York, NY, USA, 1211–1362, ISBN 978-1-00-915789-6, 2021.

Frederikse, T. and Gerkema, T.: Multi-decadal variability in seasonal mean sea level along the North Sea coast, Ocean Sci., 14, 1491–1501, https://doi.org/10.5194/os-14-1491-2018, 2018.

Frederikse, T., Riva, R., Kleinherenbrink, M., Wada, Y., Van Den Broeke, M., and Marzeion, B.: Closing the sea level budget on a regional scale: Trends and variability on the Northwestern European continental shelf, Geophys. Res. Lett., 43, 10864–10872, https://doi.org/10.1002/2016GL070750, 2016.

Frederikse, T., Buchanan, M. K., Lambert, E., Kopp, R. E., Oppenheimer, M., Rasmussen, D. J., and van de Wal, R. S. W.: Antarctic Ice Sheet and emission scenario controls on 21st-century extreme sea-level changes, Nat. Commun., 11, 390, https://doi.org/10.1038/s41467-019-14049-6, 2020a.

Frederikse, T., Landerer, F., Caron, L., Adhikari, S., Parkes, D., Humphrey, V. W., Dangendorf, S., Hogarth, P., Zanna, L., Cheng, L., and Wu, Y.-H.: The causes of sea-level rise since 1900, Nature, 584, 393–397, https://doi.org/10.1038/s41586-020-2591-3, 2020b.

Garbe, J., Albrecht, T., Levermann, A., Donges, J. F., and Winkelmann, R.: The hysteresis of the Antarctic Ice Sheet, Nature, 585, 538–544, https://doi.org/10.1038/s41586-020-2727-5, 2020.

Garner, G. G., Hermans, T., Kopp, R. E., Slangen, A. B. A., Edwards, T. L., Levermann, A., Nowicki, S., Palmer, M. D., Smith, C., Fox-Kemper, B., Hewitt, H. T., Xiao, C., Aðalgeirsdóttir, G., Drijfhout, S. S., Golledge, N. R., Hemer, M., Krinner, G., Mix, A., Notz, D., Nurhati, I. S., Ruiz, L., Sallée, J.-B., Yu, Y., Hua, L., Palmer, T., and Pearson, B.: IPCC AR6 Sea Level Projections (Version 20210809), Zenodo [data set], https://doi.org/10.5281/zenodo.5914709, 2021.

Garrote, J., Díaz-Álvarez, A., Nganhane, H., and Garzón Heydt, G.: The Severe 2013–14 Winter Storms in the Historical Evolution of Cantabrian (Northern Spain) Beach-Dune Systems, Geosciences, 8, 459, https://doi.org/10.3390/geosciences8120459, 2018.

Gerkema, T. and Duran-Matute, M.: Interannual variability of mean sea level and its sensitivity to wind climate in an inter-tidal basin, Earth Syst. Dynam., 8, 1223–1235, https://doi.org/10.5194/esd-8-1223-2017, 2017.

Gerritsen, H.: What happened in 1953? The Big Flood in the Netherlands in retrospect, Philos. Trans. R. Soc. Math. Phys. Eng. Sci., 363, 1271–1291, https://doi.org/10.1098/rsta.2005.1568, 2005.

Giesen, R., Clementi, E., Bajo, M., Federico, I., Stoffelen, A., and Santoleri, R.: The November 2019 record highwater levels in Venice, in: Copernicus Marine Service Ocean State Report, Issue 5, vol. 14, s140–s148, https://doi.org/10.1080/1755876X.2021.1946240, 2021.

Gilbert, S. and Horner, R.: The Thames Barrier, Thomas Telford Ltd, ISBN 978-0727702494, 1986.

Girjatowicz, J. P.: Ice thrusts and piles on the shores of the Southern Baltic Sea coast (Poland) lagoons, Balt. Coast. Zone J. Ecol. Prot. Coastline, 8, 5–22, 2004.

Goelzer, H., Nowicki, S., Payne, A., Larour, E., Seroussi, H., Lipscomb, W. H., Gregory, J., Abe-Ouchi, A., Shepherd, A., Simon, E., Agosta, C., Alexander, P., Aschwanden, A., Barthel, A., Calov, R., Chambers, C., Choi, Y., Cuzzone, J., Dumas, C., Edwards, T., Felikson, D., Fettweis, X., Golledge, N. R., Greve, R., Humbert, A., Huybrechts, P., Le clec'h, S., Lee, V., Leguy, G., Little, C., Lowry, D. P., Morlighem, M., Nias, I., Quiquet, A., Rückamp, M., Schlegel, N.-J., Slater, D. A., Smith, R. S., Straneo, F., Tarasov, L., van de Wal, R., and van den Broeke, M.: The future sea-level contribution of the Greenland ice sheet: a multi-model ensemble study of ISMIP6, The Cryosphere, 14, 3071–3096, https://doi.org/10.5194/tc-14-3071-2020, 2020.

Golledge, N. R., Keller, E. D., Gomez, N., Naughten, K. A., Bernales, J., Trusel, L. D., and Edwards, T. L.: Global environmental consequences of twenty-first-century ice-sheet melt, Nature, 566, 65–72, https://doi.org/10.1038/s41586-019-0889-9, 2019.

Golledge, N. R., Clark, P. U., He, F., Dutton, A., Turney, C. S. M., Fogwill, C. J., Naish, T. R., Levy, R. H., McKay, R. M., Lowry, D. P., Bertler, N. A. N., Dunbar, G. B., and Carlson, A. E.: Retreat of the Antarctic Ice Sheet During the Last Interglaciation and Implications for Future Change, Geophys. Res. Lett., 48, e2021GL094513, https://doi.org/10.1029/2021GL094513, 2021.

Gomis, D., Álvarez-Fanjul, E., Jordà, G., Marcos, M., Aznar, R., Rodríguez-Camino, E., Sánchez-Perrino, J. C., Rodríguez-González, J. M., Martínez-Asensio, A., Llasses, J., Pérez, B., and Sotillo, M. G.: Regional marine climate scenarios in the NE Atlantic sector close to the Spanish shores, Sci. Mar., 80, 215–234, https://doi.org/10.3989/scimar.04328.07A, 2016.

Gönnert, G., Dube, S. K., Murty, T. S., and Siefert, W.: Global Storm Surges: Theory Observation and Applications, Westholsteinische Verlagsanstalt Boyens & Co, Heide in Holstein, 623 pp., ISBN 9783804210547, 2001.

González-Alemán, J. J., Pascale, S., Gutierrez-Fernandez, J., Murakami, H., Gaertner, M. A., and Vecchi, G. A.: Potential Increase in Hazard From Mediterranean Hurricane Activity With Global Warming, Geophys. Res. Lett., 46, 1754–1764, https://doi.org/10.1029/2018GL081253, 2019.

Görmüş, T. and Ayat, B.: GüneybatıKaradeniz kıyılarının kırılganlık analizi, Gazi Üniversitesi Mühendis. Mimar. Fakültesi Derg., 35, 663–682, https://doi.org/10.17341/gazimmfd.504954, 2019.

Gräwe, U. and Burchard, H.: Storm surges in the Western Baltic Sea: the present and a possible future, Clim. Dynam., 39, 165–183, https://doi.org/10.1007/s00382-011-1185-z, 2012.

Gräwe, U., Klingbeil, K., Kelln, J., and Dangendorf, S.: Decomposing Mean Sea Level Rise in a Semi-Enclosed Basin, the Baltic Sea, J. Climate, 32, 3089–3108, https://doi.org/10.1175/JCLI-D-18-0174.1, 2019.

Greene, C. A., Gardner, A. S., Schlegel, N.-J., and Fraser, A. D.: Antarctic calving loss rivals ice-shelf thinning, Nature, 609, 948–953, https://doi.org/10.1038/s41586-022-05037-w, 2022.

Greenspan, M.: Propagation of Sound in Five Monatomic Gases, J. Acoust. Soc. Am., 28, 644–648, https://doi.org/10.1121/1.1908432, 1956.

Gregory, J. M., Griffies, S. M., Hughes, C. W., Lowe, J. A., Church, J. A., Fukimori, I., Gomez, N., Kopp, R. E., Landerer, F., Le Cozannet, G., Ponte, R. M., Stammer, D., Tamisiea, M. E., and Van De Wal, R. S. W.: Concepts and Terminology for Sea Level: Mean, Variability and Change, Both Local and Global, Surv. Geophys., 1251–1289, https://doi.org/10.1007/s10712-019-09525-z, 2019.

Gregory, J. M., George, S. E., and Smith, R. S.: Large and irreversible future decline of the Greenland ice sheet, The Cryosphere, 14, 4299–4322, https://doi.org/10.5194/tc-14-4299-2020, 2020.

Grinsted, A., Jevrejeva, S., Riva, R., and Dahl-Jensen, D.: Sea level rise projections for northern Europe under RCP8.5, Clim. Res., 64, 15–23, https://doi.org/10.3354/cr01309, 2015.

Gröger, M., Dieterich, C., Haapala, J., Ho-Hagemann, H. T. M., Hagemann, S., Jakacki, J., May, W., Meier, H. E. M., Miller, P. A., Rutgersson, A., and Wu, L.: Coupled regional Earth system modeling in the Baltic Sea region, Earth Syst. Dynam., 12, 939–973, https://doi.org/10.5194/esd-12-939-2021, 2021.

Groh, A., Richter, A., and Dietrich, C.: Recent Baltic Sea level changes induced by past and present ice masses, in: Coastline Changes of the Baltic Sea from South to East: Past and Future Projection, edited by: Harff, J., Furmanczyk, K., and von Storch, H., Springer, 55–68, ISBN 978-3319842660, 2017.

Gudmundsson, G. H.: Ice-shelf buttressing and the stability of marine ice sheets, The Cryosphere, 7, 647–655, https://doi.org/10.5194/tc-7-647-2013, 2013.

Gudmundsson, G. H., Paolo, F. S., Adusumilli, S., and Fricker, H. A.: Instantaneous Antarctic ice sheet mass loss driven by thinning ice shelves, Geophys. Res. Lett., 46, 13903–13909, https://doi.org/10.1029/2019GL085027, 2019.

Guérou, A., Meyssignac, B., Prandi, P., Ablain, M., Ribes, A., and Bignalet-Cazalet, F.: Current observed global mean sea level rise and acceleration estimated from satellite altimetry and the associated measurement uncertainty, Ocean Sci., 19, 431–451, https://doi.org/10.5194/os-19-431-2023, 2023.

Gutiérrez, J. M., Jones, R. G., Narisma, G. T., Alves, L. M., Amjad, M., Gorodetskaya, I. V., Grose, M., Klutse, N. A. B., Krakovska, S., Li, J., Martínez-Castro, D., Mearns, L. O., Mernild, S. H., Ngo-Duc, T., van den Hurk, B., and Yoon, J.-H.: Atlas, in: Climate Change 2021: The Physical Science Basis. Contribution of Working Group I to the Sixth Assessment Report of the Intergovernmental Panel on Climate Change, edited by: Masson-Delmotte, V., Zhai, P., Pirani, A., Connors, S. L., Péan, C., Berger, S., Caud, N., Chen, Y., Goldfarb, L., Gomis, M. I., Huang, M., Leitzell, K., Lonnoy, E., Matthews, J. B. R., Maycock, T. K., Waterfield, T., Yelekçi, O., Yu, R., and Zhou, B., Cambridge University Press, ISBN 978-1-00-915789-6, 2021.

Haarsma, R. J., Roberts, M. J., Vidale, P. L., Senior, C. A., Bellucci, A., Bao, Q., Chang, P., Corti, S., Fučkar, N. S., Guemas, V., von Hardenberg, J., Hazeleger, W., Kodama, C., Koenigk, T., Leung, L. R., Lu, J., Luo, J.-J., Mao, J., Mizielinski, M. S., Mizuta, R., Nobre, P., Satoh, M., Scoccimarro, E., Semmler, T., Small, J., and von Storch, J.-S.: High Resolution Model Intercomparison Project (HighResMIP v1.0) for CMIP6, Geosci. Model Dev., 9, 4185–4208, https://doi.org/10.5194/gmd-9-4185-2016, 2016.

Haasnoot, M., Brown, S., Scussolini, P., Jimenez, J. A., Vafeidis, A. T., and Nicholls, R. J.: Generic adaptation pathways for coastal archetypes under uncertain sea-level rise, Environ. Res. Commun., 1, 071006, https://doi.org/10.1088/2515-7620/ab1871, 2019.

Haasnoot, M., Lawrence, J., and Magnan, A. K.: Pathways to coastal retreat: The shrinking solution space for adaptation calls for long-term dynamic planning starting now, Science, 372, 1287–1290,, https://doi.org/10.1126/science.abi6594, 2021.

Haigh, I., Nicholls, R., and Wells, N.: Mean sea level trends around the English Channel over the 20th century and their wider context, Cont. Shelf Res., 29, 2083–2098, https://doi.org/10.1016/j.csr.2009.07.013, 2009.

Haigh, I. D., Nicholls, R., and Wells, N.: Assessing changes in extreme sea levels: Application to the English Channel, 1900–2006, Cont. Shelf Res., 30, 1042–1055, https://doi.org/10.1016/j.csr.2010.02.002, 2010.

Haigh, I. D., Wadey, M. P., Gallop, S. L., Loehr, H., Nicholls, R. J., Horsburgh, K., Brown, J. M., and Bradshaw, E.: A user-friendly database of coastal flooding in the United Kingdom from 1915–2014, Sci. Data, 2, 150021, https://doi.org/10.1038/sdata.2015.21, 2015.

Haigh, I. D., Ozsoy, O., Wadey, M. P., Nicholls, R. J., Gallop, S. L., Wahl, T., and Brown, J. M.: An improved database of coastal flooding in the United Kingdom from 1915 to 2016, Sci. Data, 4, 170100, https://doi.org/10.1038/sdata.2017.100, 2017.

Haigh, I. D., Pickering, M. D., Green, J. A. M., Arbic, B. K., Arns, A., Dangendorf, S., Hill, D. F., Horsburgh, K., Howard, T., Idier, D., Jay, D. A., Jänicke, L., Lee, S. B., Müller, M., Schindelegger, M., Talke, S. A., Wilmes, S., and Woodworth, P. L.: The Tides They Are A-Changin': A Comprehensive Review of Past and Future Nonastronomical Changes in Tides, Their Driving Mechanisms, and Future Implications, Rev. Geophys., 58, e2018RG000636, https://doi.org/10.1029/2018RG000636, 2020.

Haigh, I. D., Marcos, M., Talke, S. A., Woodworth, P. L., Hunter, J. R., Hague, B. S., Arns, A., Bradshaw, E., and Thompson, P.: GESLA Version 3: A major update to the global higher-frequency sea-level dataset, Geosci. Data J., 10, 293–314, https://doi.org/10.1002/gdj3.174, 2022.

Hallberg, R.: Using a resolution function to regulate parameterizations of oceanic mesoscale eddy effects, Ocean Model., 72, 92–103, https://doi.org/10.1016/j.ocemod.2013.08.007, 2013.

Hamlington, B. D., Piecuch, C. G., Reager, J. T., Chandanpurkar, H., Frederikse, T., Nerem, R. S., Fasullo, J. T., and Cheon, S.-H.: Origin of interannual variability in global mean sea level, P. Natl. Acad. Sci. USA, 117, 13983–13990, https://doi.org/10.1073/pnas.1922190117, 2020.

Hammarklint, T.: Swedish Sea Level Series – A Climate Indicator, Swedish Meteorological and Hydrological Institute (SMHI), 5 pp., https://www.smhi.se/polopoly_fs/1.8963!/Swedish_Sea_Level_Series_-_A_Climate_Indicator.pdf (last access: 2 July 2024), 2009.

Hammond, W. C., Blewitt, G., Kreemer, C., and Nerem, R. S.: GPS Imaging of Global Vertical Land Motion for Studies of Sea Level Rise, J. Geophys. Res.-Sol. Ea., 126, e2021JB022355, https://doi.org/10.1029/2021JB022355, 2021.

Hanna, E., Fettweis, X., and Hall, R. J.: Brief communication: Recent changes in summer Greenland blocking captured by none of the CMIP5 models, The Cryosphere, 12, 3287–3292, https://doi.org/10.5194/tc-12-3287-2018, 2018.

Hanna, E., Cappelen, J., Fettweis, X., Mernild, S. H., Mote, T. L., Mottram, R., Steffen, K., Ballinger, T. J., and Hall, R. J.: Greenland surface air temperature changes from 1981 to 2019 and implications for ice-sheet melt and mass-balance change, Int. J. Climatol., 41, E1336–E1352, https://doi.org/10.1002/joc.6771, 2021.

Haseloff, M. and Sergienko, O. V.: The effect of buttressing on grounding line dynamics, J. Glaciol., 64, 417–431, https://doi.org/10.1017/jog.2018.30, 2018.

Henry, O., Prandi, P., Llovel, W., Cazenave, A., Jevrejeva, S., Stammer, D., Meyssignac, B., and Koldunov, N.: Tide gauge-based sea level variations since 1950 along the Norwegian and Russian coasts of the Arctic Ocean: Contribution of the steric and mass components, J. Geophys. Res.-Oceans, 117, 2011JC007706, https://doi.org/10.1029/2011JC007706, 2012.

Henry, O., Ablain, M., Meyssignac, B., Cazenave, A., Masters, D., Nerem, S., and Garric, G.: Effect of the processing methodology on satellite altimetry-based global mean sea level rise over the Jason-1 operating period, J. Geod., 88, 351–361, https://doi.org/10.1007/s00190-013-0687-3, 2014.

Hermans, T. H. J., Tinker, J., Palmer, M. D., Katsman, C. A., Vermeersen, B. L. A., and Slangen, A. B. A.: Improving sea-level projections on the Northwestern European shelf us-

ing dynamical downscaling, Clim. Dynam., 54, 1987–2011, https://doi.org/10.1007/s00382-019-05104-5, 2020.

Hermans, T. H. J., Gregory, J. M., Palmer, M. D., Ringer, M. A., Katsman, C. A., and Slangen, A. B. A.: Projecting Global Mean Sea-Level Change Using CMIP6 Models, Geophys. Res. Lett., 48, e2020GL092064, https://doi.org/10.1029/2020GL092064, 2021.

Hermans, T. H. J., Katsman, C. A., Camargo, C. M. L., Garner, G. G., Kopp, R. E., and Slangen, A. B. A.: The Effect of Wind Stress on Seasonal Sea-Level Change on the Northwestern European Shelf, J. Climate, 35, 1745–1759, https://doi.org/10.1175/JCLI-D-21-0636.1, 2022.

Hermans, T. H. J., Malagón-Santos, V., Katsman, C. A., Jane, R. A., Rasmussen, D. J., Haasnoot, M., Garner, G. G., Kopp, R. E., Oppenheimer, M., and Slangen, A. B. A.: The timing of decreasing coastal flood protection due to sea-level rise, Nat. Clim. Change, 13, 359–366, https://doi.org/10.1038/s41558-023-01616-5, 2023.

Hieronymus, M. and Kalén, O.: Sea-level rise projections for Sweden based on the new IPCC special report: The ocean and cryosphere in a changing climate, Ambio, 49, 1587–1600, https://doi.org/10.1007/s13280-019-01313-8, 2020.

Hill, E. A., Rosier, S. H. R., Gudmundsson, G. H., and Collins, M.: Quantifying the potential future contribution to global mean sea level from the Filchner–Ronne basin, Antarctica, The Cryosphere, 15, 4675–4702, https://doi.org/10.5194/tc-15-4675-2021, 2021.

Hill, E. A., Urruty, B., Reese, R., Garbe, J., Gagliardini, O., Durand, G., Gillet-Chaulet, F., Gudmundsson, G. H., Winkelmann, R., Chekki, M., Chandler, D., and Langebroek, P. M.: The stability of present-day Antarctic grounding lines – Part 1: No indication of marine ice sheet instability in the current geometry, The Cryosphere, 17, 3739–3759, https://doi.org/10.5194/tc-17-3739-2023, 2023.

Hill, E. M., Davis, J. L., Tamisiea, M. E., and Lidberg, M.: Combination of geodetic observations and models for glacial isostatic adjustment fields in Fennoscandia, J. Geophys. Res.-Sol. Ea., 115, B07403, https://doi.org/10.1029/2009jb006967, 2010.

Hogarth, P., Hughes, C. W., Williams, S. D. P., and Wilson, C.: Improved and extended tide gauge records for the British Isles leading to more consistent estimates of sea level rise and acceleration since 1958, Prog. Oceanogr., 184, 102333, https://doi.org/10.1016/j.pocean.2020.102333, 2020.

Hogarth, P., Pugh, D. T., Hughes, C. W., and Williams, S. D. P.: Changes in mean sea level around Great Britain over the past 200 years, Prog. Oceanogr., 192, 102521, https://doi.org/10.1016/j.pocean.2021.102521, 2021.

Holgate, S. J., Matthews, A., Woodworth, P. L., Rickards, L. J., Tamisiea, M. E., Bradshaw, E., Foden, P. R., Gordon, K. M., Jevrejeva, S., and Pugh, J.: New Data Systems and Products at the Permanent Service for Mean Sea Level, J. Coast. Res., 29, 493–504, https://doi.org/10.2112/JCOASTRES-D-12-00175.1, 2013.

Holland, D. M., Thomas, R. H., De Young, B., Ribergaard, M. H., and Lyberth, B.: Acceleration of Jakobshavn Isbræ triggered by warm subsurface ocean waters, Nat. Geosci., 1, 659–664, https://doi.org/10.1038/ngeo316, 2008.

Horsburgh, K. J. and Wilson, C.: Tide-surge interaction and its role in the distribution of surge residuals in the North Sea, J. Geophys. Res., 112, C08003, https://doi.org/10.1029/2006JC004033, 2007.

Howard, T., Palmer, M. D., and Bricheno, L. M.: Contributions to 21st century projections of extreme sea-level change around the UK, Environ. Res. Commun., 1, 095002, https://doi.org/10.1088/2515-7620/ab42d7, 2019.

Hughes, C. W., Fukumori, I., Griffies, S. M., Huthnance, J. M., Minobe, S., Spence, P., Thompson, K. R., and Wise, A.: Sea Level and the Role of Coastal Trapped Waves in Mediating the Influence of the Open Ocean on the Coast, Surv. Geophys., 40, 1467–1492, https://doi.org/10.1007/s10712-019-09535-x, 2019.

Hünicke, B. and Zorita, E.: Trends in the amplitude of Baltic Sea level annual cycle, Tellus Dyn. Meteorol. Oceanogr., 60, 154–164, https://doi.org/10.1111/j.1600-0870.2007.00277.x, 2008.

Hünicke, B. and Zorita, E.: Statistical Analysis of the Acceleration of Baltic Mean Sea-Level Rise, 1900–2012, Front. Mar. Sci., 3, 125, https://doi.org/10.3389/fmars.2016.00125, 2016.

Hünicke, B., Zorita, E., Soomere, T., Madsen, K. S., Johansson, M., and Suursaar, Ü.: Recent Change – Sea Level and Wind Waves, in: Second Assessment of Climate Change for the Baltic Sea Basin, edited by: The BACC II Author Team, Springer International Publishing, Cham, 155–185, https://doi.org/10.1007/978-3-319-16006-1_9, 2015.

Hunter, J.: A simple technique for estimating an allowance for uncertain sea-level rise, Clim. Change, 113, 239–252, https://doi.org/10.1007/s10584-011-0332-1, 2012.

Hunter, J. R., Church, J. A., White, N. J., and Zhang, X.: Towards a global regionally varying allowance for sea-level rise, Ocean Eng., 71, 17–27, https://doi.org/10.1016/j.oceaneng.2012.12.041, 2013.

Hurrell, J. W.: Decadal Trends in the North Atlantic Oscillation: Regional Temperatures and Precipitation, Science, 269, 676–679, https://doi.org/10.1126/science.269.5224.676, 1995.

Hurrell, J. W. and Deser, C.: North Atlantic climate variability: The role of the North Atlantic Oscillation, J. Mar. Syst., 79, 231–244, https://doi.org/10.1016/j.jmarsys.2009.11.002, 2010.

Hurrell, J. W., Kushnir, Y., Ottersen, G., and Visbeck, M.: An overview of the North Atlantic Oscillation, in: Geophysical Monograph Series, edited by: Hurrell, J. W., Kushnir, Y., Ottersen, G., and Visbeck, M., American Geophysical Union, Washington, D. C., vol. 134, 1–35, https://doi.org/10.1029/134GM01, 2003.

Huthnance, J. M. and Gould, W. J.: On the Northeast Atlantic Slope Current, in: Poleward Flows Along Eastern Ocean Boundaries, edited by: Neshyba, S. J., Mooers, C. N. K., Smith, R. L., and Barber, R. T., Springer New York, New York, NY, 76–81, https://doi.org/10.1007/978-1-4613-8963-7_7, 1989.

Idier, D., Dumas, F., and Muller, H.: Tide-surge interaction in the English Channel, Nat. Hazards Earth Syst. Sci., 12, 3709–3718, https://doi.org/10.5194/nhess-12-3709-2012, 2012.

Idier, D., Paris, F., Cozannet, G. L., Boulahya, F., and Dumas, F.: Sea-level rise impacts on the tides of the European Shelf, Cont. Shelf Res., 137, 56–71, https://doi.org/10.1016/j.csr.2017.01.007, 2017.

Idier, D., Bertin, X., Thompson, P., and Pickering, M. D.: Interactions Between Mean Sea Level, Tide, Surge, Waves and Flooding: Mechanisms and Contributions to Sea Level Variations at the Coast, Surv. Geophys., 40, 1603–1630, https://doi.org/10.1007/s10712-019-09549-5, 2019.

IPCC: Climate Change 2013: The Physical Science Basis. Contribution of Working Group I to the Fifth Assessment Report of the Intergovernmental Panel on Climate Change, edited by: Stocker, T. F., Qin, D., Plattner, G.-K., Tignor, M., Allen, S. K., Boschung, J., Nauels, A., Xia, Y., Bex, V., and Midgley, P. M., Cambridge University Press, Cambridge, United Kingdom and New York, NY, USA, 1535 pp., https://doi.org/10.1017/CBO9781107415324, 2013.

IPCC: Special report on the Ocean and Cryosphere in a Changing Climate, edited by: Pörtner, H.-O., Roberts, D. C., Masson-Delmotte, V., Zhai, P., Tignor, M., Poloczanska, E., Mintenbeck, K., Alegría, A., Nicolai, M., Okem, A., Petzold, J., Rama, B., and Weyer, N. M., Cambridge University Press, https://www.ipcc.ch/report/srocc/ (last access: 2 July 2024), 2019.

IPCC: Climate Change 2021: The Physical Science Basis. Contribution of Working Group I to the Sixth Assessment Report of the Intergovernmental Panel on Climate Change, edited by: Masson-Delmotte, V., Zhai, P., Pirani, A., Connors, S. L., Péan, C., Berger, S., Caud, N., Chen, Y., Goldfarb, L., Gomis, M. I., Huang, M., Leitzell, K., E. Lonnoy, J. B., Matthews, R., Maycock, T. K., Waterfield, T., Yelekçi, O., And, R. Y., and Zhou, B., Cambridge University Press, ISBN 978-1-00-915789-6, 2021a.

IPCC: Summary for Policymakers, in: Climate Change 2021: The Physical Science Basis. Contribution of Working Group I to the Sixth Assessment Report of the Intergovernmental Panel on Climate Change, edited by: Masson-Delmotte, V., Zhai, P., Pirani, A., Connors, S. L., Péan, C., Berger, S., Caud, N., Chen, Y., Goldfarb, L., Gomis, M. I., Huang, M., Leitzell, K., Lonnoy, E., Matthews, J. B. R., Maycock, T. K., Waterfield, T., Yelekçi, O., Yu, R., and Zhou, B., Cambridge University Press, Cambridge, United Kingdom and New York, NY, USA, 3–32, https://doi.org/10.1017/9781009157896.001, 2021b.

Irazoqui Apecechea, M., Melet, A., and Armaroli, C.: Towards a pan-European coastal flood awareness system: Skill of extreme sea-level forecasts from the Copernicus Marine Service, Front. Mar. Sci., 9, 1091844, https://doi.org/10.3389/fmars.2022.1091844, 2023.

Jänicke, L., Ebener, A., Dangendorf, S., Arns, A., Schindelegger, M., Niehüser, S., Haigh, I. D., Woodworth, P., and Jensen, J.: Assessment of Tidal Range Changes in the North Sea From 1958 to 2014, J. Geophys. Res.-Oceans, 126, e2020JC016456, https://doi.org/10.1029/2020JC016456, 2021.

Jensen, A.: Excretion of organic carbon as function of nutrient stress, in: Lecture Notes on Coastal and Estuarine Studies, edited by: Holm-Hansen, O., Bolis, L., and Gilles, R., American Geophysical Union, Washington, D. C., vol. 8, 61–72, https://doi.org/10.1029/LN008p0061, 1984.

Jensen, J. and Mudersbach, C.: Zeitliche Anderungen in den Wasserstandszeitreihen an den Deutschen Kusten, Berichte Zur Dtsch. Landeskd., 81, 99, 2007.

Jet Propulsion Laboratory: Simulation of Glacial Isostatic Adjustment (GIA), NASA [data set], https://vesl.jpl.nasa.gov/solid-earth/gia, last access: 2 July 2024.

Jevrejeva, S., Moore, J. C., Woodworth, P. L., and Grinsted, A.: Influence of large-scale atmospheric circulation on European sea level: results based on the wavelet transform method, Tellus Dyn. Meteorol. Oceanogr., 57, 183–193, https://doi.org/10.3402/tellusa.v57i2.14609, 2005.

Jevrejeva, S., Williams, J., Vousdoukas, M. I., and Jackson, L. P.: Future sea level rise dominates changes in worst case extreme sea levels along the global coastline by 2100, Environ. Res. Lett., 18, 024037, https://doi.org/10.1088/1748-9326/acb504, 2023.

Jiang, L., Gerkema, T., Idier, D., Slangen, A. B. A., and Soetaert, K.: Effects of sea-level rise on tides and sediment dynamics in a Dutch tidal bay, Ocean Sci., 16, 307–321, https://doi.org/10.5194/os-16-307-2020, 2020.

Jiménez, J. A., Winter, G., Bonaduce, A., Depuydt, M., Galluccio, G., van den Hurk, B., Meier, H. E. M., Pinardi, N., Pomarico, L. G., and Vazquez Riveiros, N.: Sea Level Rise in Europe: Knowledge gaps identified through a participatory approach, in: Sea Level Rise in Europe: 1st Assessment Report of the Knowledge Hub on Sea Level Rise (SLRE1), edited by: van den Hurk, B., Pinardi, N., Kiefer, T., Larkin, K., Manderscheid, P., and Richter, K., Copernicus Publications, State Planet, 3-slre1, 3, https://doi.org/10.5194/sp-3-slre1-3-2024, 2024.

Jin, Y., Zhang, X., Church, J. A., and Bao, X.: Projected sea-level changes in the marginal seas near China based on dynamical downscaling, J. Climate, 1–52, https://doi.org/10.1175/JCLI-D-20-0796.1, 2021.

Joughin, I., Smith, B. E., and Medley, B.: Marine Ice Sheet Collapse Potentially Under Way for the Thwaites Glacier Basin, West Antarctica, Science, 344, 735–738, https://doi.org/10.1126/science.1249055, 2014.

Keizer, I., Le Bars, D., de Valk, C., Jüling, A., van de Wal, R., and Drijfhout, S.: The acceleration of sea-level rise along the coast of the Netherlands started in the 1960s, Ocean Sci., 19, 991–1007, https://doi.org/10.5194/os-19-991-2023, 2023.

Keller, H.: Weser and Ems, ihre Stromgebiete und ihre wichtigsten Nebenfluesse: Eine hydrographische, wasserwirtschaftlichte und wasserrechtliche Darstellung, IV., Dietrich Reimer, Berlin, ISBN 978-1144661845, 1901.

Kenyeres, A., Bellet, J. G., Bruyninx, C., Caporali, A., De Doncker, F., Droscak, B., Duret, A., Franke, P., Georgiev, I., Bingley, R., Huisman, L., Jivall, L., Khoda, O., Kollo, K., Kurt, A. I., Lahtinen, S., Legrand, J., Magyar, B., Mesmaker, D., Morozova, K., Nágl, J., Özdemir, S., Papanikolaou, X., Parseliunas, E., Stangl, G., Ryczywolski, M., Tangen, O. B., Valdes, M., Zurutuza, J., and Weber, M.: Regional integration of long-term national dense GNSS network solutions, GPS Solut., 23, 122, https://doi.org/10.1007/s10291-019-0902-7, 2019.

Kierulf, H. P., Steffen, H., Barletta, V. R., Lidberg, M., Johansson, J., Kristiansen, O., and Tarasov, L.: A GNSS velocity field for geophysical applications in Fennoscandia, J. Geodyn., 146, 101845, https://doi.org/10.1016/j.jog.2021.101845, 2021.

Kierulf, H. P., Kohler, J., Boy, J.-P., Geyman, E. C., Mémin, A., Omang, O. C. D., Steffen, H., and Steffen, R.: Time-varying uplift in Svalbard – an effect of glacial changes, Geophys. J. Int., 231, 1518–1534, https://doi.org/10.1093/gji/ggac264, 2022.

Kim, Y.-Y., Kim, B.-G., Jeong, K. Y., Lee, E., Byun, D.-S., and Cho, Y.-K.: Local Sea-Level Rise Caused by Climate Change in the Northwest Pacific Marginal Seas Using Dynamical Downscaling, Front. Mar. Sci., 8, 620570, https://doi.org/10.3389/fmars.2021.620570, 2021.

Kirezci, E., Young, I. R., Ranasinghe, R., Muis, S., Nicholls, R. J., Lincke, D., and Hinkel, J.: Projections of global-scale extreme sea levels and resulting episodic coastal flooding over the 21st

Century, Sci. Rep., 10, 11629, https://doi.org/10.1038/s41598-020-67736-6, 2020.

Kirezci, E., Young, I. R., Ranasinghe, R., Lincke, D., and Hinkel, J.: Global-scale analysis of socioeconomic impacts of coastal flooding over the 21st century, Front. Mar. Sci., 9, 1024111, https://doi.org/10.3389/fmars.2022.1024111, 2023.

Kolen, B., Slomp, R., and Jonkman, S. N.: The impacts of storm Xynthia February 27–28, 2010 in France: lessons for flood risk management: Impacts of storm Xynthia, J. Flood Risk Manag., 6, 261–278, https://doi.org/10.1111/jfr3.12011, 2013.

Kopp, R. E., Horton, R. M., Little, C. M., Mitrovica, J. X., Oppenheimer, M., Rasmussen, D. J., Strauss, B. H., and Tebaldi, C.: Probabilistic 21st and 22nd century sea-level projections at a global network of tide-gauge sites, Earths Future, 2, 383–406, https://doi.org/10.1002/2014EF000239, 2014.

Kopp, R. E., Oppenheimer, M., O'Reilly, J. L., Drijfhout, S. S., Edwards, T. L., Fox-Kemper, B., Garner, G. G., Golledge, N. R., Hermans, T. H. J., Hewitt, H. T., Horton, B. P., Krinner, G., Notz, D., Nowicki, S., Palmer, M. D., Slangen, A. B. A., and Xiao, C.: Communicating future sea-level rise uncertainty and ambiguity to assessment users, Nat. Clim. Change, 13, 648–660, https://doi.org/10.1038/s41558-023-01691-8, 2023.

Koseki, S., Mooney, P. A., Cabos, W., Gaertner, M. Á., de la Vara, A., and González-Alemán, J. J.: Modelling a tropical-like cyclone in the Mediterranean Sea under present and warmer climate, Nat. Hazards Earth Syst. Sci., 21, 53–71, https://doi.org/10.5194/nhess-21-53-2021, 2021.

Krasting, J. P., Stouffer, R. J., Griffies, S. M., Hallberg, R. W., Malyshev, S. L., Samuels, B. L., and Sentman, L. T.: Role of Ocean Model Formulation in Climate Response Uncertainty, J. Climate, 31, 9313–9333, https://doi.org/10.1175/JCLI-D-18-0035.1, 2018.

Kuhlbrodt, T. and Gregory, J. M.: Ocean heat uptake and its consequences for the magnitude of sea level rise and climate change, Geophys. Res. Lett., 39, L18608, https://doi.org/10.1029/2012GL052952, 2012.

LaCasce, J. H. and Groeskamp, S.: Baroclinic Modes over Rough Bathymetry and the Surface Deformation Radius, J. Phys. Oceanogr., 50, 2835–2847, https://doi.org/10.1175/JPO-D-20-0055.1, 2020.

Lambert, E., Rohmer, J., Le Cozannet, G., and van de Wal, R. S. W.: Adaptation time to magnified flood hazards underestimated when derived from tide gauge records, Environ. Res. Lett., 15, 074015, https://doi.org/10.1088/1748-9326/ab8336, 2020.

Lambert, E., Le Bars, D., Goelzer, H., and van de Wal, R. S. W.: Correlations Between Sea-Level Components Are Driven by Regional Climate Change, Earths Future, 9, e2020EF001825, https://doi.org/10.1029/2020EF001825, 2021.

Lang, A. and Mikolajewicz, U.: The long-term variability of extreme sea levels in the German Bight, Ocean Sci., 15, 651–668, https://doi.org/10.5194/os-15-651-2019, 2019.

Legeais, J.-F., Llovel, W., Melet, A., and Meyssignac, B.: Evidence of the TOPEX-A Altimeter Instrumental Anomaly and Acceleration of the Global Mean Sea Level, in: Copernicus Marine Service Ocean State Report, Issue 4, J. Oper. Oceanogr., 13, s77–s82, https://doi.org/10.1080/1755876X.2020.1785097, 2020.

Legeais, J.-F., Meyssignac, B., Faugère, Y., Guerou, A., Ablain, M., Pujol, M.-I., Dufau, C., and Dibarboure, G.: Copernicus Sea Level Space Observations: A Basis for Assessing Mitigation and Developing Adaptation Strategies to Sea Level Rise, Front. Mar. Sci., 8, 704721, https://doi.org/10.3389/fmars.2021.704721, 2021.

Lenton, T. M., Held, H., Kriegler, E., Hall, J. W., Lucht, W., Rahmstorf, S., and Schellnhuber, H. J.: Tipping elements in the Earth's climate system, P. Natl. Acad. Sci. USA, 105, 1786–1793, https://doi.org/10.1073/pnas.0705414105, 2008.

Leppäranta, M.: Land–ice interaction in the Baltic Sea, Est. J. Earth Sci., 62, 2–14, https://doi.org/10.3176/earth.2013.01, 2013.

Levermann, A. and Winkelmann, R.: A simple equation for the melt elevation feedback of ice sheets, The Cryosphere, 10, 1799–1807, https://doi.org/10.5194/tc-10-1799-2016, 2016.

Levermann, A., Winkelmann, R., Albrecht, T., Goelzer, H., Golledge, N. R., Greve, R., Huybrechts, P., Jordan, J., Leguy, G., Martin, D., Morlighem, M., Pattyn, F., Pollard, D., Quiquet, A., Rodehacke, C., Seroussi, H., Sutter, J., Zhang, T., Van Breedam, J., Calov, R., DeConto, R., Dumas, C., Garbe, J., Gudmundsson, G. H., Hoffman, M. J., Humbert, A., Kleiner, T., Lipscomb, W. H., Meinshausen, M., Ng, E., Nowicki, S. M. J., Perego, M., Price, S. F., Saito, F., Schlegel, N.-J., Sun, S., and van de Wal, R. S. W.: Projecting Antarctica's contribution to future sea level rise from basal ice shelf melt using linear response functions of 16 ice sheet models (LARMIP-2), Earth Syst. Dynam., 11, 35–76, https://doi.org/10.5194/esd-11-35-2020, 2020.

Lionello, P. and Sanna, A.: Mediterranean wave climate variability and its links with NAO and Indian Monsoon, Clim. Dynam., 611–623, 2005.

Lionello, P., Planton, S., and Rodo, X.: Preface: Trends and climate change in the Mediterranean region, Glob. Planet. Change, 63, 87–89, https://doi.org/10.1016/j.gloplacha.2008.06.004, 2008.

Lionello, P., Conte, D., Marzo, L., and Scarascia, L.: The contrasting effect of increasing mean sea level and decreasing storminess on the maximum water level during storms along the coast of the Mediterranean Sea in the mid 21st century, Glob. Planet. Change, 151, 80–91, https://doi.org/10.1016/j.gloplacha.2016.06.012, 2017.

Lionello, P., Barriopedro, D., Ferrarin, C., Nicholls, R. J., Orlić, M., Raicich, F., Reale, M., Umgiesser, G., Vousdoukas, M., and Zanchettin, D.: Extreme floods of Venice: characteristics, dynamics, past and future evolution (review article), Nat. Hazards Earth Syst. Sci., 21, 2705–2731, https://doi.org/10.5194/nhess-21-2705-2021, 2021a.

Lionello, P., Nicholls, R. J., Umgiesser, G., and Zanchettin, D.: Venice flooding and sea level: past evolution, present issues, and future projections (introduction to the special issue), Nat. Hazards Earth Syst. Sci., 21, 2633–2641, https://doi.org/10.5194/nhess-21-2633-2021, 2021b.

Llovel, W., Penduff, T., Meyssignac, B., Molines, J., Terray, L., Bessières, L., and Barnier, B.: Contributions of Atmospheric Forcing and Chaotic Ocean Variability to Regional Sea Level Trends Over 1993–2015, Geophys. Res. Lett., 45, 13405–13413, https://doi.org/10.1029/2018GL080838, 2018.

Lobeto, H., Menendez, M., and Losada, I. J.: Future behavior of wind wave extremes due to climate change, Sci. Rep., 11, 7869, https://doi.org/10.1038/s41598-021-86524-4, 2021a.

Lobeto, H., Menendez, M., and Losada, I. J.: Projections of Directional Spectra Help to Unravel the Future Behavior of Wind Waves, Front. Mar. Sci., 8, 655490, https://doi.org/10.3389/fmars.2021.655490, 2021b.

Lobeto, H., Menendez, M., Losada, I. J., and Hemer, M.: The effect of climate change on wind-wave directional spectra, Glob. Planet. Change, 213, 103820, https://doi.org/10.1016/j.gloplacha.2022.103820, 2022.

Maagard, L. and Krauss, W.: Spektren der Wasserstandsschwankungen der Ostsee im Jahre 1958, Kiel. Meeresforsch., 22, 155–162, 1966.

Madsen, K. S., Høyer, J. L., Suursaar, Ü., She, J., and Knudsen, P.: Sea Level Trends and Variability of the Baltic Sea From 2D Statistical Reconstruction and Altimetry, Front. Earth Sci., 7, 243, https://doi.org/10.3389/feart.2019.00243, 2019.

Mangini, F., Chafik, L., Bonaduce, A., Bertino, L., and Nilsen, J. E. Ø.: Sea-level variability and change along the Norwegian coast between 2003 and 2018 from satellite altimetry, tide gauges, and hydrography, Ocean Sci., 18, 331–359, https://doi.org/10.5194/os-18-331-2022, 2022.

Marcos, M. and Tsimplis, M. N.: Coastal sea level trends in Southern Europe, Geophys. J. Int., 175, 70–82, https://doi.org/10.1111/j.1365-246X.2008.03892.x, 2008.

Marcos, M. and Woodworth, P. L.: Spatiotemporal changes in extreme sea levels along the coasts of the North Atlantic and the Gulf of Mexico, J. Geophys. Res.-Oceans, 122, 7031–7048, https://doi.org/10.1002/2017JC013065, 2017.

Marcos, M., Tsimplis, M. N., and Shaw, A. G. P.: Sea level extremes in southern Europe, J. Geophys. Res., 114, C01007, https://doi.org/10.1029/2008JC004912, 2009.

Marcos, M., Calafat, F. M., Berihuete, Á., and Dangendorf, S.: Long-term variations in global sea level extremes, J. Geophys. Res.-Oceans, 120, 8115–8134, https://doi.org/10.1002/2015JC011173, 2015a.

Marcos, M., Calafat, F. M., Berihuete, Á., and Dangendorf, S.: Long-term variations in global sea level extremes, J. Geophys. Res.-Oceans, 120, 8115–8134, https://doi.org/10.1002/2015JC011173, 2015b.

Marcos, M., Marzeion, B., Dangendorf, S., Slangen, A. B. A., Palanisamy, H., and Fenoglio-Marc, L.: Internal Variability Versus Anthropogenic Forcing on Sea Level and Its Components, Surv. Geophys., 38, 329–348, https://doi.org/10.1007/s10712-016-9373-3, 2017.

Marcos, M., Puyol, B., Amores, A., Pérez Gómez, B., Fraile, M. Á., and Talke, S. A.: Historical tide gauge sea-level observations in Alicante and Santander (Spain) since the 19th century, Geosci. Data J., 8, 144–153, https://doi.org/10.1002/gdj3.112, 2021.

Marmer, H. A.: Tides and currents in New York harbor, U.S. Coast and Geodetic Survey, U.S. Government Printing Office, Special Publication number 111, LCCN 35026984, 198 pp., 1935.

Marshall, D. P. and Zanna, L.: A Conceptual Model of Ocean Heat Uptake under Climate Change, J. Climate, 27, 8444–8465, https://doi.org/10.1175/JCLI-D-13-00344.1, 2014.

Martínez-Asensio, A., Marcos, M., Tsimplis, M. N., Gomis, D., Josey, S., and Jordà, G.: Impact of the atmospheric climate modes on Mediterranean sea level variability, Glob. Planet. Change, 118, 1–15, https://doi.org/10.1016/j.gloplacha.2014.03.007, 2014.

Masina, M. and Lamberti, A.: A nonstationary analysis for the Northern Adriatic extreme sea levels: JGR-Oceans-March 2013-Masina-Lamberti, J. Geophys. Res.-Oceans, 118, 3999–4016, https://doi.org/10.1002/jgrc.20313, 2013.

Masina, S., Pinardi, N., Cipollone, A., Banerjee, D. S., Lyubartsev, V., Von Schuckmann, K., Jackson, L., Escudier, R., Clementi, E., Aydogdu, A., and Iovino, D.: The Atlantic Meridional Overturning Circulation forcing the mean sea level in the Mediterranean Sea through the Gibraltar transport, in: Copernicus Ocean State Report, vol. 15(sup1), 1–220, https://doi.org/10.1080/1755876X.2022.2095169, 2022.

Mauri, E., Sitz, L., Gerin, R., Poulain, P.-M., Hayes, D., and Gildor, H.: On the Variability of the Circulation and Water Mass Properties in the Eastern Levantine Sea between September 2016–August 2017, Water, 11, 1741, https://doi.org/10.3390/w11091741, 2019.

McRobie, A., Spencer, T., and Gerritsen, H.: The Big Flood: North Sea storm surge, Philos. Trans. R. Soc. Math. Phys. Eng. Sci., 363, 1263–1270, https://doi.org/10.1098/rsta.2005.1567, 2005.

Meier, H., Broman, B., and Kjellström, E.: Simulated sea level in past and future climates of the Baltic Sea, Clim. Res., 27, 59–75, https://doi.org/10.3354/cr027059, 2004.

Meier, H. E. M., Kniebusch, M., Dieterich, C., Gröger, M., Zorita, E., Elmgren, R., Myrberg, K., Ahola, M. P., Bartosova, A., Bonsdorff, E., Börgel, F., Capell, R., Carlén, I., Carlund, T., Carstensen, J., Christensen, O. B., Dierschke, V., Frauen, C., Frederiksen, M., Gaget, E., Galatius, A., Haapala, J. J., Halkka, A., Hugelius, G., Hünicke, B., Jaagus, J., Jüssi, M., Käyhkö, J., Kirchner, N., Kjellström, E., Kulinski, K., Lehmann, A., Lindström, G., May, W., Miller, P. A., Mohrholz, V., Müller-Karulis, B., Pavón-Jordán, D., Quante, M., Reckermann, M., Rutgersson, A., Savchuk, O. P., Stendel, M., Tuomi, L., Viitasalo, M., Weisse, R., and Zhang, W.: Climate change in the Baltic Sea region: a summary, Earth Syst. Dynam., 13, 457–593, https://doi.org/10.5194/esd-13-457-2022, 2022a.

Meier, H. E. M., Dieterich, C., Gröger, M., Dutheil, C., Börgel, F., Safonova, K., Christensen, O. B., and Kjellström, E.: Oceanographic regional climate projections for the Baltic Sea until 2100, Earth Syst. Dynam., 13, 159–199, https://doi.org/10.5194/esd-13-159-2022, 2022b.

Meier, H. E. M., Reckermann, M., Langner, J., Smith, B., and Didenkulova, I.: Overview: The Baltic Earth Assessment Reports (BEAR), Earth Syst. Dynam., 14, 519–531, https://doi.org/10.5194/esd-14-519-2023, 2023.

Melet, A. and Meyssignac, B.: Explaining the Spread in Global Mean Thermosteric Sea Level Rise in CMIP5 Climate Models, J. Climate, 28, 9918–9940, https://doi.org/10.1175/JCLI-D-15-0200.1, 2015.

Melet, A., Meyssignac, B., Almar, R., and Le Cozannet, G.: Underestimated wave contribution to coastal sea-level rise, Nat. Clim. Change, 8, 234–239, https://doi.org/10.1038/s41558-018-0088-y, 2018.

Melet, A., Almar, R., Hemer, M., Le Cozannet, G., Meyssignac, B., and Ruggiero, P.: Contribution of Wave Setup to Projected Coastal Sea Level Changes, J. Geophys. Res.-Oceans, 125, e2020JC016078, https://doi.org/10.1029/2020JC016078, 2020.

Melet, A., Buontempo, C., Mattiuzzi, M., Salamon, P., Bahurel, P., Breyiannis, G., Burgess, S., Crosnier, L., Le Traon, P.-Y., Mentaschi, L., Nicolas, J., Solari, L., Vamborg, F., and Voukouvalas, E.: European Copernicus Services to Inform on Sea-Level Rise Adaptation: Current Status and Perspectives, Front. Mar. Sci., 8, 703425, https://doi.org/10.3389/fmars.2021.703425, 2021.

Melet, A. V., Hallberg, R., and Marshall, D. P.: The role of ocean mixing in the climate system, in: Ocean Mixing, Elsevier, 5–34, https://doi.org/10.1016/B978-0-12-821512-8.00009-8, 2022.

Meli, M., Camargo, C. M. L., Olivieri, M., Slangen, A. B. A., and Romagnoli, C.: Sea-level trend variability in the Mediterranean during the 1993–2019 period, Front. Mar. Sci., 10, 1150488, https://doi.org/10.3389/fmars.2023.1150488, 2023.

Mengel, M. and Levermann, A.: Ice plug prevents irreversible discharge from East Antarctica, Nat. Clim. Change, 4, 451–455, https://doi.org/10.1038/nclimate2226, 2014.

Menna, M., Suarez, N. C. R., Civitarese, G., Gačić, M., Rubino, A., and Poulain, P.-M.: Decadal variations of circulation in the Central Mediterranean and its interactions with mesoscale gyres, Deep-Sea Res. Pt. II, 164, 14–24, https://doi.org/10.1016/j.dsr2.2019.02.004, 2019.

Menna, M., Gerin, R., Notarstefano, G., Mauri, E., Bussani, A., Pacciaroni, M., and Poulain, P.-M.: On the Circulation and Thermohaline Properties of the Eastern Mediterranean Sea, Front. Mar. Sci., 8, 671469, https://doi.org/10.3389/fmars.2021.671469, 2021.

Mentaschi, L., Vousdoukas, M. I., Voukouvalas, E., Dosio, A., and Feyen, L.: Global changes of extreme coastal wave energy fluxes triggered by intensified teleconnection patterns, Geophys. Res. Lett., 44, 2416–2426, https://doi.org/10.1002/2016GL072488, 2017.

Meucci, A., Young, I. R., Hemer, M., Kirezci, E., and Ranasinghe, R.: Projected 21st century changes in extreme wind-wave events, Sci. Adv., 6, eaaz7295, https://doi.org/10.1126/sciadv.aaz7295, 2020.

Meyssignac, B., Piecuch, C. G., Merchant, C. J., Racault, M.-F., Palanisamy, H., MacIntosh, C., Sathyendranath, S., and Brewin, R.: Causes of the Regional Variability in Observed Sea Level, Sea Surface Temperature and Ocean Colour Over the Period 1993–2011, Surv. Geophys., 38, 187–215, https://doi.org/10.1007/s10712-016-9383-1, 2017.

Milne, G. A., Davis, J. L., Mitrovica, J. X., Scherneck, H.-G., Johansson, J. M., Vermeer, M., and Koivula, H.: Space-Geodetic Constraints on Glacial Isostatic Adjustment in Fennoscandia, Science, 291, 2381–2385, https://doi.org/10.1126/science.1057022, 2001.

Mitrovica, J. X., Hay, C. C., Kopp, R. E., Harig, C., and Latychev, K.: Quantifying the Sensitivity of Sea Level Change in Coastal Localities to the Geometry of Polar Ice Mass Flux, J. Climate, 31, 3701–3709, https://doi.org/10.1175/JCLI-D-17-0465.1, 2018.

Mohamed, B. and Skiliris, N.: Steric and atmospheric contributions to interannual sea level variability in the eastern mediterranean sea over 1993–2019, Oceanologia, 64, 50–62, https://doi.org/10.1016/j.oceano.2021.09.001, 2022.

Mohamed, B., Abdallah, A. M., Alam El-Din, K., Nagy, H., and Shaltout, M.: Inter-Annual Variability and Trends of Sea Level and Sea Surface Temperature in the Mediterranean Sea over the Last 25 Years, Pure Appl. Geophys., 176, 3787–3810, https://doi.org/10.1007/s00024-019-02156-w, 2019.

Monserrat, S., Vilibić, I., and Rabinovich, A. B.: Meteotsunamis: atmospherically induced destructive ocean waves in the tsunami frequency band, Nat. Hazards Earth Syst. Sci., 6, 1035–1051, https://doi.org/10.5194/nhess-6-1035-2006, 2006.

Morim, J., Hemer, M., Cartwright, N., Strauss, D., and Andutta, F.: On the concordance of 21st century wind-wave climate projections, Glob. Planet. Change, 167, 160–171, https://doi.org/10.1016/j.gloplacha.2018.05.005, 2018.

Morim, J., Hemer, M., Wang, X. L., Cartwright, N., Trenham, C., Semedo, A., Young, I., Bricheno, L., Camus, P., Casas-Prat, M., Erikson, L., Mentaschi, L., Mori, N., Shimura, T., Timmermans, B., Aarnes, O., Breivik, O., Behrens, A., Dobrynin, M., Menendez, M., Staneva, J., Wehner, M., Wolf, J., Kamranzad, B., Webb, A., Stopa, J., and Andutta, F.: Robustness and uncertainties in global multivariate wind-wave climate projections, Nat. Clim. Change, 9, 711–718, https://doi.org/10.1038/s41558-019-0542-5, 2019.

Morim, J., Vitousek, S., Hemer, M., Reguero, B., Erikson, L., Casas-Prat, M., Wang, X. L., Semedo, A., Mori, N., Shimura, T., Mentaschi, L., and Timmermans, B.: Global-scale changes to extreme ocean wave events due to anthropogenic warming, Environ. Res. Lett., 16, 074056, https://doi.org/10.1088/1748-9326/ac1013, 2021.

Morim, J., Wahl, T., Vitousek, S., Santamaria-Aguilar, S., Young, I., and Hemer, M.: Understanding uncertainties in contemporary and future extreme wave events for broad-scale impact and adaptation planning, Sci. Adv., 9, eade3170, https://doi.org/10.1126/sciadv.ade3170, 2023.

Mourre, B., Santana, A., Builes, A., Gautreau, L., Ličer, M., Jansà, A., Casas, B., Amengual, B., and Tintoré, J.: On the potential of ensemble forecasting for the prediction of meteotsunamis in the Balearic Islands: sensitivity to atmospheric model parameterizations, Nat. Hazards, 106, 1315–1336, https://doi.org/10.1007/s11069-020-03908-x, 2021.

Mudersbach, C., Wahl, T., Haigh, I. D., and Jensen, J.: Trends in high sea levels of German North Sea gauges compared to regional mean sea level changes, Cont. Shelf Res., 65, 111–120, https://doi.org/10.1016/j.csr.2013.06.016, 2013.

Muis, S., Apecechea, M. I., Dullaart, J., de Lima Rego, J., Madsen, K. S., Su, J., Yan, K., and Verlaan, M.: A High-Resolution Global Dataset of Extreme Sea Levels, Tides, and Storm Surges, Including Future Projections, Front. Mar. Sci., 7, 263, https://doi.org/10.3389/fmars.2020.00263, 2020.

Muis, S., Aerts, J., Álvarez Antolínez, J. A., Dullaart, J., Duong, T. M., Erikson, L., Haarmsa, R., Irazoqui Apecechea, M., Mengel, M., Le Bars, D., O'Neill, A., Ranasinghe, R., Roberts, M., Verlaan, M., Ward, P. J., and Yan, K.: Global projections of storm surges using high-resolution CMIP6 climate models, Earths Future, 11, e2023EF003479, https://doi.org/10.1029/2023EF003479, 2023.

Musić, S. and Nicković, S.: 44-year wave hindcast for the Eastern Mediterranean, Coast. Eng., 55, 872–880, https://doi.org/10.1016/j.coastaleng.2008.02.024, 2008.

Naughten, K. A., Holland, P. R., and De Rydt, J.: Unavoidable future increase in West Antarctic ice-shelf melting over the twenty-first century, Nat. Clim. Change, 13, 1222–1228, https://doi.org/10.1038/s41558-023-01818-x, 2023.

Neumann, B., Vafeidis, A. T., Zimmermann, J., and Nicholls, R. J.: Future Coastal Population Growth and Exposure to Sea-Level Rise and Coastal Flooding - A Global Assessment, PLOS ONE, 10, e0118571, https://doi.org/10.1371/journal.pone.0118571, 2015.

Neumann, G.: Eigenschwingungen der Ostsee, Archiv der Deutschen Seewarte und des Marineobservatoriums, Bd. 61, No. 4, Hamburg, 1941.

Nias, I. J., Nowicki, S., Felikson, D., and Loomis, B.: Modeling the Greenland Ice Sheet's Committed Contribution to Sea Level During the 21st Century, J. Geophys. Res.-Earth Surf., 128, e2022JF006914, https://doi.org/10.1029/2022JF006914, 2023.

Nicholls, R. J., Lincke, D., Hinkel, J., Brown, S., Vafeidis, A. T., Meyssignac, B., Hanson, S. E., Merkens, J.-L., and Fang, J.: A global analysis of subsidence, relative sea-level change and coastal flood exposure, Nat. Clim. Change, 11, 338–342, https://doi.org/10.1038/s41558-021-00993-z, 2021.

Oelsmann, J., Marcos, M., Passaro, M., Sanchez, L., Dettmering, D., Dangendorf, S., and Seitz, F.: Regional variations in relative sea-level changes influenced by nonlinear vertical land motion, Nat. Geosci., 17, 137–144, https://doi.org/10.1038/s41561-023-01357-2, 2024.

Okal, E. A.: On the possibility of seismic recording of meteotsunamis, Nat. Hazards, 106, 1125–1147, https://doi.org/10.1007/s11069-020-04146-x, 2021.

Oppenheimer, M., Glavovic, B., Hinkel, J., van de Wal, R. S. W., Magnan, A., Abd-Elgawad, A., Cai, R., Cifuentes-Jara, M., DeConto, R. M., Ghosh, T., Hay, J., Isla, F. I., Marzeion, B., Meyssignac, B., and Sebesvari, Z.: Sea Level Rise and Implications for Low-Lying Islands, Coasts and Communities, in: IPCC Special Report on the Ocean and Cryosphere in a Changing Climate, edited by: Pörtner, H.-O., Roberts, D. C., Masson-Delmotte, V., Zhai, P., Tignor, M., Poloczanska, E., Mintenbeck, K., Alegría, A., Nicolai, M., Okem, A., Petzold, J., Rama, B., and Weyer, N. M., Cambridge University Press, Cambridge, UK and New York, NY, USA, 321–445, https://doi.org/10.1017/9781009157964.006, 2019.

Orlić, M.: The first attempt at cataloguing tsunami-like waves of meteorological origin in Croatian coastal waters, Acta Adriat. Int. J. Mar. Sci., 56, 83–96, 2015.

Orviku, K., Jaagus, J., and Tonisson, H.: Sea ice shaping the shores, J. Coast. Res., 681–685, 2011.

Otosaka, I. N., Shepherd, A., Ivins, E. R., Schlegel, N.-J., Amory, C., van den Broeke, M. R., Horwath, M., Joughin, I., King, M. D., Krinner, G., Nowicki, S., Payne, A. J., Rignot, E., Scambos, T., Simon, K. M., Smith, B. E., Sørensen, L. S., Velicogna, I., Whitehouse, P. L., A, G., Agosta, C., Ahlstrøm, A. P., Blazquez, A., Colgan, W., Engdahl, M. E., Fettweis, X., Forsberg, R., Gallée, H., Gardner, A., Gilbert, L., Gourmelen, N., Groh, A., Gunter, B. C., Harig, C., Helm, V., Khan, S. A., Kittel, C., Konrad, H., Langen, P. L., Lecavalier, B. S., Liang, C.-C., Loomis, B. D., McMillan, M., Melini, D., Mernild, S. H., Mottram, R., Mouginot, J., Nilsson, J., Noël, B., Pattle, M. E., Peltier, W. R., Pie, N., Roca, M., Sasgen, I., Save, H. V., Seo, K.-W., Scheuchl, B., Schrama, E. J. O., Schröder, L., Simonsen, S. B., Slater, T., Spada, G., Sutterley, T. C., Vishwakarma, B. D., van Wessem, J. M., Wiese, D., van der Wal, W., and Wouters, B.: Mass balance of the Greenland and Antarctic ice sheets from 1992 to 2020, Earth Syst. Sci. Data, 15, 1597–1616, https://doi.org/10.5194/essd-15-1597-2023, 2023.

Ozsahin, E., Ozdes, M., Ozturk, M., and Yang, D.: Coastal Vulnerability Assessment of Thrace Peninsula: Implications for Climate Change and Sea Level Rise, Remote Sens., 15, 5592, https://doi.org/10.3390/rs15235592, 2023.

Palmer, M. D., Howard, T., Tinker, J., Lowe, J. A., Bricheno, L., Calvert, D., Edwards, T., Gregory, J., Harris, G., Krijnen, J., Pickering, M., Roberts, C. D., and Wolf, J.: UKCP18 marine report, MetOffice Report, 133 pp., https://nora.nerc.ac.uk/id/eprint/522257 (last access: 2 July 2024), 2018.

Paprotny, D., Morales-Nápoles, O., and Jonkman, S. N.: HANZE: a pan-European database of exposure to natural hazards and damaging historical floods since 1870, Earth Syst. Sci. Data, 10, 565–581, https://doi.org/10.5194/essd-10-565-2018, 2018.

Pardaens, A. K., Gregory, J. M., and Lowe, J. A.: A model study of factors influencing projected changes in regional sea level over the twenty-first century, Clim. Dynam., 36, 2015–2033, https://doi.org/10.1007/s00382-009-0738-x, 2011.

Park, J.-Y., Schloesser, F., Timmermann, A., Choudhury, D., Lee, J.-Y., and Nellikkattil, A. B.: Future sea-level projections with a coupled atmosphere-ocean-ice-sheet model, Nat. Commun., 14, 636, https://doi.org/10.1038/s41467-023-36051-9, 2023.

Passaro, M., Müller, F. L., Oelsmann, J., Rautiainen, L., Dettmering, D., Hart-Davis, M. G., Abulaitijiang, A., Andersen, O. B., Høyer, J. L., Madsen, K. S., Ringgaard, I. M., Särkkä, J., Scarrott, R., Schwatke, C., Seitz, F., Tuomi, L., Restano, M., and Benveniste, J.: Absolute Baltic Sea Level Trends in the Satellite Altimetry Era: A Revisit, Front. Mar. Sci., 8, 647607, https://doi.org/10.3389/fmars.2021.647607, 2021.

Payne, A. J., Nowicki, S., Abe-Ouchi, A., Agosta, C., Alexander, P., Albrecht, T., Asay-Davis, X., Aschwanden, A., Barthel, A., Bracegirdle, T. J., Calov, R., Chambers, C., Choi, Y., Cullather, R., Cuzzone, J., Dumas, C., Edwards, T. L., Felikson, D., Fettweis, X., Galton-Fenzi, B. K., Goelzer, H., Gladstone, R., Golledge, N. R., Gregory, J. M., Greve, R., Hattermann, T., Hoffman, M. J., Humbert, A., Huybrechts, P., Jourdain, N. C., Kleiner, T., Munneke, P. K., Larour, E., Le Clec'H, S., Lee, V., Leguy, G., Lipscomb, W. H., Little, C. M., Lowry, D. P., Morlighem, M., Nias, I., Pattyn, F., Pelle, T., Price, S. F., Quiquet, A., Reese, R., Rückamp, M., Schlegel, N., Seroussi, H., Shepherd, A., Simon, E., Slater, D., Smith, R. S., Straneo, F., Sun, S., Tarasov, L., Trusel, L. D., Van Breedam, J., Van De Wal, R., Van Den Broeke, M., Winkelmann, R., Zhao, C., Zhang, T., and Zwinger, T.: Future Sea Level Change Under Coupled Model Intercomparison Project Phase 5 and Phase 6 Scenarios From the Greenland and Antarctic Ice Sheets, Geophys. Res. Lett., 48, e2020GL091741, https://doi.org/10.1029/2020GL091741, 2021.

Pegler, S. S.: Marine ice sheet dynamics: the impacts of ice-shelf buttressing, J. Fluid Mech., 857, 605–647, https://doi.org/10.1017/jfm.2018.741, 2018.

Pellikka, H., Leijala, U., Johansson, M. M., Leinonen, K., and Kahma, K. K.: Future probabilities of coastal floods in Finland, Cont. Shelf Res., 157, 32–42, https://doi.org/10.1016/j.csr.2018.02.006, 2018.

Pellikka, H., Sarkka, J., Johansson, J., and Pettersson, H.: Probability distributions for mean sea level and storm contribution up to 2100 AD at Forsmark, Swedish Nuclear Fuel and Waste Management Company (SKB), https://www.skb.com/publication/2494748/TR-19-23.pdf (last access: 2 July 2024), 2020.

Peltier, W. R.: Global glacial isostasy and the surface of the ice-age Earth: The ICE-5G (VM2) Model and Grace, Annu. Rev. Earth Planet. Sci., 32, 111–149, https://doi.org/10.1146/annurev.earth.32.082503.144359, 2004.

Peltier, W. R., Argus, D. F., and Drummond, R.: Space geodesy constrains ice age terminal deglaciation: The global ICE-6G_C

(VM5a) model, J. Geophys. Res.-Sol. Ea., 120, 450–487, https://doi.org/10.1002/2014JB011176, 2015.

Pérez-Gómez, B., García-León, M., García-Valdecasas, J., Clementi, E., Mösso Aranda, C., Pérez-Rubio, S., Masina, S., Coppini, G., Molina-Sánchez, R., Muñoz-Cubillo, A., García Fletcher, A., Sánchez González, J. F., Sánchez-Arcilla, A., and Álvarez Fanjul, E.: Understanding Sea Level Processes During Western Mediterranean Storm Gloria, Front. Mar. Sci., 8, 647437, https://doi.org/10.3389/fmars.2021.647437, 2021.

Pérez Gómez, B., Vilibić, I., Šepić, J., Međugorac, I., Ličer, M., Testut, L., Fraboul, C., Marcos, M., Abdellaoui, H., Álvarez Fanjul, E., Barbalić, D., Casas, B., Castaño-Tierno, A., Čupić, S., Drago, A., Fraile, M. A., Galliano, D. A., Gauci, A., Gloginja, B., Martín Guijarro, V., Jeromel, M., Larrad Revuelto, M., Lazar, A., Keskin, I. H., Medvedev, I., Menassri, A., Meslem, M. A., Mihanović, H., Morucci, S., Niculescu, D., Quijano de Benito, J. M., Pascual, J., Palazov, A., Picone, M., Raicich, F., Said, M., Salat, J., Sezen, E., Simav, M., Sylaios, G., Tel, E., Tintoré, J., Zaimi, K., and Zodiatis, G.: Coastal sea level monitoring in the Mediterranean and Black seas, Ocean Sci., 18, 997–1053, https://doi.org/10.5194/os-18-997-2022, 2022.

Permanent Service for Mean Sea Level (PSMSL): Tide Gauge Data, PSMSL [data set], http://www.psmsl.org/data/obtaining/ (last access: 2 July 2024), 2024.

Pickering, M. D., Horsburgh, K. J., Blundell, J. R., Hirschi, J. J.-M., Nicholls, R. J., Verlaan, M., and Wells, N. C.: The impact of future sea-level rise on the global tides, Cont. Shelf Res., 142, 50–68, https://doi.org/10.1016/j.csr.2017.02.004, 2017.

Piecuch, C. G. and Quinn, K. J.: El Niño, La Niña, and the global sea level budget, Ocean Sci., 12, 1165–1177, https://doi.org/10.5194/os-12-1165-2016, 2016.

Pinardi, N., Bonaduce, A., Navarra, A., Dobricic, S., and Oddo, P.: The Mean Sea Level Equation and Its Application to the Mediterranean Sea, J. Climate, 27, 442–447, https://doi.org/10.1175/JCLI-D-13-00139.1, 2014.

Piña-Valdés, J., Socquet, A., Beauval, C., Doin, M., D'Agostino, N., and Shen, Z.: 3D GNSS Velocity Field Sheds Light on the Deformation Mechanisms in Europe: Effects of the Vertical Crustal Motion on the Distribution of Seismicity, J. Geophys. Res.-Sol. Ea., 127, e2021JB023451, https://doi.org/10.1029/2021JB023451, 2022.

Pineau-Guillou, L., Lazure, P., and Wöppelmann, G.: Large-scale changes of the semidiurnal tide along North Atlantic coasts from 1846 to 2018, Ocean Sci., 17, 17–34, https://doi.org/10.5194/os-17-17-2021, 2021.

Pomaro, A., Cavaleri, L., and Lionello, P.: Climatology and trends of the Adriatic Sea wind waves: analysis of a 37-year long instrumental data set, Int. J. Climatol., 37, 4237–4250, https://doi.org/10.1002/joc.5066, 2017.

Prandi, P., Meyssignac, B., Ablain, M., Spada, G., Ribes, A., and Benveniste, J.: Local sea level trends, accelerations and uncertainties over 1993–2019, Sci. Data, 8, 1, https://doi.org/10.1038/s41597-020-00786-7, 2021.

Prandle, D. and Wolf, J.: The interaction of surge and tide in the North Sea and River Thames, Geophys. J. Int., 55, 203–216, https://doi.org/10.1111/j.1365-246X.1978.tb04758.x, 1978.

Proudman, J.: The Effects on the Sea of Changes in Atmospheric Pressure, Geophys. J. Int., 2, 197–209, https://doi.org/10.1111/j.1365-246X.1929.tb05408.x, 1929.

Proudman, J.: The propagation of tide and surge in an estuary, Proc. R. Soc. Lond. Ser. Math. Phys. Sci., 231, 8–24, https://doi.org/10.1098/rspa.1955.0153, 1955.

Proudman, J.: Oscillations of tide and surge in an estuary of finite length, J. Fluid Mech., 2, 371–382, https://doi.org/10.1017/S002211205700018X, 1957.

Pugh, D.: Changing sea levels: effects of tides, weather and climate, Cambridge University Press, 265 pp., ISBN 978-1934309094, 2004.

Pugh, D. and Woodworth, P.: Sea-Level Science: Understanding Tides, Surges, Tsunamis and Mean Sea-Level Changes, 1st edn., Cambridge University Press, https://doi.org/10.1017/CBO9781139235778, 2014.

Purkey, S. G., Johnson, G. C., and Chambers, D. P.: Relative contributions of ocean mass and deep steric changes to sea level rise between 1993 and 2013, J. Geophys. Res.-Oceans, 119, 7509–7522, https://doi.org/10.1002/2014JC010180, 2014.

Rabinovich, A. B. and Monserrat, S.: Generation of Meteorological Tsunamis (Large Amplitude Seiches) Near the Balearic and Kuril Islands, Nat. Hazards, 18, 27–55, https://doi.org/10.1023/A:1008096627047, 1998.

Raicich, F.: Recent evolution of sea-level extremes at Trieste (Northern Adriatic), Cont. Shelf Res., 23, 225–235, https://doi.org/10.1016/S0278-4343(02)00224-8, 2003.

Raicich, F.: A 1782–1794 sea level record at Trieste (northern Adriatic), Hist. Geo Space. Sci., 11, 1–14, https://doi.org/10.5194/hgss-11-1-2020, 2020.

Räisänen, J.: Future Climate Change in the Baltic Sea Region and Environmental Impacts, Oxford University Press, https://doi.org/10.1093/acrefore/9780190228620.013.634, 2017.

Ranasinghe, R., Ruane, A. C., Vautard, R., Arnell, E., Coppola, E., Cruz, F. A., Dessai, S., Islam, A. S., Rahimi, M., Ruiz Carrascal, D., Silliman, J., Sylla, M. B., Tebaldi, C., Wang, W., and Zaaboul, R.: Climate Change Information for Regional Impact and for Risk Assessment, in: Climate Change 2021: The Physical Science Basis. Contribution of Working Group I to the Sixth Assessment Report of the Intergovernmental Panel on Climate Change, Cambridge University Press, Cambridge, United Kingdom and New York, NY, USA, 1767–1926, ISBN 978-1-00-915789-6, 2021.

Rasmussen, D. J., Bittermann, K., Buchanan, M. K., Kulp, S., Strauss, B. H., Kopp, R. E., and Oppenheimer, M.: Extreme sea level implications of 1.5 °C, 2.0 °C, and 2.5 °C temperature stabilization targets in the 21st and 22nd centuries, Environ. Res. Lett., 13, 034040, https://doi.org/10.1088/1748-9326/aaac87, 2018.

Rasmussen, D. J., Kulp, S., Kopp, R. E., Oppenheimer, M., and Strauss, B. H.: Popular extreme sea level metrics can better communicate impacts, Clim. Change, 170, 30, https://doi.org/10.1007/s10584-021-03288-6, 2022.

Ratsimandresey, A. W., Sotillo, M. G., Carretero Albiach, J. C., Álvarez Fanjul, E., and Hajji, H.: A 44-year high-resolution ocean and atmospheric hindcast for the Mediterranean Basin developed within the HIPOCAS Project, Coast. Eng., 55, 827–842, https://doi.org/10.1016/j.coastaleng.2008.02.025, 2008.

Ray, R. D., Loomis, B. D., and Zlotnicki, V.: The mean seasonal cycle in relative sea level from satellite altimetry and gravimetry, J. Geod., 95, 80, https://doi.org/10.1007/s00190-021-01529-1, 2021.

Reese, R., Levermann, A., Albrecht, T., Seroussi, H., and Winkelmann, R.: The role of history and strength of the oceanic forcing in sea level projections from Antarctica with the Parallel Ice Sheet Model, The Cryosphere, 14, 3097–3110, https://doi.org/10.5194/tc-14-3097-2020, 2020.

Reese, R., Garbe, J., Hill, E. A., Urruty, B., Naughten, K. A., Gagliardini, O., Durand, G., Gillet-Chaulet, F., Gudmundsson, G. H., Chandler, D., Langebroek, P. M., and Winkelmann, R.: The stability of present-day Antarctic grounding lines – Part 2: Onset of irreversible retreat of Amundsen Sea glaciers under current climate on centennial timescales cannot be excluded, The Cryosphere, 17, 3761–3783, https://doi.org/10.5194/tc-17-3761-2023, 2023.

Reinert, M., Pineau-Guillou, L., Raillard, N., and Chapron, B.: Seasonal Shift in Storm Surges at Brest Revealed by Extreme Value Analysis, J. Geophys. Res.-Oceans, 126, e2021JC017794, https://doi.org/10.1029/2021JC017794, 2021.

Ribeiro, A., Barbosa, S. M., Scotto, M. G., and Donner, R. V.: Changes in extreme sea-levels in the Baltic Sea, Tellus Dyn. Meteorol. Oceanogr., 66, 20921, https://doi.org/10.3402/tellusa.v66.20921, 2014.

Richter, A., Groh, A., and Dietrich, R.: Geodetic observation of sea-level change and crustal deformation in the Baltic Sea region, Phys. Chem. Earth ABC, 53–54, 43–53, https://doi.org/10.1016/j.pce.2011.04.011, 2012.

Richter, K., Meyssignac, B., Slangen, A. B. A., Melet, A., Church, J. A., Fettweis, X., Marzeion, B., Agosta, C., Ligtenberg, S. R. M., Spada, G., Palmer, M. D., Roberts, C. D., and Champollion, N.: Detecting a forced signal in satellite-era sea-level change, Environ. Res. Lett., 15, 094079, https://doi.org/10.1088/1748-9326/ab986e, 2020.

Rignot, E., Mouginot, J., Morlighem, M., Seroussi, H., and Scheuchl, B.: Widespread, rapid grounding line retreat of Pine Island, Thwaites, Smith, and Kohler glaciers, West Antarctica, from 1992 to 2011, Geophys. Res. Lett., 41, 3502–3509, https://doi.org/10.1002/2014GL060140, 2014.

Rignot, E., Mouginot, J., Scheuchl, B., Van Den Broeke, M., Van Wessem, M. J., and Morlighem, M.: Four decades of Antarctic Ice Sheet mass balance from 1979–2017, P. Natl. Acad. Sci. USA, 116, 1095–1103, https://doi.org/10.1073/pnas.1812883116, 2019.

Robel, A. A., Seroussi, H., and Roe, G. H.: Marine ice sheet instability amplifies and skews uncertainty in projections of future sea-level rise, P. Natl. Acad. Sci. USA, 116, 14887–14892, https://doi.org/10.1073/pnas.1904822116, 2019.

Roberts, C. D., Calvert, D., Dunstone, N., Hermanson, L., Palmer, M. D., and Smith, D.: On the Drivers and Predictability of Seasonal-to-Interannual Variations in Regional Sea Level, J. Climate, 29, 7565–7585, https://doi.org/10.1175/JCLI-D-15-0886.1, 2016.

Robinson, A., Calov, R., and Ganopolski, A.: Multistability and critical thresholds of the Greenland ice sheet, Nat. Clim. Change, 2, 429–432, https://doi.org/10.1038/nclimate1449, 2012.

Roland, A., Cucco, A., Ferrarin, C., Hsu, T.-W., Liau, J.-M., Ou, S.-H., Umgiesser, G., and Zanke, U.: On the development and verification of a 2-D coupled wave-current model on unstructured meshes, J. Mar. Syst., 78, S244–S254, https://doi.org/10.1016/j.jmarsys.2009.01.026, 2009.

Romero, R. and Emanuel, K.: Medicane risk in a changing climate, J. Geophys. Res.-Atmos., 118, 5992–6001, https://doi.org/10.1002/jgrd.50475, 2013.

Romero, R. and Emanuel, K.: Climate Change and Hurricane-Like Extratropical Cyclones: Projections for North Atlantic Polar Lows and Medicanes Based on CMIP5 Models, J. Climate, 30, 279–299, https://doi.org/10.1175/JCLI-D-16-0255.1, 2017.

Romero, R., Vich, M., and Ramis, C.: A pragmatic approach for the numerical prediction of meteotsunamis in Ciutadella harbour (Balearic Islands), Ocean Model., 142, 101441, https://doi.org/10.1016/j.ocemod.2019.101441, 2019.

Rose, S. K., Andersen, O. B., Passaro, M., Ludwigsen, C. A., and Schwatke, C.: Arctic Ocean Sea Level Record from the Complete Radar Altimetry Era: 1991–2018, Remote Sens., 11, 1672, https://doi.org/10.3390/rs11141672, 2019.

Rosier, S. H. R., Reese, R., Donges, J. F., De Rydt, J., Gudmundsson, G. H., and Winkelmann, R.: The tipping points and early warning indicators for Pine Island Glacier, West Antarctica, The Cryosphere, 15, 1501–1516, https://doi.org/10.5194/tc-15-1501-2021, 2021.

Roustan, J.-B., Pineau-Guillou, L., Chapron, B., Raillard, N., and Reinert, M.: Shift of the storm surge season in Europe due to climate variability, Sci. Rep., 12, 8210, https://doi.org/10.1038/s41598-022-12356-5, 2022.

Royston, S., Dutt Vishwakarma, B., Westaway, R., Rougier, J., Sha, Z., and Bamber, J.: Can We Resolve the Basin-Scale Sea Level Trend Budget From GRACE Ocean Mass?, J. Geophys. Res.-Oceans, 125, e2019JC015535, https://doi.org/10.1029/2019JC015535, 2020.

Ruić, K., Šepić, J., Mlinar, M., and Međugorac, I.: Contribution of high-frequency ($T < 2$ h) sea level oscillations to the Adriatic sea level maxima, Nat. Hazards, 116, 3747–3777, https://doi.org/10.1007/s11069-023-05834-0, 2023.

Rutgersson, A., Kjellström, E., Haapala, J., Stendel, M., Danilovich, I., Drews, M., Jylhä, K., Kujala, P., Larsén, X. G., Halsnæs, K., Lehtonen, I., Luomaranta, A., Nilsson, E., Olsson, T., Särkkä, J., Tuomi, L., and Wasmund, N.: Natural hazards and extreme events in the Baltic Sea region, Earth Syst. Dynam., 13, 251–301, https://doi.org/10.5194/esd-13-251-2022, 2022.

Samuelsson, M. and Stigebrandt, A.: Main characteristics of the long-term sea level variability in the Baltic sea, Tellus A, 48, 672–683, https://doi.org/10.1034/j.1600-0870.1996.t01-4-00006.x, 1996.

Sannino, G., Carillo, A., Iacono, R., Napolitano, E., Palma, M., Pisacane, G., and Struglia, M.: Modelling present and future climate in the Mediterranean Sea: a focus on sea-level change, Clim. Dynam., 59, 357–391, https://doi.org/10.1007/s00382-021-06132-w, 2022.

Scharffenberg, M. G. and Stammer, D.: Time-Space Sampling-Related Uncertainties of Altimetric Global Mean Sea Level Estimates, J. Geophys. Res.-Oceans, 124, 7743–7755, https://doi.org/10.1029/2018JC014785, 2019.

Schindelegger, M., Green, J. A. M., Wilmes, S.-B., and Haigh, I. D.: Can We Model the Effect of Observed Sea Level Rise on Tides?, J. Geophys. Res.-Oceans, 123, 4593–4609, https://doi.org/10.1029/2018JC013959, 2018.

Schlemm, T., Feldmann, J., Winkelmann, R., and Levermann, A.: Stabilizing effect of mélange buttressing on the marine ice-cliff

instability of the West Antarctic Ice Sheet, The Cryosphere, 16, 1979–1996, https://doi.org/10.5194/tc-16-1979-2022, 2022.

Schoof, C.: Ice sheet grounding line dynamics: Steady states, stability, and hysteresis, J. Geophys. Res., 112, F03S28, https://doi.org/10.1029/2006JF000664, 2007.

Schureman, P.: Tides and Currents in Hudson River, in: Coast and Geodetic Survey Special Publication, U.S. Department of Commerce, ISBN 978-0266815631, 1934.

Seifert, T. and Kayser, B.: A high-resolution spherical grid topography of the Baltic Sea, Meereswiss. Ber. Warn., 9, 73–88, 1995.

Šepić, J., Rabinovich, A. B., and Sytov, V. N.: Odessa Tsunami of 27 June 2014: Observations and Numerical Modelling, Pure Appl. Geophys., 175, 1545–1572, https://doi.org/10.1007/s00024-017-1729-1, 2018.

Sérazin, G., Penduff, T., Grégorio, S., Barnier, B., Molines, J.-M., and Terray, L.: Intrinsic Variability of Sea Level from Global Ocean Simulations: Spatiotemporal Scales, J. Climate, 28, 4279–4292, https://doi.org/10.1175/JCLI-D-14-00554.1, 2015.

Sergienko, O. V. and Wingham, D. J.: Bed topography and marine ice-sheet stability, J. Glaciol., 68, 124–138, https://doi.org/10.1017/jog.2021.79, 2022.

Seroussi, H., Nowicki, S., Payne, A. J., Goelzer, H., Lipscomb, W. H., Abe-Ouchi, A., Agosta, C., Albrecht, T., Asay-Davis, X., Barthel, A., Calov, R., Cullather, R., Dumas, C., Galton-Fenzi, B. K., Gladstone, R., Golledge, N. R., Gregory, J. M., Greve, R., Hattermann, T., Hoffman, M. J., Humbert, A., Huybrechts, P., Jourdain, N. C., Kleiner, T., Larour, E., Leguy, G. R., Lowry, D. P., Little, C. M., Morlighem, M., Pattyn, F., Pelle, T., Price, S. F., Quiquet, A., Reese, R., Schlegel, N.-J., Shepherd, A., Simon, E., Smith, R. S., Straneo, F., Sun, S., Trusel, L. D., Van Breedam, J., van de Wal, R. S. W., Winkelmann, R., Zhao, C., Zhang, T., and Zwinger, T.: ISMIP6 Antarctica: a multi-model ensemble of the Antarctic ice sheet evolution over the 21st century, The Cryosphere, 14, 3033–3070, https://doi.org/10.5194/tc-14-3033-2020, 2020.

Siahaan, A., Smith, R. S., Holland, P. R., Jenkins, A., Gregory, J. M., Lee, V., Mathiot, P., Payne, A. J., Ridley, J. K., and Jones, C. G.: The Antarctic contribution to 21st-century sea-level rise predicted by the UK Earth System Model with an interactive ice sheet, The Cryosphere, 16, 4053–4086, https://doi.org/10.5194/tc-16-4053-2022, 2022.

Simon, B.: Statistiques des niveaux marins extrêmes de pleine mer en Manche et Atlantique, CD-Rom, Produit commun SHOM-CETMEF, 2008.

Simpson, M., Ravndal, O., Sande, H., Nilsen, J., Kierulf, H., Vestøl, O., and Steffen, H.: Projected 21st Century Sea-Level Changes, Observed Sea Level Extremes, and Sea Level Allowances for Norway, J. Mar. Sci. Eng., 5, 36, https://doi.org/10.3390/jmse5030036, 2017.

Skjong, M., Naess, A., and Næss, O. E. B.: Statistics of Extreme Sea Levels for Locations along the Norwegian Coast, J. Coast. Res., 29, 1029–1048, https://doi.org/10.2112/JCOASTRES-D-12-00208.1, 2013.

Skliris, N., Zika, J. D., Herold, L., Josey, S. A., and Marsh, R.: Mediterranean sea water budget long-term trend inferred from salinity observations, Clim. Dynam., 51, 2857–2876, https://doi.org/10.1007/s00382-017-4053-7, 2018.

Slangen, A., van de Wal, R., Reerink, T., de Winter, R., Hunter, J., Woodworth, P., and Edwards, T.: The Impact of Uncertainties in Ice Sheet Dynamics on Sea-Level Allowances at Tide Gauge Locations, J. Mar. Sci. Eng., 5, 21, https://doi.org/10.3390/jmse5020021, 2017.

Slangen, A. B. A., Church, J. A., Agosta, C., Fettweis, X., Marzeion, B., and Richter, K.: Anthropogenic forcing dominates global mean sea-level rise since 1970, Nat. Clim. Change, 6, 701–705, https://doi.org/10.1038/nclimate2991, 2016.

Slangen, A. B. A., Haasnoot, M., and Winter, G.: Rethinking Sea-Level Projections Using Families and Timing Differences, Earths Future, 10, e2021EF002576, https://doi.org/10.1029/2021EF002576, 2022.

Slangen, A. B. A., Palmer, M. D., Camargo, C. M. L., Church, J. A., Edwards, T. L., Hermans, T. H. J., Hewitt, H. T., Garner, G. G., Gregory, J. M., Kopp, R. E., Santos, V. M., and van de Wal, R. S. W.: The evolution of 21st century sea-level projections from IPCC AR5 to AR6 and beyond, Camb. Prisms Coast. Futur., 1, e7, https://doi.org/10.1017/cft.2022.8, 2023.

Slater, D. A., Felikson, D., Straneo, F., Goelzer, H., Little, C. M., Morlighem, M., Fettweis, X., and Nowicki, S.: Twenty-first century ocean forcing of the Greenland ice sheet for modelling of sea level contribution , The Cryosphere, 14, 985–1008, https://doi.org/10.5194/tc-14-985-2020, 2020.

Slater, T., Shepherd, A., McMillan, M., Leeson, A., Gilbert, L., Muir, A., Munneke, P. K., Noël, B., Fettweis, X., Van Den Broeke, M., and Briggs, K.: Increased variability in Greenland Ice Sheet runoff from satellite observations, Nat. Commun., 12, 6069, https://doi.org/10.1038/s41467-021-26229-4, 2021.

Smith, B., Fricker, H. A., Gardner, A. S., Medley, B., Nilsson, J., Paolo, F. S., Holschuh, N., Adusumilli, S., Brunt, K., Csatho, B., Harbeck, K., Markus, T., Neumann, T., Siegfried, M. R., and Zwally, H. J.: Pervasive ice sheet mass loss reflects competing ocean and atmosphere processes, Science, 368, 1239–1242, https://doi.org/10.1126/science.aaz5845, 2020.

Spencer, T., Brooks, S. M., Evans, B. R., Tempest, J. A., and Möller, I.: Southern North Sea storm surge event of 5 December 2013: Water levels, waves and coastal impacts, Earth-Sci. Rev., 146, 120–145, https://doi.org/10.1016/j.earscirev.2015.04.002, 2015.

Staneva, J., Alari, V., Breivik, Ø., Bidlot, J.-R., and Mogensen, K.: Effects of wave-induced forcing on a circulation model of the North Sea, Ocean Dynam., 67, 81–101, https://doi.org/10.1007/s10236-016-1009-0, 2017.

Staneva, J., Grayek, S., Behrens, A., and Günther, H.: GCOAST: Skill assessments of coupling wave and circulation models (NEMO-WAM), J. Phys. Conf. Ser., 1730, 012071, https://doi.org/10.1088/1742-6596/1730/1/012071, 2021.

Steffelbauer, D. B., Riva, R. E. M., Timmermans, J. S., Kwakkel, J. H., and Bakker, M.: Evidence of regional sea-level rise acceleration for the North Sea, Environ. Res. Lett., 17, 074002, https://doi.org/10.1088/1748-9326/ac753a, 2022.

Sterlini, P., Le Bars, D., De Vries, H., and Ridder, N.: Understanding the spatial variation of sea level rise in the North Sea using satellite altimetry, J. Geophys. Res.-Oceans, 122, 6498–6511, https://doi.org/10.1002/2017JC012907, 2017.

Stramska, M. and Chudziak, N.: Recent multiyear trends in the Baltic Sea level, Oceanologia, 55, 319–337, https://doi.org/10.5697/oc.55-2.319, 2013.

Straneo, F. and Heimbach, P.: North Atlantic warming and the retreat of Greenland's outlet glaciers, Nature, 504, 36–43, https://doi.org/10.1038/nature12854, 2013.

Sun, S., Pattyn, F., Simon, E. G., Albrecht, T., Cornford, S., Calov, R., Dumas, C., Gillet-Chaulet, F., Goelzer, H., Golledge, N. R., Greve, R., Hoffman, M. J., Humbert, A., Kazmierczak, E., Kleiner, T., Leguy, G. R., Lipscomb, W. H., Martin, D., Morlighem, M., Nowicki, S., Pollard, D., Price, S., Quiquet, A., Seroussi, H., Schlemm, T., Sutter, J., van de Wal, R. S. W., Winkelmann, R., and Zhang, T.: Antarctic ice sheet response to sudden and sustained ice-shelf collapse (ABUMIP), J. Glaciol., 66, 891–904, https://doi.org/10.1017/jog.2020.67, 2020.

Sündermann, J. and Pohlmann, T.: A brief analysis of North Sea physics, Oceanologia, 53, 663–689, https://doi.org/10.5697/oc.53-3.663, 2011.

Sweet, W. V., Hamlington, B. D., Kopp, R. E., Weaver, C. P., Barnard, P. L., Bekaert, D., Brooks, W., Craghan, M., Dusek, G., Frederikse, T., Garner, G. G., Genz, A. S., Krasting, J. P., Larour, E., Marcy, D., Marra, J. J., Obeysekera, J., Osler, M., Pendleton, M., Roman, D., Schmied, L., Veatch, W., White, K. D., and Zuzak, C.: Global and Regional Sea Level Rise Scenarios for the United States: Updated Mean Projections and Extreme Water Level Probabilities Along U.S. Coastlines, NOAA Technical Report NOS 01, National Oceanic and Atmospheric Administration, National Ocean Service, Silver Spring, MD, 111 pp., https://oceanservice.noaa.gov/hazards/sealevelrise/noaa-nos-techrpt01-global-regional-SLR-scenarios-US.pdf (last access: 2 July 2024), 2022.

Tadesse, M., Wahl, T., and Cid, A.: Data-Driven Modeling of Global Storm Surges, Front. Mar. Sci., 7, 260, https://doi.org/10.3389/fmars.2020.00260, 2020.

Tadesse, M. G. and Wahl, T.: A database of global storm surge reconstructions, Sci. Data, 8, 125, https://doi.org/10.1038/s41597-021-00906-x, 2021.

Tadesse, M. G., Wahl, T., Rashid, M. M., Dangendorf, S., Rodríguez-Enríquez, A., and Talke, S. A.: Long-term trends in storm surge climate derived from an ensemble of global surge reconstructions, Sci. Rep., 12, 13307, https://doi.org/10.1038/s41598-022-17099-x, 2022.

Tamisiea, M. E.: Ongoing glacial isostatic contributions to observations of sea level change, Geophys. J. Int., 186, 1036–1044, 2011.

Tamisiea, M. E., Hughes, C. W., Williams, S. D. P., and Bingley, R. M.: Sea level: measuring the bounding surfaces of the ocean, Philos. Trans. R. Soc. Math. Phys. Eng. Sci., 372, 20130336, https://doi.org/10.1098/rsta.2013.0336, 2014.

Teatini, P., Tosi, L., Strozzi, T., Carbognin, L., Cecconi, G., Rosselli, R., and Libardo, S.: Resolving land subsi- dence within the Venice Lagoon by persistent scatterer SAR interferometry, Phys. Chem. Earth, 40–41, 72–79, 2012.

Tebaldi, C., Ranasinghe, R., Vousdoukas, M., Rasmussen, D. J., Vega-Westhoff, B., Kirezci, E., Kopp, R. E., Sriver, R., and Mentaschi, L.: Extreme sea levels at different global warming levels, Nat. Clim. Change, 11, 746–751, https://doi.org/10.1038/s41558-021-01127-1, 2021.

Teferle, F. N., Bingley, R. M., Orliac, E. J., Williams, S. D. P., Woodworth, P. L., McLaughlin, D., Baker, T. F., Shennan, I., Milne, G. A., Bradley, S. L., and Hansen, D. N.: Crustal motions in Great Britain: evidence from continuous GPS, absolute gravity and Holocene sea level data, Geophys. J. Int., 178, 23–46, https://doi.org/10.1111/j.1365-246X.2009.04185.x, 2009.

The Climate Change Initiative Coastal Sea Level Team, Benveniste, J., Birol, F., Calafat, F., Cazenave, A., Dieng, H., Gouzenes, Y., Legeais, J. F., Léger, F., Niño, F., Passaro, M., Schwatke, C., and Shaw, A.: Coastal sea level anomalies and associated trends from Jason satellite altimetry over 2002–2018, Sci. Data, 7, 357, https://doi.org/10.1038/s41597-020-00694-w, 2020.

The IMBIE team: Mass balance of the Antarctic Ice Sheet from 1992 to 2017, Nature, 558, 219–222, https://doi.org/10.1038/s41586-018-0179-y, 2018.

The IMBIE Team: Mass balance of the Greenland Ice Sheet from 1992 to 2018, Nature, 579, 233–239, https://doi.org/10.1038/s41586-019-1855-2, 2020.

Tinker, J., Palmer, M. D., Copsey, D., Howard, T., Lowe, J. A., and Hermans, T. H. J.: Dynamical downscaling of unforced interannual sea-level variability in the North-West European shelf seas, Clim. Dynam., 55, 2207–2236, https://doi.org/10.1007/s00382-020-05378-0, 2020.

Todd, A., Zanna, L., Couldrey, M., Gregory, J., Wu, Q., Church, J. A., Farneti, R., Navarro-Labastida, R., Lyu, K., Saenko, O., Yang, D., and Zhang, X.: Ocean-Only FAFMIP: Understanding Regional Patterns of Ocean Heat Content and Dynamic Sea Level Change, J. Adv. Model. Earth Syst., 12, e2019MS002027TS141, https://doi.org/10.1029/2019MS002027, 2020.

Toimil, A., Losada, I. J., Díaz-Simal, P., Izaguirre, C., and Camus, P.: Multi-sectoral, high-resolution assessment of climate change consequences of coastal flooding, Clim. Change, 145, 431–444, https://doi.org/10.1007/s10584-017-2104-z, 2017.

Toomey, T., Amores, A., Marcos, M., Orfila, A., and Romero, R.: Coastal Hazards of Tropical-Like Cyclones Over the Mediterranean Sea, J. Geophys. Res.-Oceans, 127, e2021JC017964, https://doi.org/10.1029/2021JC017964, 2022a.

Toomey, T., Amores, A., Marcos, M., and Orfila, A.: Coastal sea levels and wind-waves in the Mediterranean Sea since 1950 from a high-resolution ocean reanalysis, Front. Mar. Sci., 9, 991504, https://doi.org/10.3389/fmars.2022.991504, 2022b.

Tsimplis, M. N., Josey, S. A., Rixen, M., and Stanev, E. V.: On the forcing of sea level in the Black Sea: Sea Level Forcing in the Black Sea, J. Geophys. Res.-Oceans, 109, C08015, https://doi.org/10.1029/2003JC002185, 2004.

Umgiesser, G., Bajo, M., Ferrarin, C., Cucco, A., Lionello, P., Zanchettin, D., Papa, A., Tosoni, A., Ferla, M., Coraci, E., Morucci, S., Crosato, F., Bonometto, A., Valentini, A., Orlić, M., Haigh, I. D., Nielsen, J. W., Bertin, X., Fortunato, A. B., Pérez Gómez, B., Alvarez Fanjul, E., Paradis, D., Jourdan, D., Pasquet, A., Mourre, B., Tintoré, J., and Nicholls, R. J.: The prediction of floods in Venice: methods, models and uncertainty (review article), Nat. Hazards Earth Syst. Sci., 21, 2679–2704, https://doi.org/10.5194/nhess-21-2679-2021, 2021.

Vacchi, M., Ghilardi, M., Melis, R. T., Spada, G., Giaime, M., Marriner, N., Lorscheid, T., Morhange, C., Burjachs, F., and Rovere, A.: New relative sea-level insights into the isostatic history of the Western Mediterranean, Quaternary Sci. Rev., 201, 396–408, https://doi.org/10.1016/j.quascirev.2018.10.025, 2018.

van den Broeke, M. R., Enderlin, E. M., Howat, I. M., Kuipers Munneke, P., Noël, B. P. Y., van de Berg, W. J., van Meijgaard, E., and Wouters, B.: On the recent contribution of the Greenland ice sheet to sea level change, The Cryosphere, 10, 1933–1946, https://doi.org/10.5194/tc-10-1933-2016, 2016.

van den Hurk, B., Bisaro, A., Haasnoot, M., Nicholls, R. J., Rehdanz, K., and Stuparu, D.: Living with sea-level rise in North-West Europe: Science-policy challenges across scales, Clim. Risk Manag., 35, 100403, https://doi.org/10.1016/j.crm.2022.100403, 2022.

Van De Wal, R. S. W., Nicholls, R. J., Behar, D., McInnes, K., Stammer, D., Lowe, J. A., Church, J. A., DeConto, R., Fettweis, X., Goelzer, H., Haasnoot, M., Haigh, I. D., Hinkel, J., Horton, B. P., James, T. S., Jenkins, A., LeCozannet, G., Levermann, A., Lipscomb, W. H., Marzeion, B., Pattyn, F., Payne, A. J., Pfeffer, W. T., Price, S. F., Seroussi, H., Sun, S., Veatch, W., and White, K.: A High-End Estimate of Sea Level Rise for Practitioners, Earths Future, 10, e2022EF002751, https://doi.org/10.1029/2022EF002751, 2022.

van de Wal, R., Melet, A., Bellafiore, D., Camus, P., Ferrarin, C., Oude Essink, G., Haigh, I. D., Lionello, P., Luijendijk, A., Toimil, A., Staneva, J., and Vousdoukas, M.: Sea Level Rise in Europe: Impacts and consequences, in: Sea Level Rise in Europe: 1st Assessment Report of the Knowledge Hub on Sea Level Rise (SLRE1), edited by: van den Hurk, B., Pinardi, N., Kiefer, T., Larkin, K., Manderscheid, P., and Richter, K., Copernicus Publications, State Planet, 3-slre1, 5, https://doi.org/10.5194/sp-3-slre1-5-2024, 2024.

van Wessem, J. M., van den Broeke, M. R., Wouters, B., and Lhermitte, S.: Variable temperature thresholds of melt pond formation on Antarctic ice shelves, Nat. Clim. Change, 13, 161–166, https://doi.org/10.1038/s41558-022-01577-1, 2023.

Vellinga, N. E., Hoitink, A. J. F., Van Der Vegt, M., Zhang, W., and Hoekstra, P.: Human impacts on tides overwhelm the effect of sea level rise on extreme water levels in the Rhine–Meuse delta, Coast. Eng., 90, 40–50, https://doi.org/10.1016/j.coastaleng.2014.04.005, 2014.

Vestøl, O., Ågren, J., Steffen, H., Kierulf, H., and Tarasov, L.: NKG2016LU: a new land uplift model for Fennoscandia and the Baltic Region, J. Geod., 93, 1759–1779, https://doi.org/10.1007/s00190-019-01280-8, 2019.

Vignudelli, S., Birol, F., Benveniste, J., Fu, L.-L., Picot, N., Raynal, M., and Roinard, H.: Satellite Altimetry Measurements of Sea Level in the Coastal Zone, Surv. Geophys., 40, 1319–1349, https://doi.org/10.1007/s10712-019-09569-1, 2019.

Vilibić, I. and Šepić, J.: Global mapping of nonseismic sea level oscillations at tsunami timescales, Sci. Rep., 7, 40818, https://doi.org/10.1038/srep40818, 2017.

Vilibić, I., Šepić, J., Dunić, N., Sevault, F., Monserrat, S., and Jordà, G.: Proxy-Based Assessment of Strength and Frequency of Meteotsunamis in Future Climate, Geophys. Res. Lett., 45, 10501–10508, https://doi.org/10.1029/2018GL079566, 2018.

Vilibić, I., Rabinovich, A. B., and Anderson, E. J.: Special issue on the global perspective on meteotsunami science: editorial, Nat. Hazards, 106, 1087–1104, https://doi.org/10.1007/s11069-021-04679-9, 2021.

Villalonga, J., Amores, À., Monserrat, S., Marcos, M., Gomis, D., and Jordà, G.: Observational study of the heterogeneous global meteotsunami generated after the Hunga Tonga–Hunga Ha'apai Volcano eruption, Sci. Rep., 13, 8649, https://doi.org/10.1038/s41598-023-35800-6, 2023.

Vinet, F., Lumbroso, D., Defossez, S., and Boissier, L.: A comparative analysis of the loss of life during two recent floods in France: the sea surge caused by the storm Xynthia and the flash flood in Var, Nat. Hazards, 61, 1179–1201, https://doi.org/10.1007/s11069-011-9975-5, 2012.

Volkov, D. L. and Landerer, F. W.: Internal and external forcing of sea level variability in the Black Sea, Clim. Dynam., 45, 2633–2646, https://doi.org/10.1007/s00382-015-2498-0, 2015.

Volkov, D. L., Johns, W. E., and Belonenko, T. V.: Dynamic response of the Black Sea elevation to intraseasonal fluctuations of the Mediterranean sea level, Geophys. Res. Lett., 43, 283–290, https://doi.org/10.1002/2015GL066876, 2016.

von Schuckmann, K., Cheng, L., Palmer, M. D., Hansen, J., Tassone, C., Aich, V., Adusumilli, S., Beltrami, H., Boyer, T., Cuesta-Valero, F. J., Desbruyères, D., Domingues, C., García-García, A., Gentine, P., Gilson, J., Gorfer, M., Haimberger, L., Ishii, M., Johnson, G. C., Killick, R., King, B. A., Kirchengast, G., Kolodziejczyk, N., Lyman, J., Marzeion, B., Mayer, M., Monier, M., Monselesan, D. P., Purkey, S., Roemmich, D., Schweiger, A., Seneviratne, S. I., Shepherd, A., Slater, D. A., Steiner, A. K., Straneo, F., Timmermans, M.-L., and Wijffels, S. E.: Heat stored in the Earth system: where does the energy go?, Earth Syst. Sci. Data, 12, 2013–2041, https://doi.org/10.5194/essd-12-2013-2020, 2020.

Von Storch, H. and Woth, K.: Storm surges: perspectives and options, Sustain. Sci., 3, 33–43, https://doi.org/10.1007/s11625-008-0044-2, 2008.

Vousdoukas, M. I., Voukouvalas, E., Annunziato, A., Giardino, A., and Feyen, L.: Projections of extreme storm surge levels along Europe, Clim. Dynam., 47, 3171–3190, https://doi.org/10.1007/s00382-016-3019-5, 2016.

Vousdoukas, M. I., Mentaschi, L., Voukouvalas, E., Verlaan, M., and Feyen, L.: Extreme sea levels on the rise along Europe's coasts: Extreme Sea Levels Along Europe's Coasts, Earths Future, 5, 304–323, https://doi.org/10.1002/2016EF000505, 2017.

Vousdoukas, M. I., Mentaschi, L., Voukouvalas, E., Verlaan, M., Jevrejeva, S., Jackson, L. P., and Feyen, L.: Global probabilistic projections of extreme sea levels show intensification of coastal flood hazard, Nat. Commun., 9, 2360, https://doi.org/10.1038/s41467-018-04692-w, 2018.

Wahl, T. and Chambers, D. P.: Climate controls multidecadal variability in U. S. extreme sea level records: U.S. Extreme Sea Levels and Climate, J. Geophys. Res.-Oceans, 121, 1274–1290, https://doi.org/10.1002/2015JC011057, 2016.

Wahl, T., Haigh, I. D., Woodworth, P. L., Albrecht, F., Dillingh, D., Jensen, J., Nicholls, R. J., Weisse, R., and Wöppelmann, G.: Observed mean sea level changes around the North Sea coastline from 1800 to present, Earth-Sci. Rev., 124, 51–67, https://doi.org/10.1016/j.earscirev.2013.05.003, 2013.

Wahl, T., Haigh, I. D., Nicholls, R. J., Arns, A., Dangendorf, S., Hinkel, J., and Slangen, A. B. A.: Understanding extreme sea levels for broad-scale coastal impact and adaptation analysis, Nat. Commun., 8, 16075, https://doi.org/10.1038/ncomms16075, 2017.

Wakelin, S. L., Woodworth, P. L., Flather, R. A., and Williams, J. A.: Sea-level dependence on the NAO over the NW European Continental Shelf: Sea Level Dependence on the NAO, Geophys. Res. Lett., 30, 1403, https://doi.org/10.1029/2003GL017041, 2003.

WCRP Global Sea Level Budget Group: Global sea-level budget 1993–present, Earth Syst. Sci. Data, 10, 1551–1590, https://doi.org/10.5194/essd-10-1551-2018, 2018.

Weertman, J.: Stability of ice-age ice sheets, J. Geophys. Res., 66, 3783–3792, https://doi.org/10.1029/JZ066i011p03783, 1961.

Weertman, J.: Stability of the Junction of an Ice Sheet and an Ice Shelf, J. Glaciol., 13, 3–11, https://doi.org/10.3189/S0022143000023327, 1974.

Weisse, R., Bellafiore, D., Menéndez, M., Méndez, F., Nicholls, R. J., Umgiesser, G., and Willems, P.: Changing extreme sea levels along European coasts, Coast. Eng., 87, 4–14, https://doi.org/10.1016/j.coastaleng.2013.10.017, 2014.

Weisse, R., Dailidienė, I., Hünicke, B., Kahma, K., Madsen, K., Omstedt, A., Parnell, K., Schöne, T., Soomere, T., Zhang, W., and Zorita, E.: Sea level dynamics and coastal erosion in the Baltic Sea region, Earth Syst. Dynam., 12, 871–898, https://doi.org/10.5194/esd-12-871-2021, 2021.

Widlansky, M. J., Long, X., and Schloesser, F.: Increase in sea level variability with ocean warming associated with the nonlinear thermal expansion of seawater, Commun. Earth Environ., 1, 9, https://doi.org/10.1038/s43247-020-0008-8, 2020.

Williams, J., Horsburgh, K. J., Williams, J. A., and Proctor, R. N. F.: Tide and skew surge independence: New insights for flood risk, Geophys. Res. Lett., 43, 6410–6417, https://doi.org/10.1002/2016GL069522, 2016.

Wolf, J.: Surge-Tide Interaction in the North Sea and River Thames, in: Floods due to High Winds and Tides, edited by: Peregrine, D., Elsevier, New York, 75–94, ISBN 978-0125518208, 1981.

Wolski, T., Wiśniewski, B., Giza, A., Kowalewska-Kalkowska, H., Boman, H., Grabbi-Kaiv, S., Hammarklint, T., Holfort, J., and Lydeikaitė, Ž.: Extreme sea levels at selected stations on the Baltic Sea coast, Oceanologia, 56, 259–290, https://doi.org/10.5697/oc.56-2.259, 2014.

Woodworth, P., Wöppelmann, G., Marcos, M., Gravelle, M., and Bingley, R.: Why We Must Tie Satellite Positioning to Tide Gauge Data, Eos, 98, https://doi.org/10.1029/2017EO064037, 2017.

Woodworth, P. L. and Blackman, D.: Evidence for systematic changes in extreme high waters since the mid-1970s, J. Climate, 17, 1190–1197, 2004.

Woodworth, P. L., Shaw, S. M., and Blackman, D. L.: Secular trends in mean tidal range around the British Isles and along the adjacent European coastline, Geophys. J. Int., 104, 593–609, https://doi.org/10.1111/j.1365-246X.1991.tb05704.x, 1991.

Woodworth, P. L., Tsimplis, M. N., Flather, R. A., and Shennan, I.: A review of the trends observed in British Isles mean sea level data measured by tide gauges, Geophys. J. Int., 136, 651–670, https://doi.org/10.1046/j.1365-246x.1999.00751.x, 1999.

Woodworth, P. L., Teferle, F. N., Bingley, R. M., Shennan, I., and Williams, S. D. P.: Trends in UK mean sea level revisited, Geophys. J. Int., 176, 19–30, https://doi.org/10.1111/j.1365-246X.2008.03942.x, 2009.

Woodworth, P. L., Menendez, M., and Gehrels, W. R.: Evidence for century-timescale acceleration in mean sea levels and for recent changes in extreme sea levels, Surv. Geophys., 32, 603–618, 2011.

Woodworth, P. L., Hunter, J. R., Marcos, M., Caldwell, P., Menéndez, M., and Haigh, I.: Towards a global higher-frequency sea level dataset, Geosci. Data J., 3, 50–59, https://doi.org/10.1002/gdj3.42, 2016.

Woodworth, P. L., Melet, A., Marcos, M., Ray, R. D., Wöppelmann, G., Sasaki, Y. N., Cirano, M., Hibbert, A., Huthnance, J. M., Monserrat, S., and Merrifield, M. A.: Forcing Factors Affecting Sea Level Changes at the Coast, Surv. Geophys., 40, 1351–1397, https://doi.org/10.1007/s10712-019-09531-1, 2019.

Woodworth, P. L., Hunter, J. R., Marcos, M., and Hughes, C. W.: Towards reliable global allowances for sea level rise, Glob. Planet. Change, 203, 103522, https://doi.org/10.1016/j.gloplacha.2021.103522, 2021.

Wöppelmann, G. and Marcos, M.: Coastal sea level rise in southern Europe and the nonclimate contribution of vertical land motion: Sea Level Rise in Southern Europe, J. Geophys. Res.-Oceans, 117, C01007, https://doi.org/10.1029/2011JC007469, 2012.

Wöppelmann, G. and Marcos, M.: Vertical land motion as a key to understanding sea level change and variability: Vertical Land Motion and Sea Level Change, Rev. Geophys., 54, 64–92, https://doi.org/10.1002/2015RG000502, 2016.

Wöppelmann, G., Marcos, M., Coulomb, A., Martín Míguez, B., Bonnetain, P., Boucher, C., Gravelle, M., Simon, B., and Tiphaneau, P.: Rescue of the historical sea level record of Marseille (France) from 1885 to 1988 and its extension back to 1849–1851, J. Geod., 88, 869–885, https://doi.org/10.1007/s00190-014-0728-6, 2014.

Woth, K.: North Sea storm surge statistics based on projections in a warmer climate: How important are the driving GCM and the chosen emission scenario?, Geophys. Res. Lett., 32, 2005GL023762, https://doi.org/10.1029/2005GL023762, 2005.

Woth, K., Weisse, R., and Von Storch, H.: Climate change and North Sea storm surge extremes: an ensemble study of storm surge extremes expected in a changed climate projected by four different regional climate models, Ocean Dynam., 56, 3–15, https://doi.org/10.1007/s10236-005-0024-3, 2006.

Wu, P., Wei, M., and D'Hondt, S.: Subsidence in Coastal Cities Throughout the World Observed by InSAR, Geophys. Res. Lett., 49, e2022GL098477, https://doi.org/10.1029/2022GL098477, 2022.

Wubber, C. and Krauss, W.: The two dimensional seiches of the Baltic Sea, Oceanol. Acta, 2, 435–446, 1979.

Wunsch, C. and Stammer, D.: Atmospheric loading and the oceanic "inverted barometer" effect, Rev. Geophys., 35, 79–107, 1997.

Yan, K., Muis, S., Irazoqui, M., and Verlaan, M.: Water level change time series for the European coast from 1977 to 2100 derived from climate projections, Copernicus Climate Change Service (C3S) Climate Data Store (CDS) [data set], https://doi.org/10.24381/cds.8c59054f, 2020.

Zanchettin, D., Bruni, S., Raicich, F., Lionello, P., Adloff, F., Androsov, A., Antonioli, F., Artale, V., Carminati, E., Ferrarin, C., Fofonova, V., Nicholls, R. J., Rubinetti, S., Rubino, A., Sannino, G., Spada, G., Thiéblemont, R., Tsimplis, M., Umgiesser, G., Vignudelli, S., Wöppelmann, G., and Zerbini, S.: Sea-level rise in Venice: historic and future trends (review article), Nat. Hazards Earth Syst. Sci., 21, 2643–2678, https://doi.org/10.5194/nhess-21-2643-2021, 2021.

Zanna, L., Khatiwala, S., Gregory, J. M., Ison, J., and Heimbach, P.: Global reconstruction of historical ocean heat storage and transport, P. Natl. Acad. Sci. USA, 116, 1126–1131, https://doi.org/10.1073/pnas.1808838115, 2019.

Zemunik, P., Denamiel, C., Williams, J., and Vilibić, I.: High-frequency sea-level extremes: Global correlations to synoptic atmospheric patterns, Weather Clim. Extrem., 38, 100516, https://doi.org/10.1016/j.wace.2022.100516, 2022.

Zickfeld, K., Solomon, S., and Gilford, D. M.: Centuries of thermal sea-level rise due to anthropogenic emissions of short-lived greenhouse gases, P. Natl. Acad. Sci. USA, 114, 657–662, https://doi.org/10.1073/pnas.1612066114, 2017.